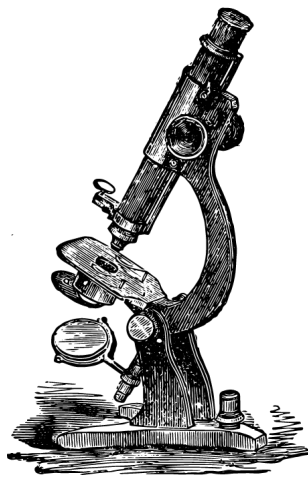


TOOLS TO EXAMINE MECHANOTRANSDUCTION

ARDON Z. SHORR



Ardon Z. Shorr: *Tools to Examine Mechanotransduction.*

A dissertation submitted in partial fulfillment of the requirements
for the degree of Doctor of Philosophy

Carnegie Mellon University
Department of Biological Sciences

COMMITTEE:

Dr. Philip R. LeDuc
Dr. Jonathan S. Minden
Dr. Frederick Lanni
Dr. John L. Woolford, Jr.
Dr. Rebecca Taylor

September 13, 2018

“Since the initial publication of the chart
of the electromagnetic spectrum,
humans have learned that
what they can touch, smell, see, and hear
is less than one-millionth of reality.”

— R. Buckminster Fuller

ABSTRACT

Organisms experience acute and chronic mechanical forces. Acute mechanical stimulation in *Drosophila* induces the ectopic expression of developmental regulatory genes. Chronic exposure to microgravity and hypergravity causes many changes in mRNA levels and cell behavior. These transcriptional changes occur downstream of mechanical transduction pathways yet to be identified. To investigate pathways of mechanotransduction, this thesis developed tools to apply acute and chronic mechanical stimulation *in vivo* with high-throughput:

- A mesofluidic device to automatic align, immobilize, compress, image, and recover hundreds of live *Drosophila* embryos
- A custom centrifuge to apply hypergravity to hundreds of *Drosophila* and zebrafish embryos
- A 3D-printed stamp to align zebrafish embryos for imaging
- A visual processing algorithm to segment Rohon-Beard neurons
- A series of macros to automate hyperstack and [DIGE](#) analysis

Using these methods, we:

- Show mechanical induction of *twist* in *Drosophila*
- Show gravitational induction of *neurogenin* in zebrafish
- Map and quantify the ectopic distribution of *twist*
- Measure *Drosophila* embryo stiffness
- Blueprint the development of future mesofluidic devices
- Run comparative proteomics across three mechanical modes, identifying 14 reciprocal changes between simulated microgravity and hypergravity, 7 of which are shared with compression

Taken together, this thesis is a study in interdisciplinary collaboration to create a pipeline of tools. The unifying theme is high-throughput *in vivo* mechanotransduction. A "mesomechanics" approach combines the high-throughput automation and precision of microfluidics, automated image processing, and proteomics, with the biological relevance of live embryos to examine mechanotransduction. The long-term goal is to uncover and dissect pathways of mechanotransduction required for normal cell function, development, and disease.

PUBLIC ABSTRACT

Life on Earth evolved under the influence of gravity. After gravity deprivation, astronauts come back with health problems that look like premature aging. It's still unclear how living things sense gravity, partly because our experiments have been limited. They've been limited to a few animals at a time, or to simple groups of cells instead of a whole, complex, living organism. In this thesis, I developed new tools across several fields to study how living things sense mechanical force. In other words, how does life turn the outside physical world into the inside chemical world? And what does it do with that information?

Three projects delivered a mechanical intervention to many animals at once, and then measured what happens. This involved building devices to align and image embryonic flies and fish, building tools to carefully apply a force, and writing code to analyze the results. Using these methods, I found intriguing responses we hadn't seen before.

This matters because if we can figure out how living things sense mechanical force, eventually, we can develop new treatments for when that goes wrong. For example, mechanical dysfunctions lead to age-related diseases, and many cancers seem to have a mechanical component. With a better understanding of how living things sense gravity, we can improve the safety of long-term space travel.

But for me, the bigger picture is building tools across disciplines. Tools change the questions we can ask. The microscope opened up an entire world inside us all along. In my own small way, I'm trying to find new ways to make visible the invisible.

I used to think of biology as chemical reactions. Now I see a web of communication with mechanics – tension, compression, and gravity, intimately bound together in a living dance.

CONTENTS

I INTRODUCTION

1	MECHANOTRANSDUCTION	3
2	ACUTE MECHANICS: DEVELOPMENT	5
2.1	Ventral furrow formation in <i>Drosophila</i>	5
2.2	Mechanical induction of <i>twist</i> and Myo-II	7
3	CHRONIC MECHANICS: GRAVITY	9
3.1	Humans in microgravity	9
3.2	Model organisms in microgravity	11
3.3	Hypergravity	12
3.4	Gene expression in altered gravity	13
4	TECHNIQUES TO STUDY MECHANOTRANSDUCTION	17
4.1	Simulating microgravity with a clinostat	17
4.2	Microfluidics	18
4.3	Proteomics	20

II MESOFLUIDICS

5	BACKGROUND	27
	METHODS	31
5.1	Mesofluidic device fabrication	31
5.2	Animals	34
5.3	Numerical simulation	34
5.4	Experimental setup	35
5.5	Image acquisition and processing	35
	RESULTS & DISCUSSION	37
5.6	Analytical model for wall deflection	37
5.7	Design and operation of the mesofluidic device	40
5.8	Design optimization	41
5.9	Determining Young's modulus of PDMS and <i>Drosophila</i>	48
5.10	Embryo development	49
5.11	Mechanical induction of <i>twist</i>	56
	CONCLUSIONS	59

III GRAVITROPISM

6	BACKGROUND	63
	METHODS	67
6.1	Animals	67
6.2	Confocal multi-photon imaging	67

6.3	Statistics	67
6.4	Simulated Microgravity	68
	RESULTS & DISCUSSION	71
6.5	Construction of a custom centrifuge	71
6.6	Dorsal alignment by 3D-printed stamp	73
6.7	Computational image analysis	74
6.8	Biological results	77
	CONCLUSIONS	80
IV MECHANOPROTEOMICS		
7	BACKGROUND	85
7.1	Gravity causes diverse biological responses	85
7.2	Developmental mechanical deformation	86
7.3	High-throughput proteomic approaches	86
	METHODS	89
7.4	Animals	89
7.5	Application of mechanical force	89
7.6	Lysis	91
7.7	DIGE	91
	RESULTS & DISCUSSION	93
7.8	Microgravity and hypergravity reciprocate	93
7.9	Compression follows hypergravity	96
7.10	Proteomic comparison in adult <i>Drosophila</i>	96
	CONCLUSIONS	97
V CONCLUSIONS		
8	THE HOW AND THE WHY	105
	BIBLIOGRAPHY	107
	ACKNOWLEDGMENTS	137

LIST OF FIGURES

2.1	Morphogenetic movement in <i>Drosophila</i> development	6
2.2	Twist-mediated coordination of VFF	6
2.3	Mechanogenetic network regulating VFF	7
4.1	Principle of <i>smg</i> by clinorotation in a RWV	18
4.2	Overview of 2D-DIGE	23
5.1	Overview of a mesofluidic device	29
5.2	Photolithography and PDMS replica molding	32
5.3	Post-bake setup for curing PDMS	33
5.4	Analytical model of deformable sidewalls	38
5.5	Mesofluidic compression channels	42
5.6	Compressed embryo micrographs	43
5.7	Optimizing parameters for a mesofluidic device	44
5.8	Simulation results of variable wall thickness	46
5.9	Mesofluidic optimization, continued	47
5.10	Simulation results of variable wall rigidity	50
5.11	Survival in the mesofluidic channel	51
5.12	Timelapse of embryos inside the channel	52
5.13	Compression between rigid walls	53
5.14	Flexible walls compress more consistently	54
5.15	Channel compression does not induce anoxia	55
5.16	Mechanical induction of ectopic <i>twist:eGFP</i>	57
5.17	Quantifying mechanical induction of <i>twist</i>	58
5.18	Timelapse of embryos under 50% normoxia	59
6.1	Measuring single-cell responses to gravity	65
6.2	Photograph of RWV clinostat	68
6.3	Schematic: adapter for custom centrifuge	69
6.4	Schematic: 3D-printed stamp	69
6.5	A custom centrifuge to apply hypergravity	72
6.6	Systematic bias in lateral imaging	74
6.7	Anatomy of Rohon-Beard neurons (RBN)	75
6.8	Rapid dorsal alignment by 3D-printed stamp	76
6.9	Pipeline of image processing for segmentation	78
6.10	Gravity-induced neurogenin expression	79
7.1	Custom centrifuge setup for <i>Drosophila</i>	90
7.2	Representative proteomic comparison by DIGE	94
7.3	Confirmation of changes by reciprocal labeling	95
7.4	Shared differences across mechanical contexts	95
7.5	Shared protein differences in 3g and 22% compression	97
7.6	DIGE of adult <i>Drosophila</i> after 6g	97
7.7	Digitally morphing DIGE gels	99

LIST OF TABLES

5.1	Embryo strain with varying wall thickness	48
5.2	Embryo strain with varying wall rigidity	48
5.3	Inference of compression from shape change	53
5.4	Consistency of uniaxial compression methods	54
6.1	Descriptive statistics of Rohon-Beard neurons	80
7.1	Summary of DIGE difference-proteins	100
7.2	LC-MS identification of proteins enriched in adult <i>Drosophila</i> after 6g	101

ACRONYMS

CoV	Coefficient of Variation
2DE	two-dimensional electrophoresis
DIC	differential interference contrast microscopy
DIGE	difference gel electrophoresis
ECM	extracellular matrix
Fog	Folded Gastrulation
GFP	green fluorescent protein
eGFP	enhanced green fluorescent protein
hpf	hours post-fertilization
IPA	isopropyl alcohol
IEF	isoelectric focusing
ISS	international space station
LC-MS	liquid chromatography-mass spectrometry
LEO	low Earth orbit
LUT	look-up table
MSE	mean squared error

Myo-II	Myosin-2
ngn3.1	-3.1 neurogenin 1
PDMS	Polydimethylsiloxane
PR	photoresist
PSI	pounds per square inch
PTM	post-translational modification
RCF	relative centrifugal force
RBN	Rohon-Beard neurons
RPM	revolutions per minute
ROI	region of interest
RWV	rotating wall vessel
SDS-PAGE	sodium dodecyl sulfate–polyacrylamide gel electrophoresis
VFF	ventral furrow formation
μg	microgravity
$s\mu g$	simulated microgravity

Part I

INTRODUCTION

Life exists in a mechanical context. Our understanding of mechanical cues has expanded to recognize their direct impact on gene expression in development, tissue maintenance, and disease. While much is known about mechanotransduction in specific sensory systems, little is known about generalized mechanosensation, especially which proteins transduce mechanics into biochemical signals. This section reviews modes of mechanosensation, molecular pathways involved in mechanotransduction, specifically acute mechanics in *Drosophila* development, and chronic mechanics in sensing gravity. A historical context discusses emerging techniques to understand mechanotransduction.

MECHANOTRANSDUCTION

Life exists in a mechanical context. Some mechanical forces are transient – the shear stresses on endothelial cells in vasculature [1] and kidneys [2], or the folding of developing tissue [3, 4]. Other mechanical forces are chronic – compression on chondrocytes [5] and bones [6], the stiffness of substrates [7], and the constant mechanical force exerted by gravity [8].

The activation of biochemical signaling pathways in response to mechanical cues is known as mechanotransduction. Organisms across the evolutionary spectrum show mechanosensitivity [9]. The ability to sense and respond to mechanical cues is critical for many biological processes such as development [10–12] and maintaining tissue integrity [13, 14]. Dysregulation of mechanotransduction cascades into a wide range of pathologies [4, 15, 16], including muscular dystrophies [17], cardiomyopathies [18], osteoporosis [19], arteriosclerosis [20], polycystic kidney disease [21], asthma [22], developmental disorders [11, 23, 24], and cancer [16, 25–28].

Early lines of evidence for mechanosensation came from specialized neurosensory cells. For example, in hearing and balance, mechanical force from soundwaves, pressure, and gravity deflect stereocilia in the inner ear, which causes tension in extracellular filaments that link cilia tips, pulling open ion channels to allow a rapid influx of calcium [29]. Adaptation to resting tension (persistent stimulation) is achieved by contraction and relaxation of motor proteins in these linker filaments [30, 31]. A similar process occurs in sensing touch and proprioception in *Drosophila* and *C. elegans* [32, 33].

Another form of mechanosensation is found in internal regulation, such as muscle tension and blood pressure [34, 35]. In bone tissue, gravity and compressive forces from movement create pressure gradients that drive interstitial fluid flow through a network of connected cavities, which is sensed by osteocytes [6]. A similar process occurs in lungs [36]. In kidneys, shear stress from urine flow deflects primary cilia to regulate morphogenesis [2, 37].

Understanding the molecular pathways involved in mechanosensing is still in progress [3, 15, 38, 39]. Several mechanosensitive elements have been identified:

STRETCH-ACTIVATED ION CHANNELS Certain ion channels open in response to strain in the plasma membrane, allowing influx of ions such as calcium [40].

GLYCOCALIX A layer of carbohydrate-rich proteins localized at the surface of endothelial cells transduce fluid shear stress [15].

CELL-CELL JUNCTION RECEPTORS Cells sense mechanical changes in their surrounding environment through cell-cell junction receptors [41].

EXTRACELLULAR MATRIX PROTEINS Outside the cell, extracellular matrix (ECM) proteins such as fibronectin unfold under force to initiate mechanotransduction [39, 42].

CYTOSKELETON Cytoskeletal elements undergo conformational changes from intracellular strain [28].

PHYSICAL CHEMISTRY Mechanotransduction may occur through changes in physical chemistry when compression of intracellular space increases the effective concentration of signaling molecules.

NUCLEUS Multiple mechanisms have been proposed by which the nucleus itself integrates mechanical force [43–45]. Surprisingly, applying mechanical force can directly affect chromatin organization [46] and stretching sufficient to express a reporter transgene [47]. Considering that the nucleus is functionally connected to the cytoskeleton which transduces tension from outside the cell [48], one way to reconceptualize the nucleus is as a spherical vertex of the ECM that happens to be anchored within the cell [44].

For the initial mechanosensor, several models have been proposed:

- Transduction occurs at the plasma membrane via mechano-sensitive ion channels, tyrosine kinase receptors, and G-proteins [49]
- Transduction occurs at the site of cell-cell junctions or cell-matrix interactions via integrins, platelet/endothelial cell adhesion molecules, or the VEGFR2-VE-cadherin- β -catenin complex [50]
- Transduction is delocalized, transmitted from the cell surface via the cytoskeleton to other locations, potentially the nucleus, where it triggers transcription events [51]

As of this writing, it remains unclear which molecules function as initial mechanosensors, whether they act independently, or to what extent their pathways integrate [49].

*It is not birth, marriage or death, but gastrulation
which is truly the most important time in your life.*

— Lewis Wolpert

A challenge in characterizing mechanical transduction pathways is that many organ systems are affected and interconnected. Using whole organisms *in vivo* has the advantage of capturing the complexity of a multicellular systems, and using model organisms adds over a century of knowledge. One model system in which to investigate mechanotransduction is in the developing fruit fly, *Drosophila melanogaster*.

During *Drosophila* development, embryonic patterning is regulated by developmental genes that operate anteroposteriorly [52] and dorso-ventrally [53]. In embryogenesis, nuclei proliferate in a single cytoplasmic mass called a syncytium. After 13 synchronized mitotic cycles, nuclei desynchronize and form mitotic domains genetically patterned by chemical gradients called morphogens [54].

2.1 VENTRAL FURROW FORMATION IN *DROSOPHILA*

Developing embryos experience acute mechanical forces during gastrulation, the process by which a single-layered blastula folds into a multi-layered structure (Fig. 2.1). In *Drosophila*, gastrulation begins with ventral furrow formation (VFF), when a swath of ventral cells' apical membranes flatten stochastically [55, 56]. Then nuclei dislodge from their apical position of the ventral cells, which is followed by apical constriction, changing the cell shape from columnar to wedge (Fig. 2.2). Coordinated shape change induces a bending force to collapse the ventral furrow inwards, initiating mesoderm invagination [57].

The collective shape change during VFF is regulated by internal mechanical forces and the transcription factor Twist [10, 57, 58]. Twist induces the expression of the secreted factor Folded Gastrulation (Fog) [58], which activates the G-protein Concertina [59], leading to the reorganization of the actin cytoskeleton [59–61]. Without Twist, VFF does not occur properly [53]; ventral cells release their nuclei but fail to constrict their apical membranes.

The expression of Twist itself is regulated both by genetics and by internal mechanical forces (Fig. 2.2). **Genetically**, *twist* is selectively

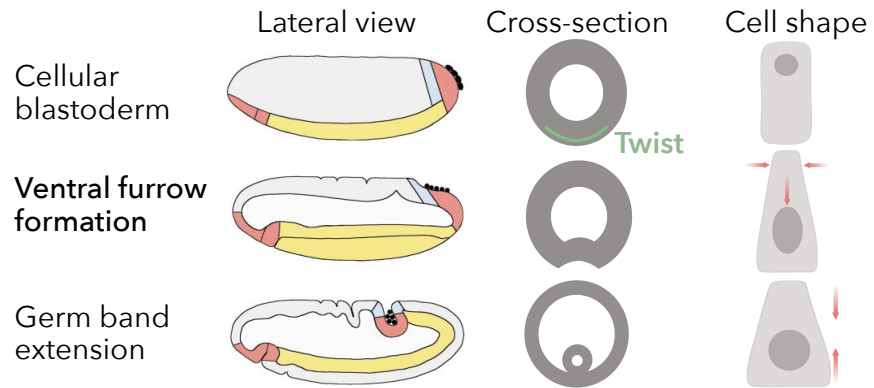


Figure 2.1: Morphogenetic movement in *Drosophila* development. Gastrulation involves collective movement through selective expression of patterning genes. Cells expressing *twist* (green) are fated to become mesoderm. *Twist* coordinates a collective change in cell shape (Fig. 2.2) to fold a group of cells into the interior of the embryo.

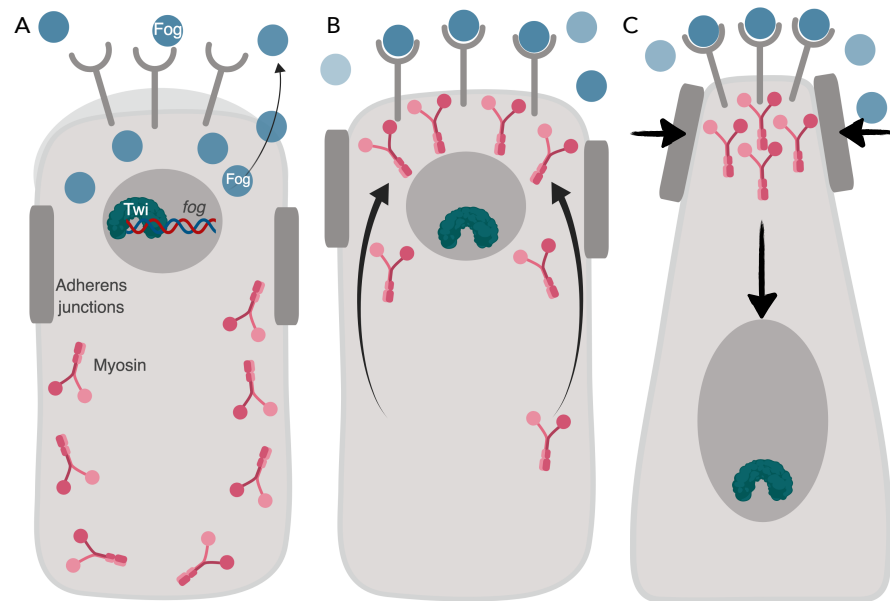


Figure 2.2: Schematic of Twist-mediated coordination of VFF (A) *Twist* directs transcription of *fog* which is secreted on the apical side to activate Snail-mediated receptor *Mist*. (B) *Fog* signaling leads to apical concentration of *Myo-II*, pulling adherens junctions to flatten the apical surface. (C) As the adherens junctions are pulled together, the nucleus detaches and migrates basally, allowing the apical side to constrict, changing its shape from columnar to wedge. Collective shape change collapses the ventral furrow, bringing those cells into the interior of the embryo.

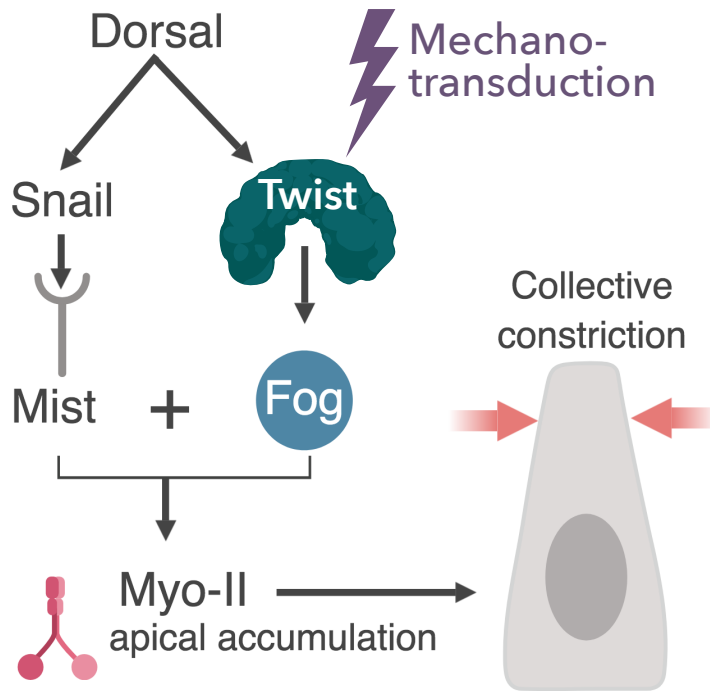


Figure 2.3: Mechanogenetic network regulating VFF. The maternal Dorsal gradient signals transcription of *twist* and *snail*. These transcription factors lead to the selective expression of *Fog* and its receptor *Mist*, which coregulate concentration of *Myo-II*, leading to collective constriction (Fig. 2.2). Mechanical induction of *twist* operates independently of Dorsal.

expressed in ventral furrow cells by a signaling cascade that activates the transmembrane receptor protein Toll on the ventral side of the embryo [62]. Toll signaling releases Dorsal (*Drosophila* NF κ B) from a cytoplasmic heterodimer Cactus, which translocates to the nucleus to transcribe *twist* in ventral cells [63], priming shape change [64].

Mechanically, *twist* is amplified from endogenous morphogenetic movements at gastrulation (namely germ-band extension) that compress stomodeal cells at the anterior pole [65]. When stomodeal compression is prevented, either by mutants defective in germ-band extension, or by laser microsurgery, *twist* is no longer amplified in stomodeal primordia. The endogenous mechanical induction of *twist* depends on *armadillo* (*arm*, *Drosophila* β -catenin); in mutants where *arm* is not transcribed, stomodeal *twist* remains attenuated [10, 65].

2.2 MECHANICAL INDUCTION OF TWIST AND MYO-II

Surprisingly, both *twist* and VFF can also be regulated by the acute application of exogenous mechanical force [4, 66]. Although *twist* is normally expressed in ventral cells [63], acute mechanical deformation just before gastrulation leads to the expression of *twist* in all tissues, leading

to a ventralized phenotype [65]. When *twist* expression is reduced by mutations in upstream genes or laser microsurgery, exogenous compression (indentation) with a blunt micro-needle recovers strong *twist* expression [3, 10, 65, 67].

Further evidence for the mechanotransductive developmental pathway comes from indentation of *Snail*-mutant (*sna*⁻) embryos. Tissue morphogenesis is initiated when developmental patterning genes drive the selective expression of an intracellular molecular motor Myosin-2 (*Myo-II*). Twist-induced *Fog* is not sufficient to accumulate medioapical *Myo-II*; co-expression of Snail is also required [10, 67]. Snail, like Twist, is established by the *dorsal* gradient, and acts through the *Fog* receptor Mist [68]. Curiously, artificial ectopic expression of *Fog* accumulates *Myo-II* in domains that do not express Snail [69]. This can be explained by a mechanotransductive link between the Snail and Twist pathway to co-regulate *Myo-II* [4, 10]. Specifically, Snail leads to the transient apical nucleation of *Myo-II*, which generates stochastic mechanical constriction [70] which can activate *Myo-II* in absence of Snail. Indeed, *sna*⁻ embryos do not accumulate *Myo-II* and fail to undergo mesoderm invagination, yet they can be rescued by mechanical indentation [10, 67]. These observations suggesting a feedback loop in which acute mechanical forces control gene expression to coordinate development.

CHRONIC MECHANICS: GRAVITY

Life on Earth evolved under the influence of gravity. Since the early Russian and American space programs of the 1960's, several biological responses have been observed in the mechanical deprivation of microgravity (μg) in space. Although some space-adaptation responses are attributable to the increased exposure to radiation [71, 72], carefully controlled ground-based simulation has revealed responses exacerbated [73] or directly attributable to changes in gravity [37, 74, 75].

When considering biological responses to μg , we would expect some to be explainable by indirect effects of altered physics. In μg , many familiar processes operate counter to our terrestrial intuition: rain does not fall, water does not drain, fire burns in a sphere, and heat does not dissipate. Gone are the gravity-driven flows of buoyancy, sedimentation, and convection. Likewise, many changes across many organ systems can be understood as consequences of fluid dysregulation [76], lack of loading, or altered cues:

3.1 HUMANS IN MICROGRAVITY

MUSCULOSKELETAL Bone demineralization was first discovered by accident; excess urinary calcium complexed with the sulfuric acid treatment in the first international space station (ISS) toilet, precipitating CaSO_4 salts that were not accounted for in ground testing [77]. Since then, rapid bone loss coupled with increased calcium in urine has been consistently observed in astronauts [78, 79] *in vivo* models [80], and osteoblast cultures [81, 82], though the mechanism of onset remains incompletely understood [82]. Although osteoporosis risk is higher for women, no such difference was seen in spaceflight [83]. Other major findings include loss of lean body mass, muscle loss due to decreased protein synthesis [84], especially postural (gravity resisting) muscles [85]. Some effects can be mitigated with resistance training and pharmacological intervention [86].

NEUROVESTIBULAR Neurovestibular systems show a constellation of postural instability and disorientation, collectively called "space adaptation syndrome." In early flight, crew struggle to maintain vertical alignment by relying on touch and sight. In later flight, alignment be-

comes internal relative to the feet. Most people report motion sickness, headache, fullness in the face and eyes [72].

RENAL In the renal system, the main concern was kidney stones due to rapid demineralization of bones and subsequent hypercalciuria of urine [87, 88]. Kidney stones are the most common complication that does not reverse after return to Earth; one retrospective analysis found 14 cases among 12 astronauts [89]. These urinary effects may be indirectly related to μg , at least partially a consequence of dehydration and limited movement because they are phenocopied in extended bedrest [90].

CARDIOVASCULATURE Major findings include a shift of fluid towards the head, reduced plasma volume, and difficulty standing [91, 92].

CIRCADIAN CLOCKS Altered circadian clocks are unsurprising given the unusual *zeitgebers* of spaceflight [93–95].

As interest in μg grew, so too did methods for simulated microgravity (*s μg*), discussed in section 4.1.

Microgravity as a model of aging

The effects of μg phenocopy those of aging in several ways: both see a deterioration of muscle quantity and quality [96], a reduction in VO_2 max [97], decreased bone mass [79], decreased immune function [98], impaired wound healing [99], impaired balance and posture [100], impaired sleep pattern [101] and disrupted circadian cycles [94]. *Drosophila* show accelerated aging as measured by mating [102] gravitaxis [103] and lifespan [104–106]. One explanation is that the gravity deprivation of space mimics the gravity withdrawal of sedentary aging; adaptation to space and aging could therefore be approached as converging disciplines of mechanotransduction disorders [92, 107]. One benefit of pursuing this approach is that in μg , the onset and time-course of many deterioration processes are ten times faster than normal aging [92].

A powerful model organism to investigate human aging is *Drosophila*. Since flies conserve many human disease genes, orthologues implicated in human aging can be functionally analyzed [108–113]. This led to *Drosophila* models for age-related disorders, including cardiovascular deterioration [114, 115] and Alzheimer’s disease [116–120]. By combining an alternative simulation of aging through mechanical perturbations with the well-established model of *Drosophila*, we can advance the understanding and prevention of age-related disorders.

3.2 MODEL ORGANISMS IN MICROGRAVITY

In vivo responses to μg have been observed in many model organisms, including *Drosophila* [75, 106, 121], zebrafish (*Danio rerio*) [37, 122], *E. coli* [123], yeast [124], rodents [79, 125–128], and others [74, 126, 129–132]. In vertebrate development, amphibians can ovulate, eggs develop, but fail to transition past tadpoles [133]. Rats and birds fail to develop motor skills for critical development [134].

Although gravity is usually considered negligible in cells, recent evidence suggests that eukaryotic cells are constrained in size by gravitational effects on nuclei, requiring mechanical stabilization by the F-actin scaffold [135]. Microgravity affects the function of many cell types, including lymphocytes [136], epidermal cells [137], osteoblasts [81], and tumor cells [138, 139]. Recent results show decreased counts in red blood cells, along with metabolic and aging effects [140].

Bacteria

Since the 1960's, bacteria have been known to grow differently in μg . This area received considerable attention because of the troubling implications for space crews, such as increased virulence [141, 142], resistance to antibiotics [143, 144], and more efficient genetic recombination [145]. Bacteria consistently show a shortened lag phase and increased duration of exponential growth, resulting in a denser cell population of many microbes [146, 147] up to five-fold [148]. Biofilm formation is thicker, more massive, more resilient to agitation [149], and shows a novel column-and-canopy structure [150]. simulated microgravity by clinorotation (4.1) shows similar results [151, 152].

An example of unusual μg effects that were ultimately explainable can be seen from *E. coli*. Genetic analysis supports the model that bacteria in space activate pathways associated with starvation conditions [123]. These include *thiFGHS*, a metabolic-stress response gene; *dps*, which codes for a protein that protects DNA during starvation; carbon- and nitrogen-starvation genes, and a broadened search for alternative sources of carbon [123]. Although the bulk pH remained the same, almost all genes associated with acid resistance were upregulated [123]. This led to the hypothesis that the trigger for starvation pathways is the local acidification of the area surrounding the bacterium due to a lack of sedimentation and buoyancy normally driven by gravity. This model of altered extracellular transport also explains several other results [123], and why motile cells, which can disrupt the local fluid environment, do not show these effects in spaceflight [153].

3.3 HYPERGRAVITY

To understand how biological systems are influenced by chronic ubiquitous mechanical force, it is essential to consider hypergravity. Some responses to μg are not only absent in hypergravity, but also show a converse response. For example, platelet aggregation is reduced after exposure to μg , but increased after exposure to hypergravity [154, 155]. In hypergravity, *Drosophila* overactivate a Toll-mediated immune response to fungal infection, which they under-activate in spaceflight [75]. Immunological effects have also been observed in mice [156]. The existence of biological responses opposite under μg and hypergravity supports the hypothesis that some pathways measure gravity as chronic baseline strain and response in a dose-dependent manner. One speculated mechanism is through altering the relative positions of intracellular elements of different densities, such as the nucleus and cytoskeleton [157], but the mechanism remains an open question.

Unlike μg , hypergravity is not a simulation; acceleration is indistinguishable from gravity [158]. For theoretical considerations, see [iii 6.5](#).

Some of the earliest observed responses to hypergravity were of increased metabolic needs. Rats chronically accelerated at at 3g showed reversible decreases in mass and increases in food intake [159] and glucose use [160, 161]. In *Drosophila*, metabolic increase was indirectly inferred from females laying fewer eggs and delaying fecundity [162], an adaptation to withstand higher metabolic demand [163].

Longevity and senescence is an area of some conflict. Early reports showed a minimal effect on longevity in flies, with no effect up to 4g [164], then a small effect (reduction to 45 and 40 days) at 5g and 7g [162]. One hypothesis was that longevity may remain similar, but organisms age faster. Evidence for flies aging faster in hypergravity comes from dose-dependent declines in wall climbing [165] and reduction in spontaneous locomotor activity [166]. Subsequent observations complicated this interpretation: the detection threshold to sucrose increases with age but was unaffected by hypergravity [167] nor was memory and learning, as measured by conditioned suppression of proboscis extension response [168]. The authors concluded that hypergravity as an accelerator of aging is too simple.

A subsequent hypothesis was that hypergravity is a stress to which an organism develops an adaptive response. Hypergravity as a stressor led to two testable implications, and both showed restricted results:

First, *acclimation*, whereby exposure to stress increases resistance to other stresses [169]. Hypergravity acclimation was not observed for starvation, desiccation, or cold exposure [170, 171], but was observed in resistance to heat, as measured by survival time at 37 °C [170]. The mechanism of action remains unknown, especially since hypergravity

was later shown not to modulate major heat shock proteins [172]. Further evidence against the stress-acclimation model comes from observations of sensitization to μg [173].

A second implication of hypergravity as a stressor was *anti-fragility*, whereby a short exposure to a stressor increases longevity [174, 175]. Anti-fragility has been observed in flies with low doses of radiation [176] and heat [177]. Again, results were restricted: flies showed a hypergravity anti-fragile effect in males, but not females, only in virgins, and only for exposure that was continuous, greater than 2 weeks, and less than 3 weeks [170, 178]. The authors concluded that hypergravity as a stressor is also too simple.

This led to the hormetic hypothesis: hypergravity shows a positive effect at low exposure, but a negative effect at higher exposures [179]. This follows observations of a critical period in zebrafish cardiovascularity in $s\mu g$ [180].

A critical period for developing mechanosensation follows the development of other sensory systems that show vulnerability during a critical period of development. For example, postnatal visual deprivation causes morphological and electrophysiological abnormalities in the lateral geniculate bodies [181] and visual cortex [182]. Permanent morphological abnormalities and functional deficits have been observed in the tactile system after tactile deprivation [183]. So too in gravity deprivation, zebrafish show critical periods of sensitivity for both the vestibular system [184] and vascular development [180]. Depriving the zebrafish heart of shear flow during a critical period of development results in abnormalities similar to congenital heart disease [185].

3.4 GENE EXPRESSION IN ALTERED GRAVITY

Despite responses to gravity across organisms and organ systems, identifying gravity-responsive genes has been inconclusive. Many genes show widespread sub-threshold changes [186–188] or contradictory results [189, 190], even across closely related studies.

The most extensive study of gravity-induced changes in gene expression is of renal cells [191]. Hammond and colleagues grew primary cultures of human renal cortical cells for 6 days on the space shuttle, in a ground-based $s\mu g$ (by rotating wall vessel (RWV)), $2g$, and ground-based control (non-adhered bag culture). Cells were fixed in space to avoid confounds from transport. The resulting RNA was extracted and measured by automated array for the expression of 10,000 genes for > 3.0 -fold change in space. In μg , 1,632 genes were found that were not known to be shear stress response elements or heat shock proteins. In RWV, 914 genes changed, in hypergravity only 5. Notably, gene ex-

pression in μg showed random overlap with *RWV*, not just an extension from *s μg* .

In *Drosophila*, an integrative analysis of microarray data found subtle effects on the transcriptome in μg , with subtle opposite effects under hypergravity [187]. Specifically, μg and *s μg* for 4 days had dramatic effects on gene expression in *Drosophila* larvae only when combined with the constraints of spaceflight [187]. In *s μg* without environmental stressors, only five genes showed a > 2-fold change; in 10g, no genes cleared this threshold. Strikingly, the subthreshold pattern obtained in *s μg* appears inverted in hypergravity [187]. This relationship was not present between *s μg* and μg transcriptomes. This result suggests that the *Drosophila* transcriptome is finely tuned to changes in gravity. Although a small group of gravity-responsive genes have been found in unicellular *Salmonella* [192], the results from Herranz 2010 refute a gene-specific response for a genome-scale response in *Drosophila*. Later analysis of *Drosophila* pupae in 3g by RNA-Seq and qRT-PCR showed significant changes in 1,513 genes affecting ion transport, redox homeostasis, immune response, proteolysis, and cuticle development [193]. This showed some overlap with Herranz *et al.* on cuticle proteins, but not on other responses.

CG17298, CG6503,
upregulated;
Eig71Eb, cg13050
downregulated, all
protein-coding genes
of unknown function

A commonality among these studies is their focus on either mRNA or mean protein expression; they do not address protein variation directly. Transcriptomic analysis does not account for translational or post-translational regulation. Transcriptomics necessitates choosing a gene assumed to be invariant; this assumption is problematic when μg has been shown to affect expression of the housekeeping gene β -actin [8, 184, 194].

Overall, several explanations have been put forward on the lack of consensus on gravity-responsive genes:

1. Limited data, specifically a small pool of test subjects, lack of longitudinal studies, high variability in flight duration, age, nutrition, and exercise [79]
2. In *ISS* experiments, confounding suboptimal conditions [187]
3. In *s μg* experiments, variations in *RWV* usage [195–197], confounding effects from magnetic levitation [188]
4. Biological responses to altered gravity will ultimately be explainable as indirect gravitational effects such as changes in convective mixing that cascade into complex stress responses [123]
5. A narrow critical period of sensitivity to exposure [179, 184]
6. Gravity-responsive genes only exist in unicellular organisms [192] while *Drosophila* and more complex organisms show a genome-scale response [187]

7. Part of the response to gravity is gene expression stochasticity [8]
8. Responses to changes in gravity are primarily post-transcriptional, and most approaches have been transcriptional [190, 198]

Taken together, biological responses to μg are myriad, sometimes surprising. Many are ultimately understandable as a consequence of the many ways physical processes and fluid flow evolved under the assumption of gravity. These are critical to the medical community and for long-term space exploration. As with mechanotransduction, it is unclear how gravitational force is first transduced into a biological signal, or which proteins propagate that signal [34, 130, 198].

Nevertheless, there remain a set of biological responses to changes in gravity that are harder to explain. Almost all astronauts experience some form of immunodeficiency [85, 127, 136] and higher rates of cataracts than can be explained by radiation alone [72]. In hematopoietic stem cells, DNA damage repair appears impaired [73] and in renal cells, the activation of sodium-retaining systems in μg suggests that not all changes can be explained by fluid distribution alone [76]. Some antibiotic resistance is mediated genetically through an upregulation of antibiotic-resistant efflux pumps in μg [199].

Whether these effects are ultimately explainable as indirect consequences of altered gravity remains to be seen. Another possibility is the existence of a cellular-level strain gauge that experiences gravity as a chronic baseline, and becomes disrupted and adapts when that chronic baseline is altered.

TECHNIQUES TO STUDY MECHANOTRANSDUCTION

4.1 SIMULATING MICROGRAVITY WITH A CLINOSTAT

As interest grew in studying microgravity, the cost and logistics of experiments in low Earth orbit (LEO) limited sample size and depth of consideration, necessitating the use of ground-based simulated microgravity ($s\mu g$). The most common $s\mu g$ technique is the *clinostat*, a chamber that slowly rotates around an axis orthogonal to the plumb line (Fig. 4.1). Clinostats reduce time-averaged gravity vectors close to zero in any fixed direction [200–202] but equally in all directions [203]. The magnitude experienced is typically 0.01g to 0.001g [204, 205]. A common implementation of clinostats with liquid medium is the rotating wall vessel (RWV) (Fig. 6.2). An extension of the clinostat is the random-position machine, also called a “3D-clinostat,” in which two frames independently rotate.

An alternative method for $s\mu g$ is diamagnetic levitation by a superconducting magnet. However, a careful comparison to $s\mu g$ by RWV shows many effects on gene expression due to the 16.5 Tesla magnet itself [186, 188], highlighting the need for caution when interpreting these results.

Simulating microgravity by RWV has several limitations [202, 205]. Gravitational loading still occurs, just not in any fixed direction [197, 201]. Clinostats generate particle oscillations, and greater convective mixing than true weightlessness [206]. Hydrostatic pressure remains, though it operates independently of the direction of gravity. Even in optimized RWV, cell cultures experience increasing shear stresses as their size increases, eventually ripping apart aggregates and limiting their size [191].

Despite these limitations, clinostats produce results comparable to true μg [128, 139, 196, 207, 208]. Clinostats have simulated μg for over 50 years [208] empirically validated against true μg in many systems [196, 201, 208], including *Drosophila* [75, 196].

Simulating microgravity has the added benefit of eliminating confounding environmental stresses. Specifically, in *Drosophila*, genome-wide transcriptional profiling in $s\mu g$ shows more subtle effects on gene expression compared to true μg on the ISS [187]. However, the preparation for space travel and logistical constraints of spaceflight introduce hypergravity and vibration during launch, limited oxygen in sealed

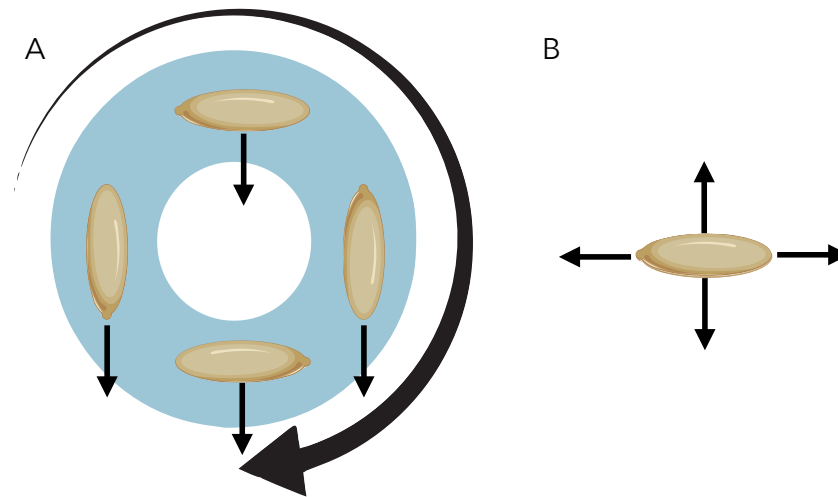


Figure 4.1: Principle of simulated microgravity ($s\mu g$) by clinorotation in a rotating wall vessel (RWV). (A) As samples rotate, they continuously fall in different directions. (B) From the sample's frame of reference, the vector average is approximately equal in all directions. If the gravity vector changes faster than the biological integration of the signal, the clinostat compensates chronic loading to simulate microgravity.

containers, increased radiation, lack of temperature control, and transportation considerations when the landing site is only known approximately. When environmental stressors are applied to $s\mu g$ on the ground, the resulting transcriptome reproduces 79% of differentially expressed genes on the ISS not seen in $s\mu g$ [187]. This suggests many transcriptomic changes in μg may be due to environmental stressors, and highlights the importance of ground-based simulations to isolate gravity responses from stress responses.

Overall, ground-based $s\mu g$ enables deeper consideration on more model organisms to interrogate biological responses to gravity. Clinostats are an essential platform to rapidly test hypotheses that would be expensive or impractical in space.

4.2 MICROFLUIDICS

A significant area of growth in biological techniques has been microscale systems. Microscale systems offer increasing functionality, operate at low volume to reduce consumption of reagents, scale physically to cellular manipulation, and scale in samples handled for increased throughput [209]. Microscale systems have led to new methods to interrogate cell properties, such as morphology, motility, behavior, biochemical interactions, and biomechanics [210, 211]. These methods have provided new insights into cell behavior and function, and enabled researchers to ask new questions otherwise impossible.

Despite this potential, collaboration has remained limited between engineers and biologists [209]. Researchers are incentivized to choose conventional and proven techniques, and face additional skepticism during grant applications, publication, and presentation. Even within collaborations, researchers face cultural divides between approaches of their discipline.

It's helpful to remember that when cell culture was first demonstrated by Ross Harrison in 1907 [212], it was also regarded with guarded skepticism [213]. Over the following decades, cell culture techniques were optimized and eventually standardized in the 1950s by what is now the Society for In Vitro Biology [213], and *in vitro* publications grew exponentially [209].

Given the relatively recent advancement in microfluidics and rarity of theses on its development in biological sciences, this work may benefit from a brief contextualization.

Historical perspective

Microfluidics is relatively younger than cell culture, with the technical groundwork laid in the 1970s with the development of soft lithography at Bell Laboratories [214]. In the 1990's, there emerged the idea of a "lab on a chip" – a miniaturized platform of laboratory equipment [215]. Research began with microscale chemistry and physics [216, 217] with few applications towards biology [218]. Much of this limitation was due to the materials: silicon and glass were popular because microfabrication techniques were first established in building circuits.

The turning point in applying microfluidics to biology was due to an advancement in materials: the development of soft lithography with Polydimethylsiloxane (PDMS) by the Whiteside lab [219]. PDMS allowed for the rapid prototyping of microscale devices that were cheap and reproducible. Accessibility and ease of use helped to rapidly expand cell-based microfluidics [209].

PDMS has several properties that facilitate biological application. Embryo manipulation is facilitated by high oxygen-permeability [220]. Low autofluorescence coupled with transparency in the visible spectrum enable high-resolution fluorescence microscopy. Deformation and elasticity help in the manufacturing process in removal from master molds and help in the biological process to orient and trap cells [221], measure traction forces [222] and actively stretch cells [223, 224].

PDMS also has some undesirable properties. Diffusion of oxygen in bulk PDMS is similar to bulk media, which may produce a hyperoxic microenvironment and cell stress [225]. PDMS is extremely permeable to water vapor [226] which can lead to evaporation that shifts media con-

centration and disrupts chemical gradients [227]. PDMS is permeable, prone to bulk absorption of hydrophobic compounds [228]. This property has been demonstrated to disrupt estrogen in culture media [229] and Prozac in human embryonic kidney cells [230]. PDMS can leach uncured oligomers into the membranes of culture cells [229]. Some mitigations have been developed for these effects [231–233] and future work will determine the biological ramifications. As with all experimental methods, awareness and careful controls are essential.

Overall, PDMS remains the best material available for patterning, bonding, prototyping, surface modification, optics, and gas permeability [209]. Care must be taken to mitigate the inherent limitations regarding biointertness and evaporation. With creative collaboration and a willingness to take risk, microfluidics has a unique ability to open new doors of inquiry into understanding the behavior of biological systems.

Towards high-throughput in vivo biomechanics

Microfluidic approaches have led to semi-automated tools for embryo manipulation. Current designs can sort [234], align [221, 235], immobilize [236, 237], image [238], and recover processed embryos with minimal intervention.

Microfluidic approaches also provide high spatiotemporal precision in several kinds of perturbation, including thermal [239], chemical [240], acoustic [241–243], geometric shape [244, 245], and RNAi [246, 247]. Mechanical interventions are mainly limited to smaller cellular systems [248, 249], and those that examine multicellular embryos have limited functionality [250, 251], especially in combining immobilization, alignment, and scalability [237, 252]. A microfluidic platform to perform all of these functions while mechanically compressing many embryos has been elusive [250]. The primary challenge is the variance in embryo size [253]. Consequently, embryo compression is performed by microaspiration [254], microindentation [255, 256], or moving a coverslip with a piezoelectric motor [65]. These methods can only process a few embryos at a time, and are labor intensive, requiring manual alignment, handling, processing, and calibration.

4.3 PROTEOMICS

When the Human Genome Project began in 1990, there was a sense that we were reaching the finish line in understanding human complexity [257]. Watson wrote, “It will explain, at the chemical level, the role of genetic factors in cancer, Alzheimer’s disease, and schizophrenia” [258]. Francis Collins predicted that within a decade we’ll have

individualized medicine [259]. There was also a healthy dose of human superiority: we would be the most complex creatures with the most genes, the apex of evolution, by orders of magnitude [260].

Reading the final publication, I sense some confusion at how much remains unexplained by “this relatively modest set of about 30,000 genes” [261]:

*“Between humans and chimpanzees, the gene number, gene structures
and functions, chromosomal and genomic organizations,
and cell types and neuroanatomies
are almost indistinguishable...*

*The number of genes or genome size
does not account for differences in complexity.”*

— J. Craig Venter *et al.*

Complexity is not in our genes, they conclude, but in regulation:

*“Rather, it is the interactions within and among these
that result in such great variation...
Now we know what we have to explain.”*

Genomics and transcriptomics have indeed transformed our understanding of the molecular basis of disease, including human heterogeneity [262, 263], developmental signaling pathway coordination [264, 265] and the discovery of non-coding genes [266, 267].

Yet genomic approaches are also fundamentally limited. Some of these limitations can be addressed by considering the more direct affectors of cell behavior: proteins. Proteins are critical because gene transcription correlates poorly with gene translation [268, 269]; transcripts encode multiple proteins through alternative splicing, and proteins exist in multiple isoforms through post-translational modification (PTM). The study of large-scale protein networks is called proteomics, and aims to bridge the gaps from transcriptomic approaches to understanding cell behavior.

The goals of proteomics as a field include identifying protein differences between healthy and diseased states in cells, tissues, and organisms. Protein differences can become targets of diagnostics and therapeutics. Specifically, protein differences predict complications in diabetes [270], heart disease [271], infectious disease [272], Parkinson’s disease [273], Alzheimer’s disease [274], and several cancers, such as colorectal [275], gastric [276], bladder [277], and prostate [278]. Protein differences are also used to screen for drug discovery and development [279, 280] with notable success in Alzheimer’s [274], alcohol dependence [281], sepsis [282], and disorders of the immune system [283].

DIGE

A powerful technique in proteomics is the separation of proteomes by isoelectric point through isoelectric focusing (IEF) and molecular weight through SDS-PAGE, together called two-dimensional electrophoresis (2DE). 2DE was first described by several groups simultaneously in 1975 for *E. coli* [284], guinea pig exocrine [285], and mouse tissue [286], foreshadowing the robustness of this technique. In 1988, isoelectric separation was improved with immobilized pH gradients [287]. Still, comparison between gels remained a challenge. Comparing spots was approached computationally, with limited success [288, 289].

Video S1:
Explanation of DIGE
through dance
<https://youtu.be/TvsvMFFBUYE>

In 1997, the Minden lab published a method of comparative 2DE called difference gel electrophoresis (DIGE) [290]. By labeling two samples with two fluorescent dyes, two proteomes can electrophorese together on the same gel, dramatically improving reproducibility. Shared proteins appear superimposed, while differences in abundance appear as a change in relative color. Since proteins remain intact throughout the detection process, DIGE allows the detection of specific changes in isoform, alternative splicing, and other PTM [290]. Differences in size or charge appear as vertical or horizontal separation. Co-electrophoresis is possible using a pair of cyanine dyes that are pH insensitive, have the same mass within 2 daltons, amine reactive, and maintain protein charge by replacing the positive charge of lysine [290, 291].

DIGE dynamic range and detection limits

DIGE detects 15% changes in abundance, responds linearly over a 10,000-fold concentration range, and is sensitive to 0.2 fmol of protein [290, 292]. By selectively masking high-abundance proteins, this range was increased to 1,000,000-fold with detection down to 10 picograms of protein [293]. Other improvements include increased protein retention by in-gel equilibration when transferring between first-dimension IEF and second-dimension SDS-PAGE [294, 295], and combination with immunoprecipitation [296, 297].

DIGE has been used to identify protein changes in many types of cells, tissues, and model organisms [291, 298], with notable results investigating prostate cancer [278], *Drosophila* VFF [64, 299], Wnt signaling [300], and microbiome-induced changes in fly behavior [301]. DIGE's properties create a unique opportunity for exploration of biological responses to mechanical forces at the proteomic level.

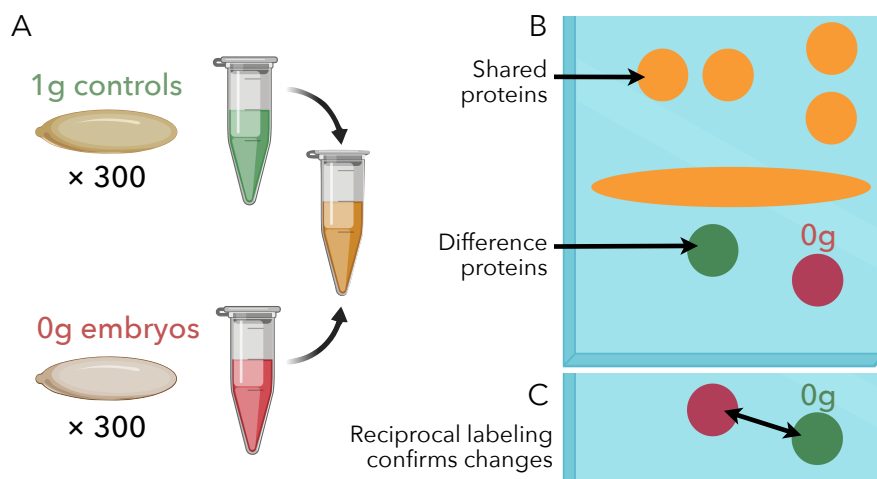


Figure 4.2: Overview of 2D-difference gel electrophoresis (DIGE). (A) Lysate from ≈ 300 *Drosophila* embryos is labeled with either Cy3 (green) or Cy5 (red) dye. (B) Proteomes are separated horizontally by isoelectric point, and then vertically by molecular weight. **Shared proteins** co-migrate and overlap in yellow. **Difference proteins** separate into red or green spots. In this example, the red spot on the right is enriched in 0g, and the green spot on the left is depleted in 0g compared to 1g controls. (C) Detail of the difference proteins under reciprocal labeling. A technical replicate swaps the labeling scheme to control for dye-dependent changes. The resulting swapped spots confirm that the right spot is enriched in 0g and the left spot is depleted in 0g compared to 1g controls. Representative gel in Fig. 7.2 with reciprocal changes in Fig. 7.3.

Part II

HIGH-THROUGHPUT MECHANOTRANSDUCTION IN *DROSOPHILA* EMBRYOS WITH MESOFLUIDICS

Developing embryos create complexity by expressing genes to coordinate movement, which generates mechanical force. An emerging theory is that mechanical force can also serve as an input signal to regulate developmental gene expression. Experimental methods to apply mechanical force to whole embryos have been limited, mainly to aspiration, indentation, or moving a coverslip; these approaches stimulate only a few embryos at a time and require manual alignment. A powerful approach for automation is microfluidic devices, which can precisely manipulate hundreds of samples. However, using microfluidics to apply mechanical intervention has been limited to small cellular systems, with fewer applications for larger scale whole embryos. We developed a mesofluidic device that applies the precision and automation of microfluidics to the *Drosophila* embryo: automatic alignment, immobilization, compression, imaging, and recovery of hundreds of live embryos. We then show using *twist:eGFP* embryos that the mechanical induction of *twist* depends on the dose and duration of compression. This device allows us to quantify responses to compression, map the distribution of ectopic *twist*, and measure embryo stiffness. For building mesofluidic devices, we use ultra-thick photolithography, derive an analytical model that predicts the deflection of sidewalls, and analyze parametric optimization. This “mesomechanics” approach combines the high-throughput automation and precision of microfluidics with the biological relevance of live embryos to examine mechanotransduction. These analytical models facilitate the design of future devices to process multicellular organisms such as larvae, organoids, and meso-scale tissue.

BACKGROUND

An emerging theory in embryonic development is that gene expression and mechanical force coordinate development in a reciprocal interplay [3, 4, 302]. It is well established that certain developmental genes generate mechanical forces that lead to tissue-specific morphogenetic movement. For example, in *Drosophila*, the transcription factor Twist controls a sequence of events that lead to the apical constriction of ventral cells, changing their shape from columnar to wedge, which collapses the ventral furrow inwards and initiates mesoderm invagination [57, 58]. The ventral furrow does not form properly in embryos mutant in *twist* [53].

Growing evidence suggests that exogenous mechanical force can be sufficient to directly activate certain genes [3, 41]. For example, although *twist* is normally expressed specifically in ventral cells of the *Drosophila* embryo, mechanical compression has been sufficient to trigger ectopic expression of *twist* [65]. The direct mechanical induction of *twist* has been observed by coverslip actuation with piezoelectrics [65], femtosecond laser pulses [303], magnetic tweezers [304], and needle indentation [67, 255]. The *Drosophila twist* pathway could be a powerful system to determine the mechanism of mechanotransduction, but these approaches are labor intensive, require manual alignment, and process only a few embryos at a time, precluding many biological assays.

One promising approach for manipulating hundreds of embryos simultaneously is microfluidics. Microfluidic approaches have led to semi-automated tools to sort [234], align [221, 235], immobilize [236, 237], image [238], and recover processed embryos with minimal intervention. In particular, fabrication using PDMS has many advantages: elasticity and high oxygen-permeability facilitate embryo manipulation, and low autofluorescence coupled with transparency in the visible spectrum enable high-resolution fluorescence microscopy. Microfluidic systems have provided spatiotemporal precision for many whole-embryo interventions, including thermal [239], chemical [240], acoustic [241–243], geometric shape [244, 245], and RNAi [246, 247]. Microfluidics could be a powerful approach to study mechanotransduction at scale, but mechanical interventions are mainly limited to smaller cellular systems [248, 249], and those that examine multicellular embryos have limited functionality [250, 251], especially in combining immobilization, alignment, and scalability [237, 252].

Here, we describe a mesofluidic device to apply the automation and precision of microfluidics to whole-embryo mechanotransduction (Fig. 5.1). This device can automatically align, immobilize, and compress hundreds of *Drosophila* embryos. It precisely applies a controlled uniaxial strain using pneumatically actuated flexible sidewalls. This flexibility compensates for the variation in size among embryos, creating a custom width that applies a consistent strain. Fabrication on a coverslip allows for live imaging during and after mechanical intervention, and embryos can be recovered for post-analysis. We describe a method for ultra-thick photolithography, derive an analytical model that predicts sidewall deflection, and discuss parametric optimization to construct future mesofluidic devices. We show this device maintains embryo development, does not induce anoxia, and can apply mechanical strain at a high-throughput scale with micrometer accuracy. Using this mesomechanics approach, we map and quantify the dose-dependent and time-dependent mechanical induction of *twist* during early *Drosophila* development.

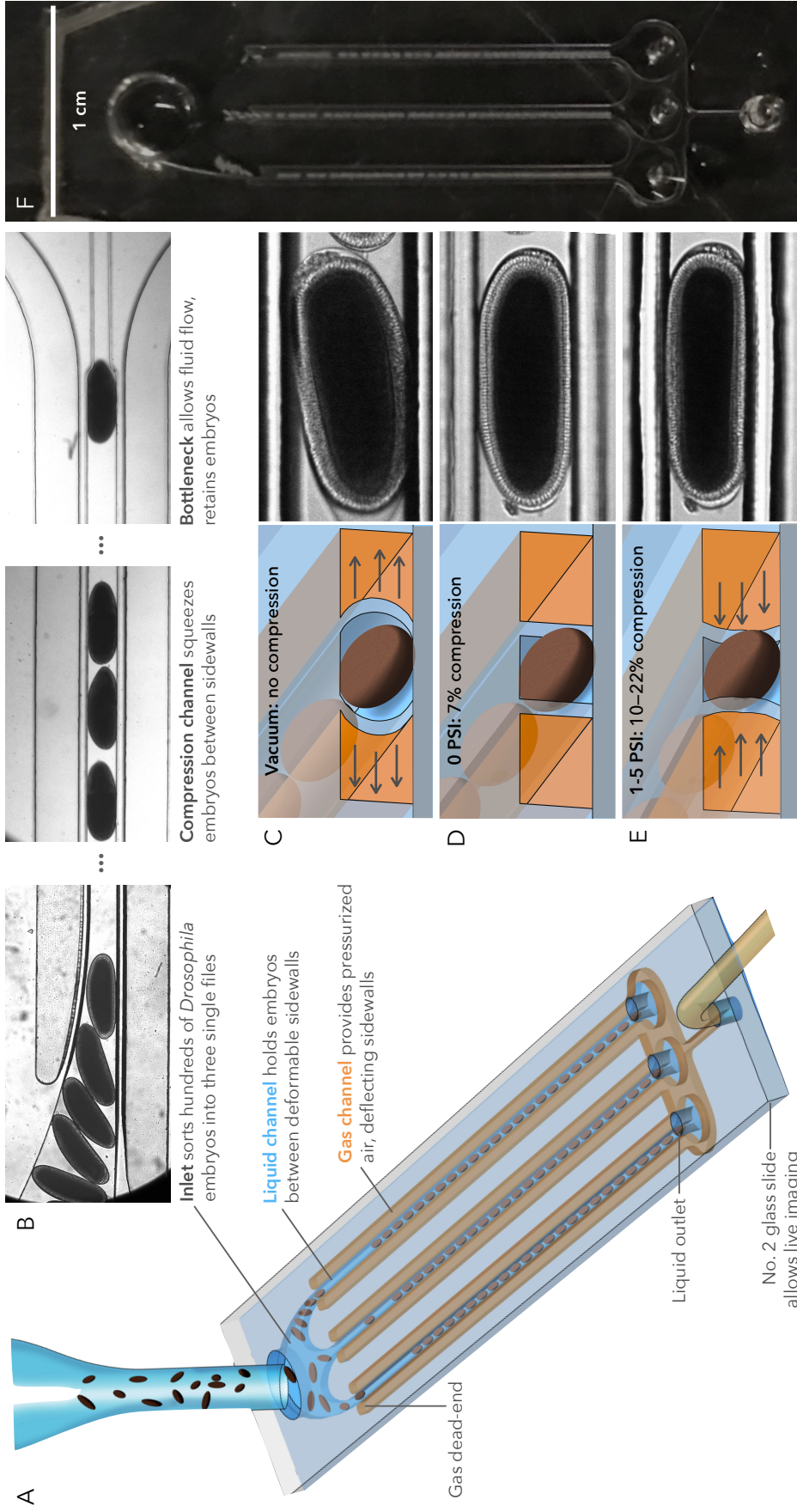


Figure 5.1: A mesofluidic device for high-throughput immobilization, imaging, compression, and recovery of *Drosophila* embryos. (A) Illustration of embryos loading into a mesofluidic device. PDMS channels form two interlaced systems: a liquid channel (blue) carries embryos suspended in buffer. A closed gas channel (orange) carries pressurized air. (B) Transmitted light micrographs of embryos in the channel. A narrowing inlet aligns embryos into a single file. The main portion of the channel compresses embryos between two deformable walls. Channels terminate in a bottleneck, allowing fluid flow while retaining embryos. (C-E) Illustrations and micrographs of sidewall deflection. (C) Under vacuum, channel walls expand to load embryos and as a control condition. (D) At rest, the channel is narrower than the embryo, providing immobilization and compression. (E) Pressurizing the surrounding chamber deflects the channel walls inwards, compressing the embryos further. (F) Photograph of the device with embryos.

METHODS

5.1 MESOFLUIDIC DEVICE FABRICATION

High aspect-ratio structures remain a fabrication challenge in microfluidic photolithography [305]. This challenge is exacerbated for continuous microscale features that cover a mesoscale footprint, such as PDMS sidewalls tens of μm thin, over 200 μm high, and 20,000 μm long. These thin, deep, and trench-like features lead to nonuniform developer exposure across the pattern, and small errors in geometry result in failure of fabrication. We fabricated devices using photolithography and PDMS replica molding (Fig. 5.2) [306] with adaptations for thick structures (film height $> 100 \mu\text{m}$) with high aspect ratio (A.R. > 5) features.

Pouring ultra-thick photoresist

Prior to spin coating, silicon wafers were cleaned with acetone, isopropyl alcohol (IPA), and deionized water, followed by a dehydration bake at 200 °C for 2 hours. Prior to pouring, ultra-thick photoresist (SU8-2100, MicroChem, MA, USA) was preheated to 60 °C to reduce the viscosity to cover the entire wafer. After the dehydration bake, the silicon wafer was transferred to a 60 °C hot plate. Preheated photoresist (PR) was poured slowly onto the silicon wafer to avoid bubble formation. The PR-coated wafer was covered and left on the hot plate for 5 minutes until the PR evenly coated the entire surface.

Spin coating

Excess PR was removed by a spin coater (WS-400B-6NPP/LITE, Laurell, USA). Pre-spin was at 250 revolutions per minute (RPM) for 30 sec, followed by 400 RPM for 15 sec (acceleration = 85 RPM/sec). PR hanging over the wafer edge was removed with an acetone-soaked cloth. Spin coating was at 500 RPM for 15 sec (85 RPM/sec) followed by 1,250 RPM for 30 sec (340 RPM/sec).

Acetone dispersion

Surface flaws are common after spin coating a thick layer of highly viscous PR. Surface flaws create uneven contact with the transparency

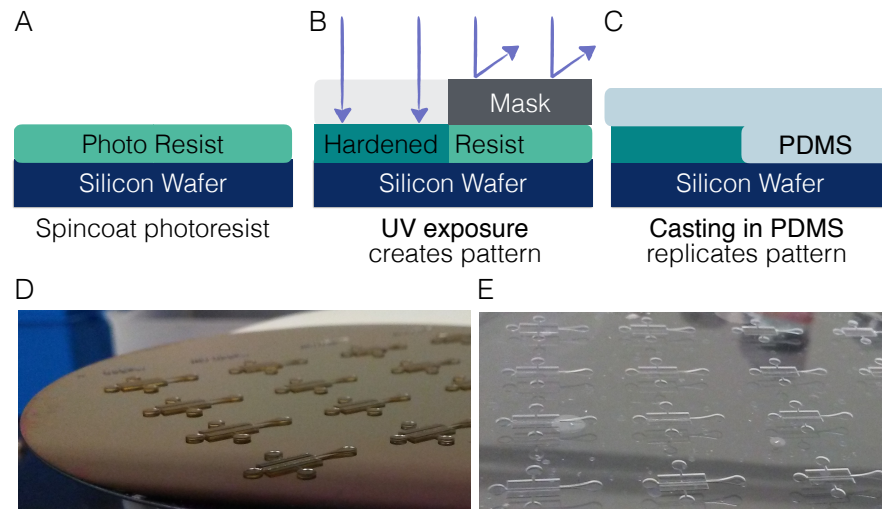


Figure 5.2: Overview of photolithography and PDMS replica molding. Photolithography is a method to write micron-scale patterns with light. (A) A light-sensitive photoresist is spun onto a silicon wafer to create an even layer. (B) A mask allows selective exposure to UV light, which selectively hardens photoresist. Unexposed photoresist is washed away. (C) The resulting negative template mold can be used hundreds of times to create PDMS microfluidic devices. (D) Photograph of Silicon wafer with negative template mold of an early version of the channel (E) Positive PDMS replica.

mask during exposure, creating inconsistent features, and small variations in height create large variations in deflection. To homogenize the PR layer, we sprayed acetone on the PR-coated wafer preheated to 50 °C on a leveled hotplate. The sprayed wafer was covered for about 15 minutes until the acetone evaporated. Acetone dispersion lowers the viscosity of PR, removes tiny bubbles and surface divots, increases the uniformity of the PR film, and eliminates the edge bead to provide even contact with the pattern mask. This provides the same benefits of overnight edge bead remover [307] in a few minutes.

Soft bake

The wafer was heated to 95 °C (3 °C/min) on a hot plate and baked for 60 minutes, followed by a slow cool down to room temperature.

Exposure

The wafer was exposed to 365 nm ultraviolet light (5 mW/cm²) for 75 seconds in mask aligner (MA65, Karl-Suss, Germany) through a 20,000 DPI (dots per inch) transparency mask (CADArt, CA, USA).

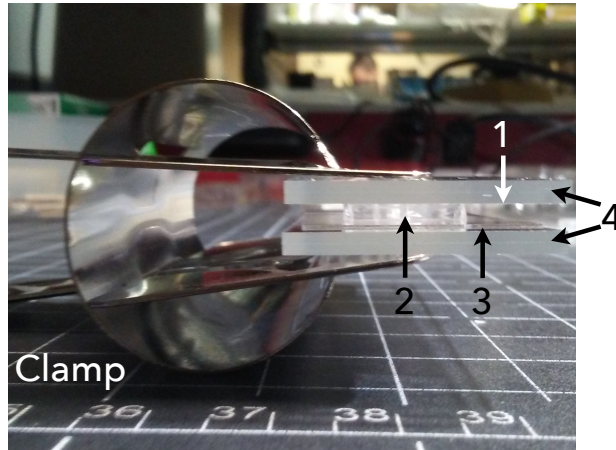


Figure 5.3: Post-bake setup for curing PDMS. Photograph of the mesofluidic device during post-bake. A polycarbonate sheet (1) was used to cover the PDMS-glass assembly (2, 3). The assembly was held between two thick glass slides (4) and clamped to ensure physical contact between PDMS and the coverslip throughout the curing process. Marks are cm.

Post-exposure bake

The exposed wafer was heated to 80 °C (3 °C/min) on a hot plate and baked for 20 minutes, followed by a slow cool down for 15 minutes. This longer post-exposure bake at a lower temperature reduces the thermal stress and risk of delamination for thick PR.

Development

The wafer was developed in SU-8 developer (MicroChem, MA, USA) for 20 minutes, then rinsed with fresh developer, IPA, and dried under nitrogen gas. The patterned wafer was coated with Tridecafluoro-1,1,2,2-tetrahydrooctyl-1-trichlorosilane (TFOCS T2492, United Chemical Technology, PA, USA) for 2 hours in a desiccator.

PDMS replica molding

Replica molding followed standard procedures [308]. Sylgard 184 PDMS (Dow Corning, Midland, Michigan, USA), was mixed with curing agent at a 10:1 mass ratio and degassed. Degassed PDMS was poured onto the silicon wafer mold and degassed again, then baked in a convection oven at 60 °C for 90 minutes. Cured PDMS was cooled, cut to size, and separated from the mold. Holes were punched for the embryo inlet (4 mm diameter biopsy punch, Integra Miltex, Pennsylvania, PSA), gas inlet (14G blunt needle), and liquid outlets (19G). The patterned sur-

face was cleaned with Scotch tape. The channel was covalently bonded to a 24 x 60 mm #2 coverglass (Warner Instruments, Cincinnati, USA) using oxygen plasma (Harrick Plasma Cleaner, 1 min, 18 W). The assembled device was sandwiched between two thick glass slides separated from the PDMS with thin polycarbonate film (McMaster-Carr, Illinois, USA). A binder clamp ensured physical contact throughout the PDMS-glass interface (Fig. 5.3). An optional post-bake increased the rigidity of PDMS sidewalls using a pre-heated oven at 150 °C (Isotemp Oven, Fischer Scientific, New Hampshire, USA).

5.2 ANIMALS

twist:eGFP flies (*w*[1118]; *Dr*[Mio]/*TM3*, *Pw*[+mC]=*GAL4-twi.G2.3*, *PUAS-2xEGFPAH2.3*, *Sb*[1] *Ser*[1]) were a gift from Emily Furbee, University of Pittsburgh. *Oregon-R* and *H2A-RFP*; *moeGFP/TM6Tb* flies were a gift from Brooke McCartney, Carnegie Mellon University. Flies were kept at room temperature in plastic bottles filled with standard *Drosophila* breeding medium. For embryo collection, flies were transferred to 100 mL tri-corner beakers and capped with 60 mm Petri dishes (Fisher Scientific, Pittsburgh, USA) partially filled with a solution containing 1.5% agarose, 2.5% sucrose, 25% apple juice, and 0.15% p-hydroxybenzoic acid methyl ester (methyl paraben to inhibit mold growth) and allowed to gel. A dab of yeast paste (1:2 parts dry yeast to water) was added to each plate. Embryos were collected for three hours, dechorionated for 90 seconds in fresh 50% bleach, washed with distilled water, collected with a cell strainer (Bellco glass), and suspended in egg wash (0.7% NaCl and 0.4% Triton-X 100 in distilled water, 0.2 μ m-filtered, light-protected). Embryos were selected under stereoscope to collect those at early cellularization (Stage 5, 2-3 hours after laying) [309] so compression would occur before gastrulation.

5.3 NUMERICAL SIMULATION

To predict the shape of the channel wrapping around an embryo, we constructed a 3D CAD model of thin PDMS sidewalls and an embryo in SolidWorks 2016 (Dassault Systèmes, Vélizy-Villacoublay, France), and modeled them in Abaqus (Dassault Systèmes, Vélizy-Villacoublay, France) as fully elastic and isotropic materials with quadratic tetrahedral elements. First, the elastic sidewall deflection was simulated without embryos. Parametric studies determined the Young's modulus of PDMS sidewalls based on experimental results. Then, *Drosophila* embryos were added to the simulation. A similar parametric study used the known Young's modulus of PDMS sidewalls to estimate the Young's modulus of *Drosophila* embryos. Simulations of embryo compression

proceeded in two steps. First, embryos received passive compression by a microchannel with a smaller width, which was simulated by displacing the wall towards the fixed embryo. In the second step, embryos received active compression, which was simulated by applying pressure to the deformable PDMS sidewall. Poisson's ratio for PDMS [310] and *Drosophila* was set to 0.4999 to avoid numerical divergence.

5.4 EXPERIMENTAL SETUP

Pneumatic connections were made with Tygon 3350 Silicone tubing with 1/32" inner diameter (Saint-Gobain, France) and fittings of the appropriate size. Consistent pressure was applied by outfitting a compressed air tank with a custom-made fine Bourdon tube pressure gauge with 0.1 pounds per square inch (PSI) resolution. Consistent vacuum was applied either by running water through a Venturi trap, or by using our in-house vacuum. Embryo wash solution was passed through 0.2 μm syringe filters to avoid clogging the microchannels. As a control for manipulation in the chamber, embryos were mounted on a coverslip glass fixed to the bottom of a plastic Petri dish. Embryos were adhered to the coverslip with a thin layer of glue prepared by dissolving the adhesive from double-sided Scotch tape in heptane. Adhered embryos were covered with a drop of halocarbon oil (series 700; Halocarbon Products, Hackensack, NJ). To apply 50% hypoxia (10% oxygen), the dish setup was placed into a stage-top environmental chamber (Live Cell; Pathology Devices, Westminster, MD) connected to an equal-pressure mixture of argon and air using a T-fitting. To apply anoxia, the dish setup was first evacuated for 10 minutes, then was placed into the environmental chamber connected only to argon.

5.5 IMAGE ACQUISITION AND PROCESSING

Images were acquired on a spinning disk confocal microscope (Nikon Eclipse Ti, running Andor iQ 3.5 software and fitted with an iXon X3 camera). 3D-image stacks were acquired with a 10x objective at 10 μm optical sections for a total depth of 200 μm . The liquid inlet of the mesofluidic device was sealed with a coverslip to prevent evaporation during extended imaging. Time-lapse DIC and fluorescent images were acquired with a 250 mW 488 nm laser with identical settings for power, exposure, and gain. Each time-lapse session comprised multi-position recordings of 60-120 embryos with 3D-image stacks captured every hour for 4 hours. The resulting hyperstacks were manually marked with an elliptical region of interest (ROI), and a custom macro recorded mean pixel values for each slice and frame in Fiji [311].

RESULTS & DISCUSSION

5.6 ANALYTICAL MODEL FOR WALL DEFLECTION

We developed an analytical model to describe the deflection of two sidewalls under pressure:

Assumptions

1. Fully elastic material
2. Isotropic material
3. Uniform pressure distribution
4. Fixed at both ends

Definitions

t = Thickness of the sidewall ($50 \times 10^{-6} \text{ m}$)

h = Height of the sidewall ($271.6 \times 10^{-6} \text{ m}$)

L = Length of the sidewall, i.e. width ($2 \times 10^{-2} \text{ m}$)

P = Pressure (5 PSI = 34473.8 N/m^2)

ω = Force per unit length (N/m)

$u(x)$ = Wall deflection (m)

E = Young's modulus (N/m^2)

I = Second moment of area (m^4)

For beams with rectangular cross-section, $I = \frac{L \cdot t^3}{12}$

ν = Poisson's ratio: $-\frac{d\epsilon_y}{d\epsilon_x}$, unitless. For PDMS [310], $\nu = 0.5$

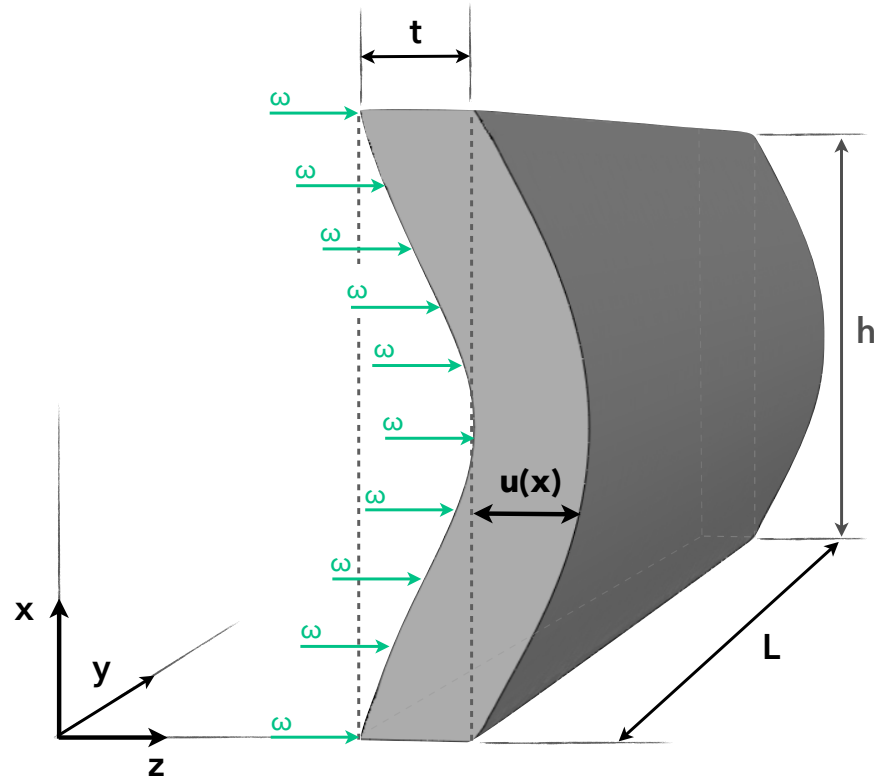


Figure 5.4: Schematic of deformable sidewalls as a uniformly loaded fixed-fixed beam. This nomenclature is somewhat counterintuitive because we're considering a sidewall as a beam. In a beam, the region between two fixed points is the length; in a sidewall, this x -dimension is the height. Likewise, the width of a beam corresponds to the length of the channel (y), and the thickness of a beam corresponds to the width of the channel (z).

Uniformly loaded fixed-fixed beams

The deflection of a beam of uniform thickness and loading fixed at both ends is described by the Euler-Bernoulli beam equation:

$$u(x) = \frac{\omega}{24EI} (x^4 - 2hx^3 + h^2x^2) \quad (5.1)$$

Shear deformation

If the aspect ratio of the sidewall (h/t) is less than 10, the contribution of shear deformation cannot be ignored. Timoshenko's beam theory [312] includes a secondary term for the contribution of shear deformation:

$$u(x) = \underbrace{\frac{\omega}{24EI} (x^4 - 2hx^3 + h^2x^2)}_{\text{Pure bending}} + \underbrace{\frac{\omega}{2\kappa GA} (hx - x^2)}_{\text{Contribution of shear}} \quad (5.2)$$

Where:

A = cross-section area of the beam ($t \times L$)

κ = shear coefficient

G = shear modulus

u_{max} at $x = h/2$ can be calculated with the following conversions:

$$\omega = P \cdot L$$

$$I = \frac{L \cdot t^3}{12} \quad \text{for rectangular cross-section}$$

$$\kappa = \frac{10(1 + \nu)}{12 + 11\nu} \quad \text{for rectangular cross-section [313]}$$

$$G = \frac{E}{2(1 + \nu)} \quad \text{assuming elastic and isotropic material}$$

Yielding:

$$u_{max} = \frac{Ph^4}{32Et^3} + \frac{Ph^2(12 + 11\nu)}{40Et} \quad (5.3)$$

$$u_{max} = \frac{Ph^4}{32Et^3} \cdot \left(1 + \frac{4t^2(12 + 11\nu)}{5h^2} \right) \quad (5.4)$$

Prevention of lateral deformation

Relatively wide beams behave more rigidly because they resist lateral deformation from fiber stresses [314]. This stiffening can be considered with a corrected term for the elastic modulus of the beam, which approaches $E/(1 - \nu^2)$ as width approaches infinity [315]. In our system, sidewalls are modeled as vertical beams (Fig. 5.4), so the beam width corresponds to microchannel length L , and the width-to-thickness ratio (L/t) is large. Therefore, the limit value is more accurate for approximating the effective elastic modulus [315, 316], yielding the final equation for deflection:

$$u_{max} = \frac{Ph^4(1 - \nu^2)}{\underbrace{32Et^3}_{\text{Bending}}} \cdot \left(1 + \frac{\underbrace{4t^2(12 + 11\nu)}_{\text{Shear}}}{5h^2} \right) \quad (5.5)$$

Extension to two deformable walls

There are two deformable walls on either side of the channel, which leads to the formula of the effective channel width as a function of the applied pressure:

$$W' = W - \frac{Ph^4(1 - \nu^2)}{16Et^3} \cdot \left(1 + \frac{4t^2(12 + 11\nu)}{5h^2} \right) \quad (5.6)$$

Where W is the initial channel width and W' is the effective channel width after applying pressure to deflect two sidewalls.

Experimental measurements

Based on experimental measurements of deflection, the channel width starts at $165 \mu\text{m}$, and decreases to $125.08 \mu\text{m}$ at 5 PSI. From this we calculate the Young's modulus of PDMS walls that were post-cured at 150°C for 2.5 hours to be 2.6 MPa.

5.7 DESIGN AND OPERATION OF THE MESOFLUIDIC DEVICE

Our mesofluidic device compresses hundreds of *Drosophila* embryos by aligning them between two walls and deflecting those walls with pressure (Fig. 5.1). The device consists of two interlaced compartments: a liquid compartment introduces and aligns embryos (Fig. 5.1A, B, 5.5).

A gas compartment uses microchannels with a closed end to create pneumatic actuation on either side of the liquid compartment, which controls the effective width of the liquid channels to load or compress embryos (Fig. 5.1E). This configuration was parallelized into three compression channels to triple the throughput of the system. When pressurization bends the sidewalls, it also creates a normal force on the roof of the gas channels, which pushes the thin sidewalls away from the glass slide, which can create leaks. To prevent such leaks, each parallel configuration was separated by a 1.5 mm region of PDMS which provides a large surface area of contact with the glass slide, functioning as a buttress (Fig. 5.5). The channels were constructed entirely from PDMS, which is optically transparent and oxygen-permeant [209]. The PDMS structure was bonded to a #2 coverglass, enabling high-resolution fluorescence microscopy.

Embryos were loaded into the device by pipetting them into the large inlet of the liquid compartment (Fig. 5.1A, supplementary video). A narrowing atrium aligned embryos into a single file (Fig. 5.1B, left). The section with deformable sidewalls was designed with a narrower width than the embryos (Fig. 5.7B), preventing embryo entry. When vacuum was applied, the PDMS sidewalls deflected outwards (Fig. 5.1C), increasing the effective width of the channels, allowing embryo entry. Tilting the device caused embryos to sediment into three parallel compression channels (Fig. 5.1F). Compression channels terminated in a bottleneck 90 μm wide (Fig. 5.1B), which allowed fluid flow while retaining embryos.

After the embryos were loaded into the compression channel, the vacuum was removed and the sidewalls recoiled, immobilizing the embryos due to PDMS elasticity (Fig. 5.1D). Higher compression was achieved by applying pressure to the gas compartment, which deformed the sidewalls inwards (Fig. 5.1E). Therefore, this system operates in two modes: without external pressure (0 PSI), for immobilization and mild passive compression, and with external pressure (1-5 PSI), to apply an active compressive strain. For post-analysis, embryos were recovered by opening the sidewalls under vacuum, tilting the channel, and collecting embryos from the inlet. Each mesofluidic device accommodated up to 120 embryos in a single run: compression channels were 20 mm long, *Drosophila* embryos were $\approx 500 \mu\text{m}$ long, and the device operated three channels in parallel. For larger sample size, we developed 40 mm channels that can accommodate 240 embryos (Fig. 5.5C).

5.8 DESIGN OPTIMIZATION

Compression can be precisely regulated by optimizing five parameters: the width and height of the compression channel, the thickness

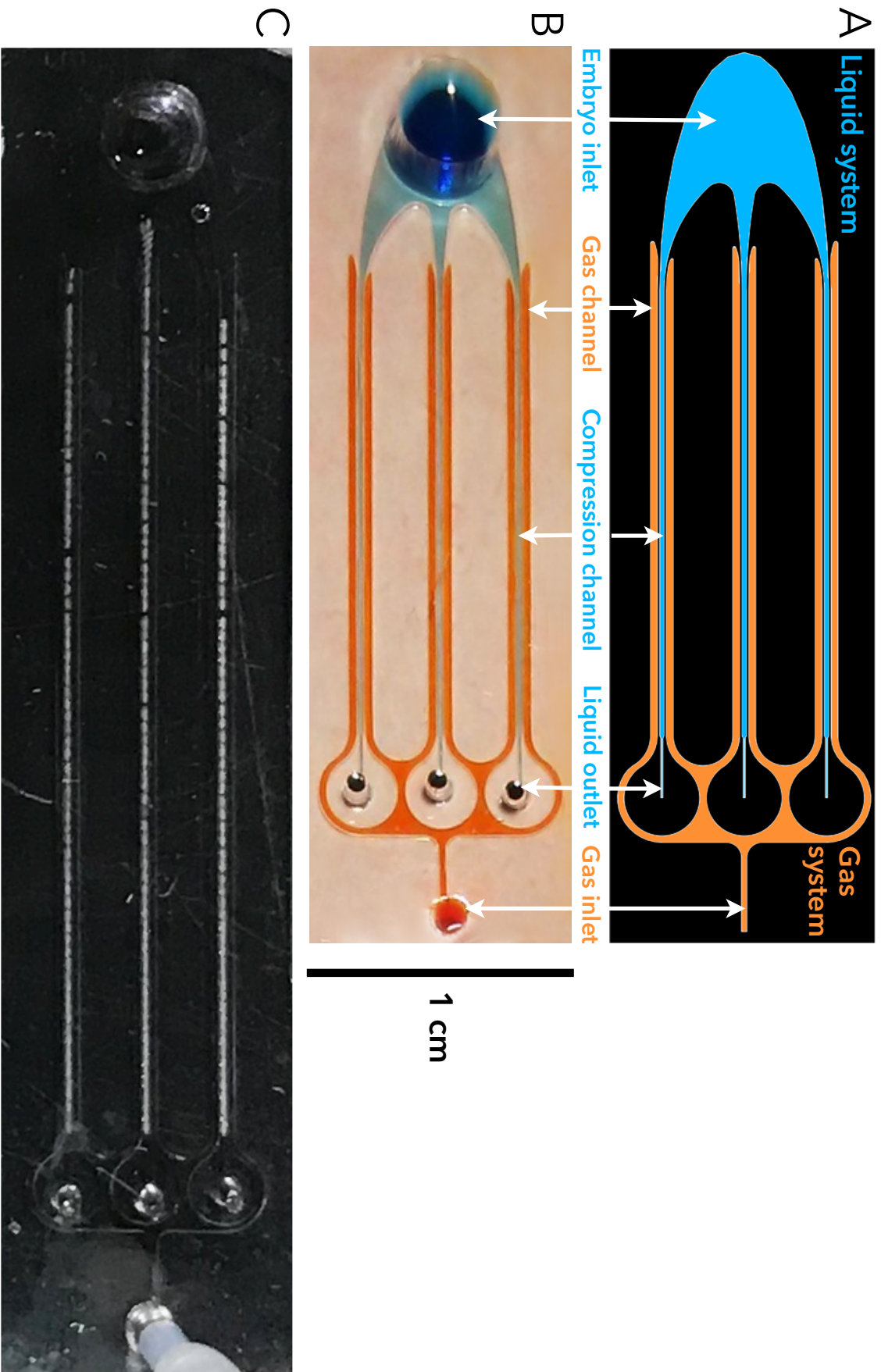


Figure 5.5: Photographs and schematic of mesofluidic PDMS compression channels. (A) Photolithography schematic shows two interlaced microfluidic systems: an open liquid system (blue) carries embryos suspended in buffer. A closed gas system (orange) carries pressurized atmospheric air. (B) Photograph of mesofluidic channel with both systems filled with dye. (C) Photograph of *Drosophila* embryos inside a longer channel.

and the rigidity of the deformable sidewalls, and the applied pressure (Fig. 5.7A). The final design optimized for *Drosophila* compression had a channel width of $165\ \mu\text{m}$ (Fig. 5.7B), channel height of $251.8\ \mu\text{m}$ (Fig. 5.7C, 5.9A), wall thickness of $50\ \mu\text{m}$ (Fig. 5.7D, E, 5.8), and a post-bake of 2.5 hours (Fig. 5.7F, G, 5.10). This resulted in a compression that could be tuned between 0–22% (Fig. 5.7H, Table 5.6) with a standard deviation less than 2.4% (Fig. 5.14, Table 5.4). Omitting the post-bake, the channel applies $< 1\%$ compression at 0 PSI to immobilize samples for timelapse imaging (Fig. 5.7G).

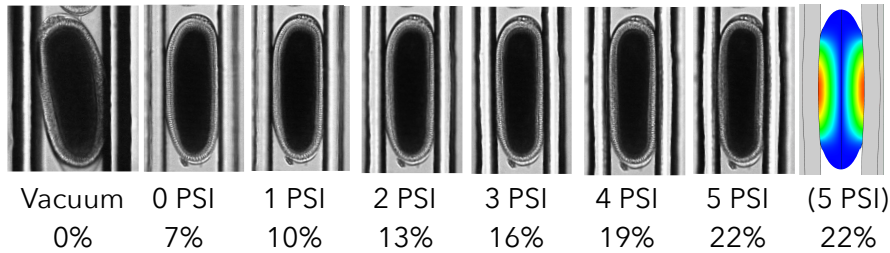


Figure 5.6: DIC micrographs of compressed embryos in the optimized device. Simulated embryo compression matches experimental results.

Channel width

We want a compression channel that is narrower than the embryo width to immobilize them passively. However, the channel must also be wide enough under vacuum to allow the biggest embryo to enter without clogging the channel. We measured the width of 140 Stage-5 Oregon-R embryos and found a normal distribution with a mean of $179.6 \pm 1\ \mu\text{m}$ (95% confidence interval, $\sigma = 6\ \mu\text{m}$, SEM = $0.5\ \mu\text{m}$, max = $194.7\ \mu\text{m}$, Fig. 5.7B). Based on this distribution, a channel width of $165\ \mu\text{m}$ can immobilize $> 99\%$ of embryos passively. When vacuum is applied, the sidewalls deflected outwards to create an effective width of about $205\ \mu\text{m}$, allowing the widest embryo to enter (Fig. 5.7B).

Applied pressure

Pressure is limited by the bond strength between the thin PDMS sidewalls and the glass slide. Any point-sized separation across any 20 mm sidewall causes a leak and failure of the entire channel. Although high pressure increases sample compression range, we found that increasing the pressure past 5 PSI led to unreliable function, and therefore used 5 PSI as an upper limit throughout this study.

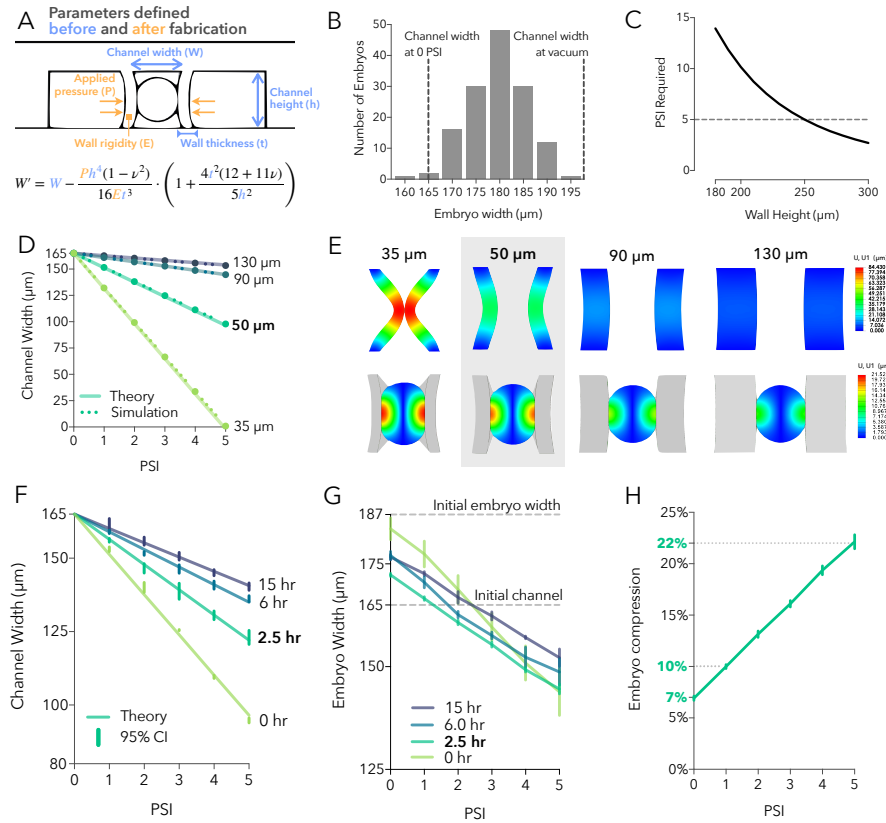


Figure 5.7: Optimization of five parameters for a mesofluidic device. (A) Overview: The effective width of a channel under pressure (W') is described by equation 5.5 with five parameters. Three were defined before fabrication (blue) and two were determined afterwards (orange). The goal was to maximize compression while limiting pressure to 5 PSI for reliable function. **(B) Initial channel width** was determined by measuring the width distribution of stage-5 Oregon R embryos ($N=140$). A channel width of $165\ \mu\text{m}$ immobilizes $> 99\%$ of embryos at rest (0 PSI) while expanding under vacuum to accommodate the widest embryo. **(C) Channel height:** Theoretical prediction of PSI required to sufficiently deflect a wall of varying height. Height was maximized at $250\ \mu\text{m}$ to enable compression at 5 PSI. Wall height has the greatest influence over deflection, as indicated by the polynomial degree of the governing equation. **(D) Wall thickness:** Deflection under pressure was calculated theoretically (solid line) and by numerical simulation (dotted line). Simulation shows $< 5\%$ difference from analytical equation (Table 5.1). **(E)** Simulated deflection of sidewalls at 5 PSI in a range of thickness with and without embryos (side view cross-section). $50\ \mu\text{m}$ walls (shaded) were selected for the greatest range of compression with the least wrapping around the embryo. **(F) Wall rigidity:** Longer post-cure baking results in stiffer walls (higher Young's Modulus) that deflect less under pressure. Continuous theoretical results with the discrete experimental measurements from 1 PSI increments (95% CI bars). **(G)** Embryo width between walls with a range of rigidity (95% CI bars). 2.5 hours post-cure bake showed the best optimization of compression. **(H) Uniaxial compressive strain** (normalized change in embryo width) in the final channel after design optimization (95% CI bars).

Channel height

A key challenge in adapting microfluidics to mesomechanics is maximizing height, which has the strongest influence over deflection (Eq. 5.5). Maximizing height creates a fabrication challenge in photolithography because the maximum aspect ratio (AR) is limited due to diffraction [317], absorption of light [318], chemical diffusion of cross-linking agents [319], which deform the final geometry and increase the risk of photoresist delaminating from the silicon wafer during curing [320]. Height must be at least greater than the largest embryo ($195\ \mu\text{m}$) to prevent clogging, with some additional allowance for vertical expansion during lateral compression. Height must be at least $250\ \mu\text{m}$ to reasonably deflect at 5 PSI, based on theoretical calculations to displace a $50\ \mu\text{m}$ PDMS wall by $15\ \mu\text{m}$ (Fig. 5.7C). Based on this target height, we used the methods described to fabricate SU-8 molds with an average height of $251.8\ \mu\text{m}$ with uniformity $> 95\%$ (Fig. 5.9A) as measured by Zygo NewView 7200 3D Optical Surface Profiler (Zygo Corporation, Middlefield, Connecticut, USA).

Wall thickness

To maximize deflection under limited pressure, we also want to minimize wall thickness, which has an inverse-cube influence over deflection (Eq. 5.5). However, reducing wall thickness reduces their surface area contact with the glass slide, which increases the chance of leaking under pressure. To optimize wall thickness, we used finite element analysis to simulate the deflection of PDMS sidewalls of 35, 50, 90, and $130\ \mu\text{m}$ thickness from 0 to 5 PSI, first by themselves and then around an embryo (Fig. 5.7E, 5.8). Simulation results were compared to analytical predictions from Eq. 5.5 (Fig. 5.7D). Although maximal displacement occurred with $35\ \mu\text{m}$ side walls, such thin walls wrap around the embryo (Fig. 5.9C, 5.8), which decreased the surface area exposed to media and could increase the risk of hypoxia. Additionally, these high aspect ratio (h/t) sidewalls create significant difficulty in fabrication for a modest gain in displacement. Walls 90 and $130\ \mu\text{m}$ thick are too stiff to provide adequate compression range (Fig. 5.7E, 5.8, Table 5.1) so we chose $50\ \mu\text{m}$ for the thickness of the deformable sidewalls. At 5 PSI, $50\ \mu\text{m}$ walls decrease the effective width of the channel by 57%, creating a 22.4% compressive strain on embryos. Over 0-5 PSI, this provides a large dynamic range of embryo compression (Fig. 5.7H, Table 5.6) within a tractable aspect ratio for fabrication.

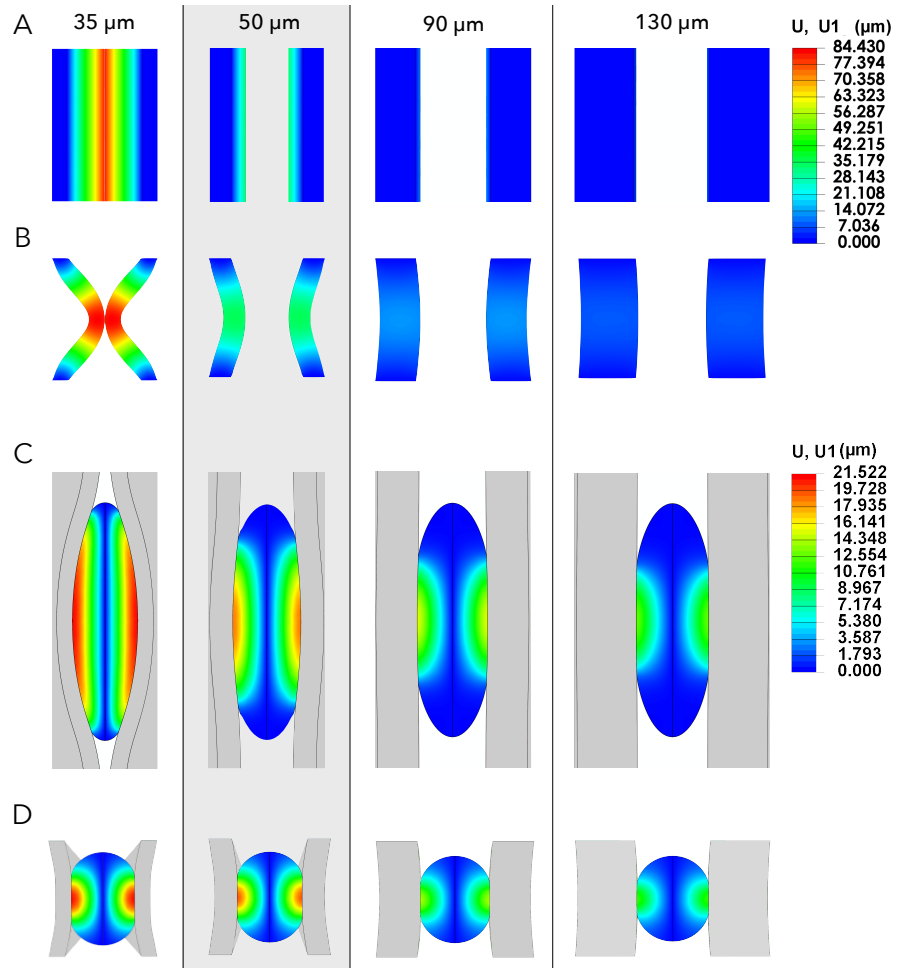


Figure 5.8: Simulation results of uniaxial node displacement at 5 PSI with variable wall thickness. (A, B) Empty channel, top view and side section. 35 μm walls close completely. (C, D) Channel with embryo, top view and side section. 35 μm walls showed heavy wrapping around the embryo, while 90 μm walls showed low displacement resulting in low compression. 50 μm walls (shaded) were selected.

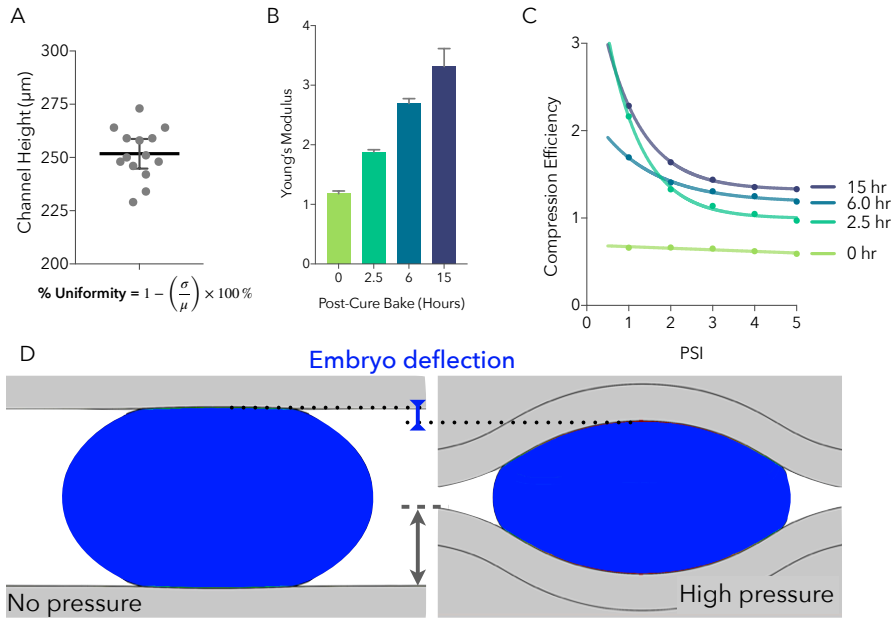


Figure 5.9: Mesofluidic optimization, continued. (A) Profilometry measurements of channel height show a mean of $251.8 \mu\text{m}$ with uniformity $> 95\%$. (B) Young's modulus of $50 \mu\text{m}$ sidewalls with differential post-cure baking. Deflection was measured at 10 points and calculated by Eq. 5.6. SEM bars. (C) Plot of compression efficiency over 5 PSI for channels with a range of post-bake durations. In the no-bake condition (0 hours), sidewalls are deflected with minimal embryo compression. As the rigidity of the walls increases, compression efficiency increases. Simulation results in Fig. 5.10. (D) Illustration of compression efficiency, the ratio of embryo deflection to wall deflection. This quantifies a deformable wall's tendency to compress instead of wrap.

WALL THICKNESS (μM):	130	90	50	35
Young's Modulus (MPa):	1.18	1.18	1.18	1.18
Aspect Ratio:	1.94	2.80	5.04	7.19
Embryo strain:	13.1%	15.9%	22.4%	23.9%
Simulation error:	10.6%	4.2%	0.3%	3.3%

Table 5.1: Simulated embryo strain at 5 PSI with varying wall thickness

Sidewall rigidity

Embryo compression requires optimizing wall rigidity. Rigid walls deflect less under pressure, but compress the embryo to a greater extent of that deflection. Conversely, soft walls deflect more, but are less compressive, instead wrapping around the embryo (Fig. 5.8). To optimize rigidity for the greatest dynamic range of compression, we added an oven bake after plasma-bond for 0, 2.5, 6, or 15 hours at 150 °C to increase the rigidity (Young's modulus) of the crosslinked PDMS (Fig. 5.9, 5.10) [321]. Deflection of differentially baked channels were simulated numerically (Fig. 5.10) and measured experimentally (Fig. 5.7F, G). As expected, longer baking time resulted in walls with an increased Young's modulus (Fig. 5.9B) that deflected less under pressure (Fig. 5.7F).

To quantify sidewall wrapping, we calculated the ratio of embryo deflection to wall deflection, which we call "compression efficiency" (Fig. 5.9D). Rigid walls have higher compression efficiency, but lower compression overall because of the decreased wall displacement. The 2.5 hour bake showed the greatest linear range of compression from 7% up to 22% at 5 PSI (Fig. 5.7H, Table 5.2).

BAKING TIME (HOURS):	0	2.5	6	15
Young's Modulus (MPa):	1.18	1.88	2.69	3.32
Aspect ratio:	5.04	5.04	5.04	5.04
Embryo strain:	22.4%	22.0%	17.4%	15.5%
Simulation Error:	0.3%	0.2%	0.2%	0.2%

Table 5.2: Experimental embryo strain at 5 PSI with varying rigidity

5.9 DETERMINING YOUNG'S MODULUS OF PDMS AND DROSOPHILA

The Young's modulus of cross-linked PDMS is highly variable, ranging 3 kPa to 3.7 MPa [322] depending on curing agent ratio, curing temperature, duration, size [323], and age [324]. The analytical model was

used to estimate the Young's modulus of PDMS to be 1.88 MPa, comparable to values reported elsewhere [321]. Simulations of embryo compression determined the Young's Modulus of *Drosophila* embryos to be 160 kPa, comparable to results from alternative approaches [325]. To determine simulation error, the experimentally observed deflection was used to calculate Young's modulus (Eq. 5.6) which was then used to run a simulation of deflection. The resulting simulated displacement was compared to the experimentally observed displacement. This process showed the simulation and analytical model to describe deflection within 0.3% across all rigidities (Table 5.2).

5.10 EMBRYO DEVELOPMENT

To test whether PDMS channels and compression affect viability, Oregon-R embryos were compressed by 7% or 22% for either 10 minutes (n = 34, 64 respectively) or 4 hours (n = 38, 100, Fig. 5.11). As a control for compression, embryos were loaded into the PDMS channel and never compressed; the walls were held open under vacuum ("vacuum control," n=68). As a control for exposure to the device, embryos were cultured in a glass dish (n=111). Embryos were recovered from the device to glass dishes and observed under a brightfield stereoscope at 24 and 48 hours, and staged as first-instar larvae, dead, or developing.

Vacuum controls showed no developmental difference from dish controls, with 75% reaching larval stage by 48 hours (Fig. 5.11B vs A) suggesting that exposure to PDMS channels alone does not affect development or survival. Surprisingly, 7% compression for 10 minutes and 4 hours showed greater survival rates compared to controls (> 90%, Fig. 5.11C, E vs A, B). One explanation is that the stiff chorion membrane mechanically constrains *Drosophila* embryos, and the standard practice of removing it decreases survival, which is recovered by mild compression. Embryos compressed by 22% for 10 minutes initially showed developmental delay at 24 hours, but ultimately reached first instar by 48 hours at rates greater than controls (Fig. 5.11D vs A). Extending 22% compression to 4 hours reduced survival to 37%; embryos that appeared alive and delayed at 24 hours did not recover (Fig. 5.11F).

To examine early development in greater detail, we took differential interference contrast microscopy (DIC) images of embryos in the channel every hour for 4 hours (Fig. 5.12). Embryos are observed at Stage 5 inside the channel (top row). Embryos compressed by 7% appear to proceed through germ-band extension, similar to uncompressed embryos. A minority of embryos compressed by 22% for 4 hours appeared to show no movement for one hour, but then proceeded through germ-band extension (Fig. 5.12E). These results contradict Farge's reports of a ventralized phenotype that fails to extend the germ band after com-

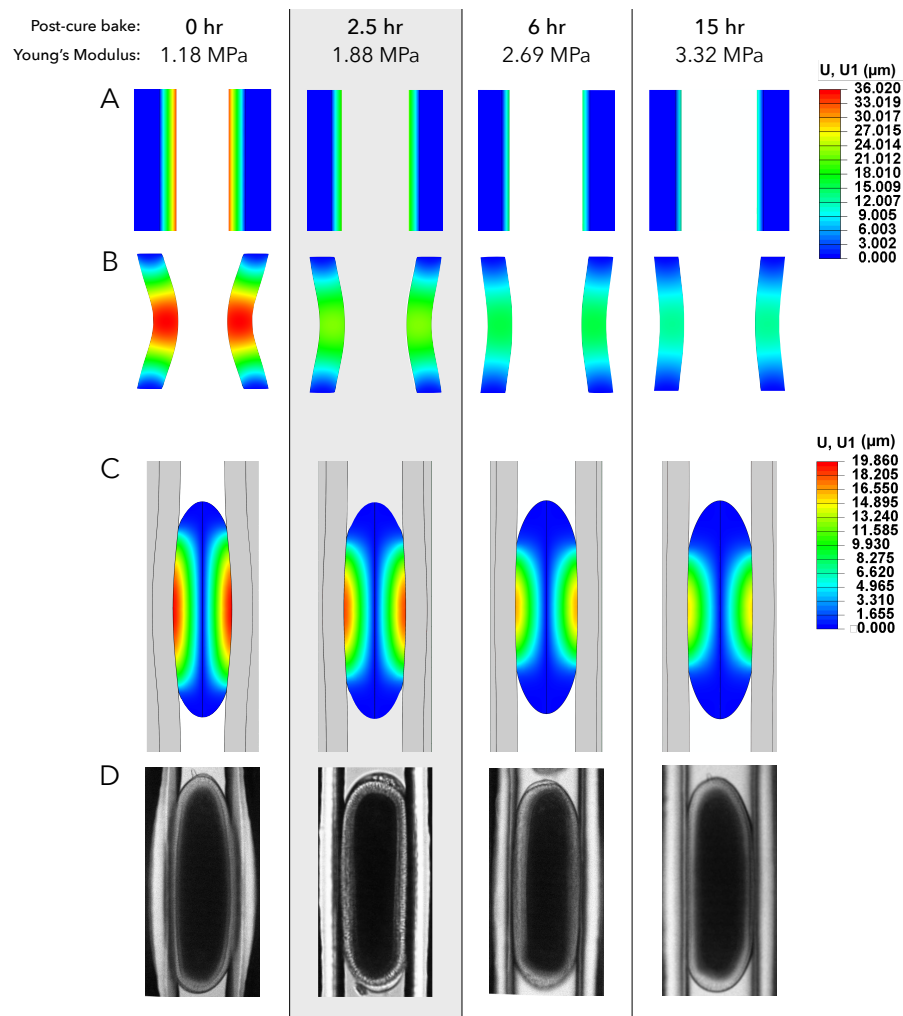


Figure 5.10: Simulation results and micrographs of embryo compression at 5 PSI with variable wall rigidity. $50\ \mu\text{m}$ thick walls were given a range of Young's modulus as a result of variable post-bake curing times (Fig 5.9B). (A, B) Empty channel, top view and side section. (C) Channel with embryo, top view (side section in Fig. 5.7E). Less rigid walls showed greater wrapping around the embryo. (D) Micrographs from experimental results. 2.5 hour post-cure bake (shaded) was selected.

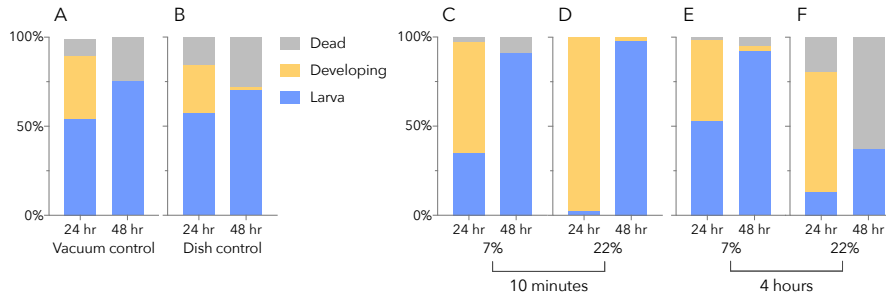


Figure 5.11: Survival in the channel. Percentage of wildtype embryos that reached first instar larva (blue), were still developing (yellow), or dead (grey), 24 and 48 hours after compression. Vacuum controls were loaded into the channel but never compressed. Embryos compressed at 7% showed greater survival rates than controls. Embryos compressed at 22% for 10 minutes show developmental delays; 22% compression for 4 hours led to low survival.

pression [65]. This difference in developmental milestones could be from several factors: (1) Farge observed embryos up to 50 minutes and concluded the phenotype was stable; observing over 4 hours shows recovery is possible (Fig. 5.12E); (2) There might be effects from the differences in genetic background in fly stocks used in these experiments; (3) There might be effects that stem from different methods of compression that result in variations in strain magnitude and consistency.

Comparison of compression methods

To compare our compression approaches in greater detail, we simulated the approach of Farge 2003 [65]. Two major differences in Farge’s approach are that (1) compression was applied vertically and observed indirectly by 10% lateral expansion, orthogonal to the direction of movement; (2) compression was applied by rigid glass. We simulated embryo deformation by a rigid plate sufficient to create a 10% lateral expansion (Fig. 5.13). The resulting compression was 25–34% (Table 5.3). Lateral expansion corresponds to larger uniaxial compression because shape change begins vertically; height decreases substantially before significant lateral expansion occurs. This larger compression may explain observed differences in developmental arrest.

Based on numerical simulations, compression by glass is more variable than compression by PDMS (Fig. 5.14). When compressed by a rigid substrate, the channel width is fixed, so wider embryos are compressed more (Fig. 5.14A). In contrast, PDMS sidewalls are flexible, so wider embryos resist wall displacement, creating a wider effective channel width unique to each embryo (Fig. 5.14B). As a result, despite the variation in embryo width, the compressive strain remains similar under flexible PDMS walls. This variation can be quantified by simulating com-

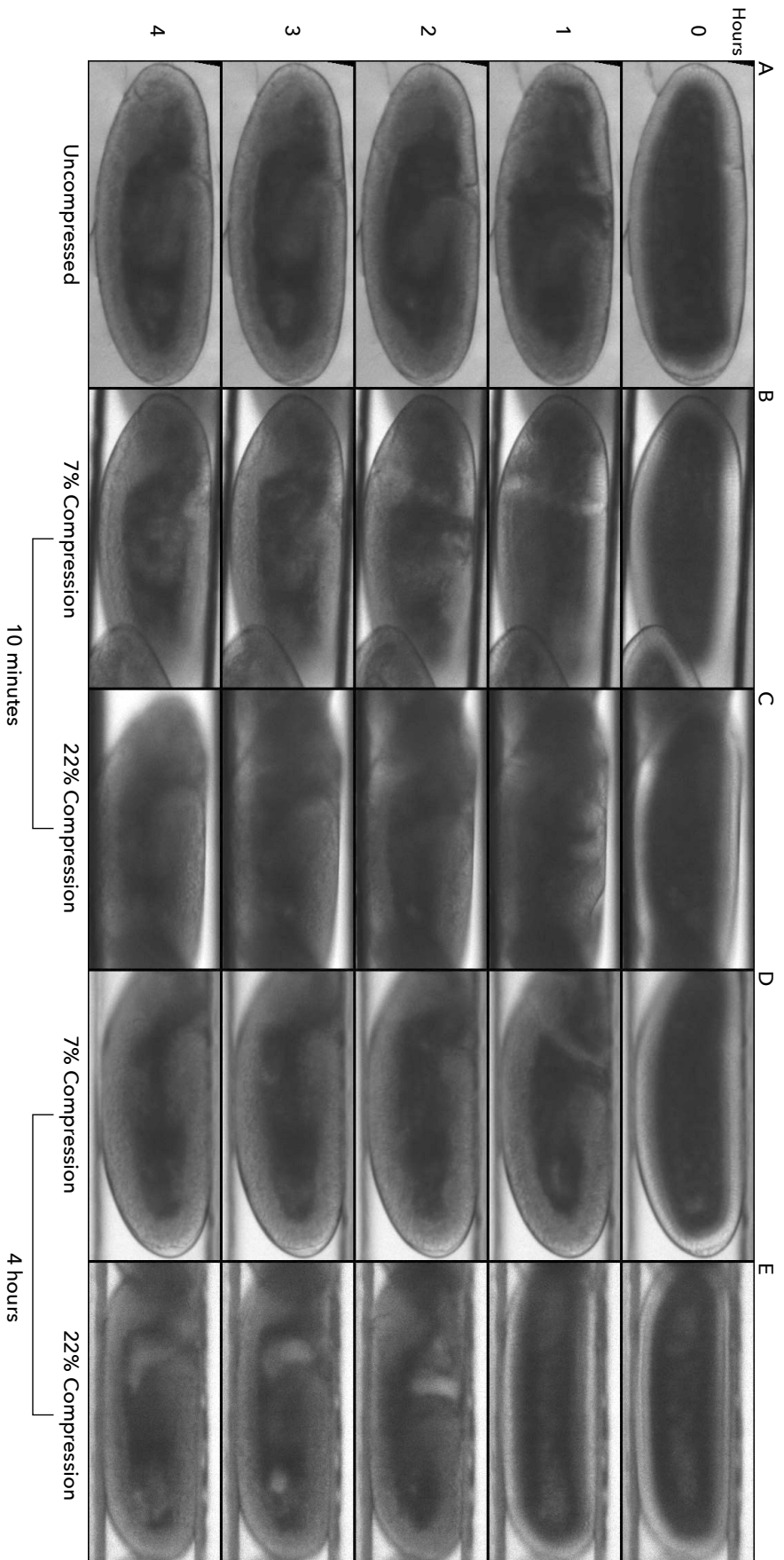


Figure 5-12: Timelapse of embryos inside the channel. DIC images taken every hour for four hours. (A) Uncompressed embryo proceeds through germ-band extension. (B–D) Compressed embryos proceed through morphological movement with some delay. (E) Some embryos compressed by 22% for 4 hours showed significant delay for 1 hour, then proceeded through germ-band extension.

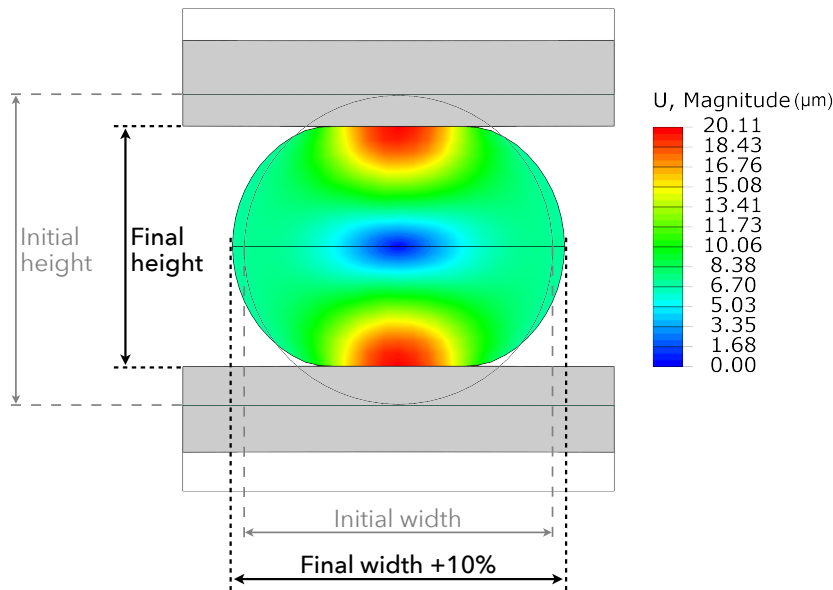


Figure 5.13: Simulation results of embryo compression between two rigid walls such that lateral expansion is 10%. Before width expands, height decreases (red). As a result, the inferred compression is substantially larger than 10% (Table 5.3).

EMBRYO WIDTH	COMPRESSION
195 μm	25.2%
180 μm	27.5%
160 μm	34.1%
STD	4.6
CoV	16.0%

Table 5.3: Inference of uniaxial compression by 10% lateral shape change

pression of embryos with mean width (180 μm), maximum width (195 μm) and minimum width (160 μm) in the same channel. Under glass, embryos are compressed with a 39% Coefficient of Variation (CoV) (Table 5.4). Compression inferred by 10% lateral shape change resulted in 16% CoV (Table 5.3). Compression by PDMS was the most consistent at 11% CoV (Table 5.4).

CoV is standard deviation as a percentage of the mean: $\frac{\sigma}{\mu} \times 100\%$

Overall, the channel itself neither delays nor destroys *Drosophila* embryos. Compression appears to switch from beneficial to harmful above a threshold of magnitude and time. These extended observations highlight the importance of long-term analysis, as developmental outcomes can drastically diverge days after mechanostimulation. Flexible PDMS sidewalls apply compression that is more consistent and directly measurable, which helps compare results across multiple studies.

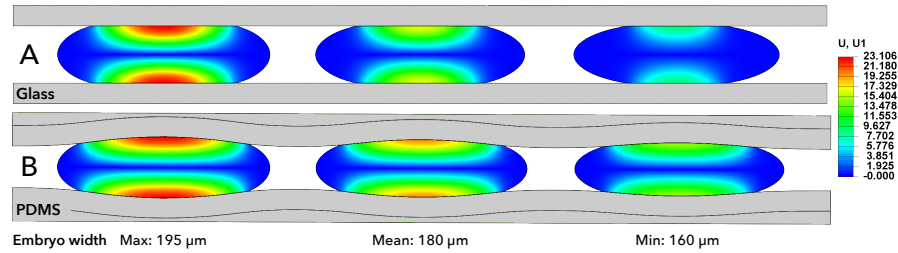


Figure 5.14: Flexible walls are more consistent than rigid glass when compressing a distribution of widths. Simulation of embryos of maximum, median, and minimum width at Stage 5. (A) When compressed by rigid glass, the channel width is consistent, applying more compression to wider embryos. (B) When compressed by flexible PDMS, the channel width is unique to each embryo, which resists deformation as a function of width. This results in a more consistent compression.

EMBRYO WIDTH	PDMS	GLASS
195 μm	23.7%	28.1%
180 μm	22.2%	22.2%
160 μm	19.1%	12.4%
STD	2.4	7.9
CoV	11.0%	38.9%

Table 5.4: Consistency of uniaxial compression methods. Compression of max, mean, and min embryo widths by PDMS at 5 PSI and simulation of compression by rigid glass such that the mean compression is the same.

Anoxia

To examine whether developmental delay at 5 PSI was due to compression or could be explained by side-effects of confinement, we tested embryos for anoxia (Fig. 5.15). Anoxia produces a rapid developmental arrest during which interphase chromosomes prematurely condense [326]. A convenient way to visualize this process is by histone H2A fused to RFP (H2A-RFP). Anoxia was induced by placing H2A-RFP embryos under vacuum for 10 minutes, then under a continuous flow of argon in a stage-top environmental chamber. As expected, anoxic embryos showed developmental arrest and chromatin condensation; no change in nuclear position indicated that development had ceased (Fig. 5.15A and c). In contrast, embryos in the PDMS compression chamber showed typical nuclear division cycles with normal chromatin condensation, mitosis, and decondensation (Fig. 5.15B). Large-scale morphogenetic movements occurred even in 22% compression when argon was used for pneumatic actuation (Fig. 5.15D). These results suggest that responses to compression cannot be explained by anoxia.

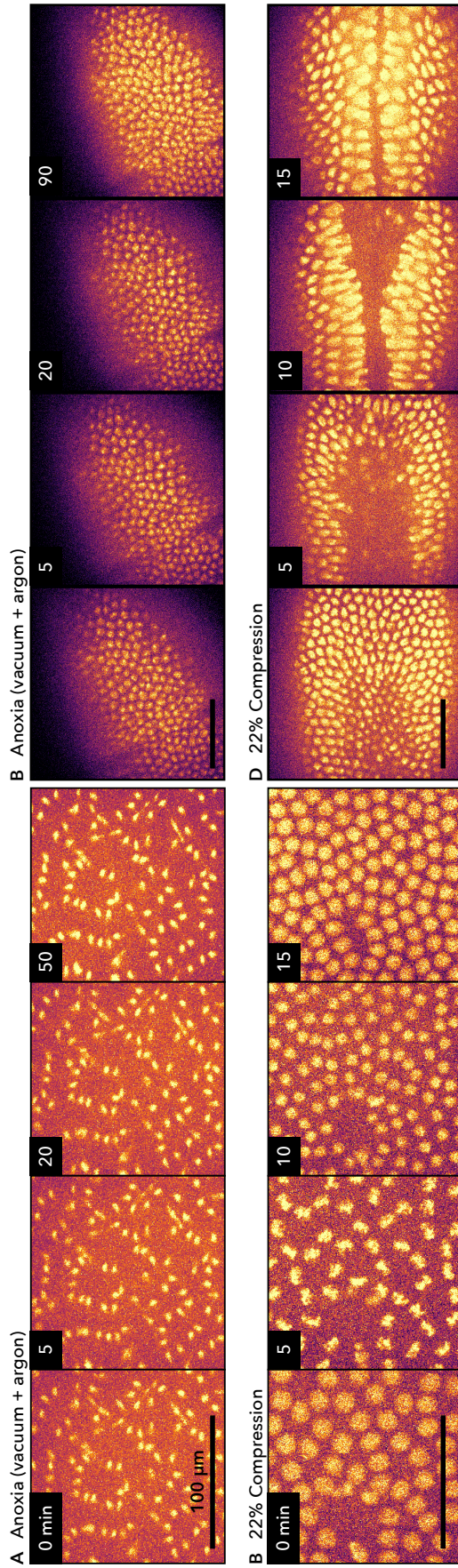


Figure 5.15: Channel compression does not induce anoxic arrest. Anoxia-induced developmental arrest can be visualized by chromatin condensation, seen in embryos expressing HzA-RFP (color by Matplotlib inferno LUT, all scale bars 100 μm). (A) Embryos kept anoxic by 10 minutes of vacuum followed by continuous argon show morphogenic freezing. An embryo in anaphase stays arrested for over 50 minutes. (B) Embryos under 22% compression pass through anaphase normally, doubling nuclei over 10 minutes. (C) Anoxic embryos show chromatin condensation, visible as puncta that remain stable over 90 minutes in nuclei that fail to divide. (D) 22% compressed embryos continue to coordinate morphogenetic movement such as ventral furrow formation (VFF).

5.11 MECHANICAL INDUCTION OF *TWIST*

Mechanical induction of *twist* was first described by Farge 2003 [65]. To examine whether mesofluidic compression also induces *twist* expression, we monitored fluorescence from the *twist* promoter driving enhanced green fluorescent protein (eGFP) every hour for 4 hours (Fig. 5.16). In unconstrained embryos, *twist:eGFP* localized to a stripe of ventral furrow cells, indicating normal expression (Fig. 5.16A). Constrained embryos showed widespread expression that was brighter and ectopic (Fig. 5.16B–E). This is consistent with the hypothesis that *twist* expression is coordinated by mechanical force – during normal development, *twist* is selectively expressed in ventral furrow cells that experience internal mechanical forces due to morphogenetic movement. When the entire embryo is compressed, the whole organism experiences mechanical force, which is sufficient to induce ectopic expression of *twist*.

To quantify the increase in *twist:eGFP* fluorescence, we measured mean fluorescence pixel intensity. As a control for compression, embryos were introduced into the chamber with the walls held open by vacuum, and all significance tests were made relative to this vacuum control. As a control for handling embryos in the channel, embryos were observed under halocarbon oil on a coverslip (dish control). Four hours after compression, all embryos showed an increase in *twist:eGFP* fluorescence (Fig. 5.17A). Embryos compressed for 10 minutes showed a significant dose-dependent increase in *twist:eGFP* when compressed by 7% ($p < 0.01$) and 22% ($p < 0.0001$; ordinary one-way ANOVA to vacuum control, Fig. 5.17). Embryos also showed a time-dependent increase in *twist:eGFP* when 7% compression was extended to 4 hours ($p < 0.0001$). In the 22% 4-hour condition, *twist:eGFP* fluorescence was not significantly different from vacuum controls in magnitude. Yet the distribution of that expression remained ectopic (Fig. 5.16E vs A). This is consistent with the idea that both the amount and the duration of compression are biologically relevant. One explanation for this lower magnitude is that embryos in this condition are already committed to die within 48 hours (Fig. 5.11F). Another interpretation is that embryos could be experiencing a mild hypoxia that interferes with the *twist:eGFP* reporter.

Hypoxia

Embryo confinement could induce a hypoxic response that would complicate the interpretation of *twist:eGFP* expression in two opposing ways: hypoxia reduces cellular eGFP fluorescence [327], and also upregulates *twist* mRNA and protein levels through hypoxia-inducible factor (HIF-1 α) binding to a hypoxia-responsive element in the proximal promoter

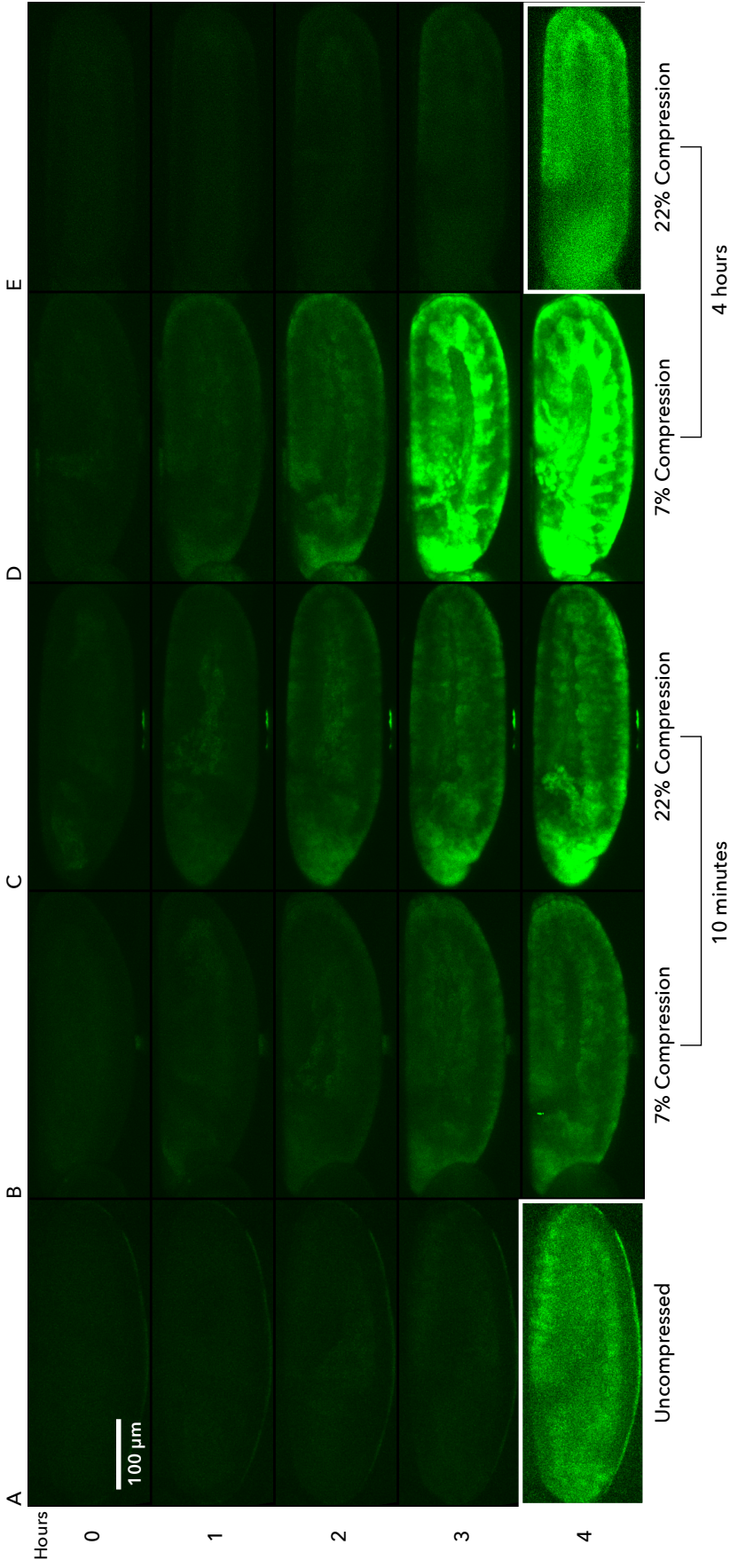


Figure 5-16: Ectopic distribution of *twist:eGFP* in compressed embryos. *twist:eGFP* fluorescence was measured every hour over 4 hours. The maximum and minimum pixel value settings are the same for all images, except for insets (bottom, white border) to show patterning. (A) Uncompressed embryos show a ventral stripe of *twist:eGFP* expression. (B, C) Embryos compressed for 10 minutes show an increase in *twist:eGFP* over 4 hours. (D) Embryos compressed by 7% continuously for 4 hours show substantial increase in fluorescence. (E) Embryos compressed by 22% for 4 hours show low fluorescence that is nevertheless ectopic.

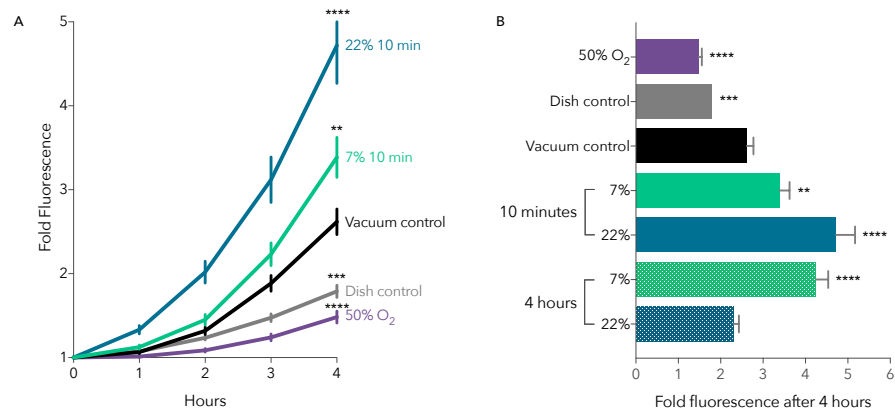


Figure 5.17: Mechanical induction of *twist* expression. (A) *twist:eGFP* fluorescence was measured every hour over 4 hours after compression. Embryos show a significant increase in mean fluorescence when compressed for 10 minutes by 7% (0 PSI, $p < 0.01$) and 22% (5 PSI, $p < 0.0001$; Ordinary one-way ANOVA to vacuum control, SEM bars). Vacuum controls were introduced into the channel with the walls held open; dish controls remained outside the channel. Hypoxia (50% O₂) decreased *twist:eGFP* expression ($p < 0.0001$). (B) Summary of *twist:eGFP* fluorescence after 4 hours. Embryos were exposed to three compression levels for either 10 minutes or 4 hours (SEM bars, ordinary one-way ANOVA to vacuum control).

of the *twist* gene [328, 329]. This pathway was demonstrated in tumor cell lines and in *C. elegans* mutant for the *twist* homolog (hlh-8), but remains unconfirmed in *Drosophila* [329]. To determine whether hypoxia could explain changes in *twist:eGFP* fluorescence, we intentionally induced an oxygen shortage in *twist:eGFP* embryos by flowing through 50% normoxia using equal pressures of compressed air and argon. Embryos continued to develop (Fig. 5.18), and the resulting *twist:eGFP* fluorescence after 4 hours was reduced compared to normoxia controls ($p < 0.0001$, Fig. 5.17, 5.18). This suggests that a decrease in *twist:eGFP* expression could be explained by hypoxic suppression of eGFP, and the indirect *twist:eGFP* system might underestimate the true value of *twist* expression. Therefore, we cannot exclude that hypoxia may underlie at least some of the observed decrease in fluorescence after 22% compression for 4 hours. Future work with this device using recovered embryos could resolve this issue.

The significant increase in vacuum control compared to dish control was unexpected (Fig. 5.17). One explanation is that when embryos in the dish crowd, they compete for oxygen, which inhibits eGFP [327]. Consistent with this hypothesis, we observed that embryos in the dish with high surface-area contact occasionally failed to develop. Embryos in the mesofluidic device did not show this effect, and may experience less hypoxia due to the surrounding oxygen-permeant PDMS sidewalls. While we cannot exclude the possibility that the chamber itself induces *twist* expression, a more likely explanation is that while switching tub-

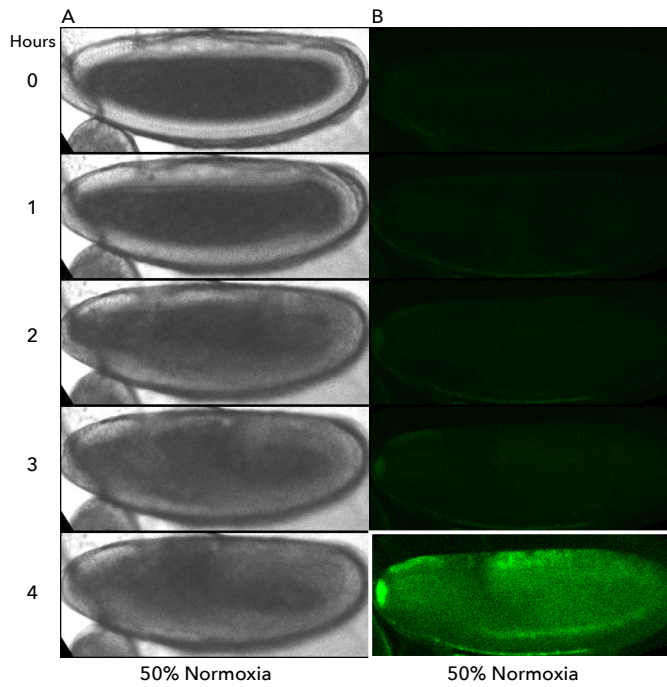


Figure 5.18: Timelapse microscopy of embryos under 50% normoxia. DIC and *twist:eGFP* fluorescence images taken every hour for 4 hours. Pixel value settings are the same as Fig. 5.16 except for bottom inset (white border) to show patterning. Fluorescence was quantified in Fig. 5.17.

ing for microscopy, the vacuum was discontinuous for approximately one minute, causing a brief flexing of the sidewalls, which triggered a *twist* response. Consistent with this hypothesis, vacuum controls in survival experiments that did not require switching tubing also did not show an intermediate response between dish control and compression. Taken together, the potential for rapid induction of *twist* expression highlights the need for precise temporal control when studying mechanotransduction. At compression less than 22% for 4 hours, the mesofluidic device provides greater access to oxygen and rates of survival than dish controls.

CONCLUSIONS

We developed a novel mesofluidic device that can automatically align and immobilize hundreds of *Drosophila* embryos without an external force. This device precisely compresses hundreds of embryos using pressure-actuated deformable sidewalls, allows for live imaging, and the retrieval of live embryos for post-analysis. We describe a method for consistent ultra-thick photolithography, derive an analytical model that describes sidewall deflection within 0.3%, and discuss the optimization of five parameters critical to the design of mesofluidic devices.

The device itself does not affect survival or development, and does not induce anoxic arrest. Using this device, we measure the Young's modulus of PDMS sidewalls and *Drosophila* embryos. Compressing embryos is sufficient to trigger the mechanical induction of *twist* that is time-dependent and dose-dependent.

Taken together, this mesomechanics approaches facilitates the design of future devices for high-throughput mechanotransduction and imaging of larvae, embryos, oocytes, organoids, or adults such as *Danio rerio* or *C. elegans*. By tuning the rigidity of PDMS, the device can operate without a pressure tank to apply a specific and consistent amount of force, including < 1% compression to immobilize samples for time-lapse imaging while maintaining access to oxygen. The bottleneck constriction at the end of the compression channels allows for the fast exchange of media around immobilized samples, enabling chemical stimulation and on-chip staining inside the microchannel. The ability to process many whole-tissue samples and precisely apply mechanical intervention makes it possible not only to interrogate the induction of *twist*, but also to map out novel mechanosensitive pathways in meso-scale organisms.

Part III

A HIGH-THROUGHPUT METHOD FOR EXPOSING ZEBRAFISH TO ALTERED GRAVITY, ALIGNING FOR IMAGING, AND SEGMENTING ROHON-BEARD NEURONS

Biological responses to gravity are challenging to identify because they show high variance. To examine single-cell variation in *ngn3.1* neurogenin 1 (*ngn3.1*) expression, we developed methods to quantify green fluorescent protein (GFP) reporter fluorescence among thousands of individual cells in the developing zebrafish. A *ngn3.1:GFP* reporter selectively labels a population of Rohon-Beard neurons (RBN) during a period of sensitivity to changes in gravity. Transgenic zebrafish embryos were exposed to simulated microgravity (*sμg*) for 24 hours using a NASA-designed clinostat, or to hypergravity using a custom-built centrifuge. We developed two methods to process dozens of embryos simultaneously at low cost: *dorsal alignment* using a 3D-printed channel-forming stamp, and *segmentation* using a human-in-the-loop visual processing algorithm. Using these methods, we measured fluorescence from over 6,000 neurons, and observed a significant decrease in mean fluorescence after exposure to *sμg*, and a reciprocal increase after exposure to hypergravity. Stochastic distribution of *ngn3.1:GFP* increased with gravity, as measured by mean squared error. These methods of alignment and segmentation balance automation with flexibility to measure stochastic protein expression.

BACKGROUND

Life on Earth evolved under the influence of gravity. The gravity deprivation of space has been shown to affect the function of many cell types, including lymphocytes [136], epidermal cells [137], osteoblasts [81], and tumor cells [138, 139]. *In vivo* responses to microgravity (μg) have been observed in *E. coli* [123], yeast [124], *Drosophila* [75, 330], zebrafish [37, 122], rodents [331], and other model organisms [126, 131]. Although some biological responses to space are attributable to the increased exposure to radiation [71, 72], carefully controlled ground-based simulation has revealed biological responses that are exacerbated or directly attributable to changes in gravity [37, 74, 75].

Despite the abundance of biological responses to gravity across organisms and organ systems, identifying gravity-responsive genes has been inconclusive. Many genes show widespread sub-threshold changes [186–188], or contradictory results [189, 190], even across closely related studies. A commonality among these studies is their focus on either mRNA or mean protein expression; they do not address protein variation directly.

Transcriptomic analysis does not account for translational or post-translational regulation; proteins are more direct affectors of cell behavior. Furthermore, transcriptomics necessitates choosing a gene that is assumed to be invariant; this assumption is problematic when μg has been shown to affect expression of the housekeeping gene β -actin [8, 184, 194].

A limitation in measuring mean protein expression is the loss of information about stochastic variation. Single-cell variation has been observed in 1,855 proteins, about 15% of the human proteome [332]. Changes in stochastic gene expression and have been implicated in μg [8, 37, 122] as well as circadian rhythms [333, 334], which may explain the disruption of circadian rhythms in μg [93, 94, 335]. Measuring mean expression dilutes changes in small organ systems; in μg , sub-threshold changes in whole embryo studies [187] belied significant changes for those same genes in the small hypochord [194]. These observations highlight the need for approaches that can measure single-cell variation at the level of proteins, especially for studying gravitational effects.

Single-cell stochastic protein approaches require a tractable system of cells and a method to quantify expression of gene products. There are several advantages to zebrafish Rohon-Beard neurons (RBN) [8]. Ze-

brafish are conducive to imaging because they are transparent during development. Zebrafish undergo a period of maximal sensitivity to μg between 24 and 72 hours post-fertilization [194], which coincides with the peak expression of RBN [336]. RBN are mechanosensory neurons that situate above the notochord just under the ventral skin in two parallel tracts [337]. RBN can be distinctly visualized because the transcription factor -3.1 neurogenin 1 (*ngn3.1*) localizes almost exclusively to RBN [338]. A transgenic zebrafish with GFP driven by a cis-regulatory element from the *ngn3.1* gene Tg(-3.1neurog1:GFP)sb2 has been described [8, 338, 339]. RBN are particularly easy to track because they do not divide. RBN have a consistent circular shape and size of about 14 μm , which reduces heterogeneity in total fluorescence due to size [340], enabling more sensitive detection of the underlying transcriptional noise. RBN are first detectable as early as 9 hours post-fertilization (hpf) at late gastrulation [336, 341]; the RBN population peaks at about 190 cells at 34 hpf [336], after which they undergo apoptosis. RBN decrease at about 5 cells/hour until 48 hpf, after which they slow down to an hourly death, with most lost by 84 hpf. Taken together, at 32 hpf we expect zebrafish RBN to be abundant, sensitive to changes in gravity, and a good candidate for computational segmentation.

Previous attempts at this system were only able to measure from six embryos at a time [8]. The two primary challenges were high-throughput dorsal alignment of zebrafish, and segmentation of RBN. Here, we aligned zebrafish with a 3D-printed channel-forming stamp; the resulting images of neurons were more tractable to segment by a human-in-the-loop visual processing algorithm specific to RBN. An overview of this method can be seen in Fig. 6.1.

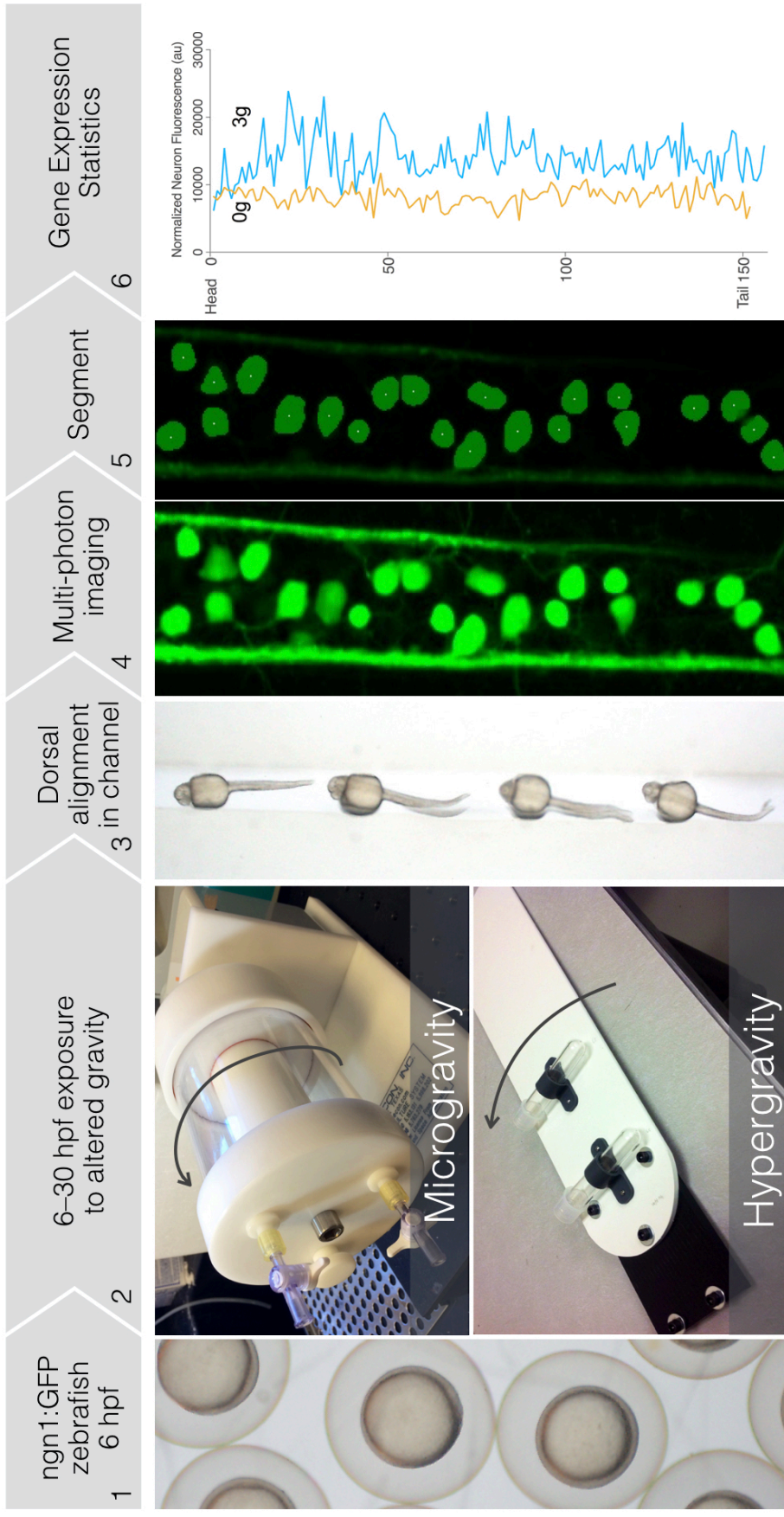


Figure 6.1: A method for measuring gravity-dependent changes in -3.1 neurogenin 1 (*ngn3.1*) expression on a single-cell level. Zebrafish embryos selectively express *ngn3.1* in Rohon-Beard neurons (RBN) during a period of sensitivity to gravity. (1) *ngn3.1:GFP* embryos were collected at 6 hours post-fertilization (hpf) and (2) exposed for 24 hours to either *shg* ($\approx 0.01g$) in a clinostat, or to hypergravity (2g and 3g) in a custom centrifuge. (3) 32-hpf embryos were aligned dorsally in agarose channels created by a 3D-printed stamp. (4) Fluorescent RBN were imaged by confocal two-photon microscopy. The resulting images were sum-projected and (5) segmented semi-automatically. These regions of interest were used to calculate (6) *ngn3.1* expression distribution among RBN.

METHODS

6.1 ANIMALS

Adult zebrafish (*Danio rerio*) were maintained according to standard husbandry protocols [342, 343] and experiments were performed in accordance with NIH guidelines. Embryos were generated by pairwise crossing to reduce genetic variation due to heterozygosity. Embryos were grown at 28°C in 30% Danieau buffer [17 mM NaCl, 2 mM KCl, 0.12 mM MgSO₄, 1.8 mM Ca(NO₃)₂, 1.5 mM HEPES] with a 14:10 h light/dark cycle. For imaging, embryo medium was supplemented with 0.003% PTU (phenylthiourea; Sigma) to prevent melanin synthesis for clearer imaging, and anesthetized with 160 µg/mL (micrograms) tricaine (3-amino benzoic acid ethylester; Sigma). The transgenic line Tg(-3.1neurog1:GFP)sb2 [339] was a gift from Dr. Mary Halloran at the University of Wisconsin. Genotype was validated by PCR amplification of GFP in fin clips as described [344].

6.2 CONFOCAL MULTI-PHOTON IMAGING

Fluorescence imaging was performed using a Leica TCS SP5 multi-photon/ confocal microscope (Leica Microsystems, Wetzlar, Germany) with an APO L 20×/1.00 water immersion objective, or an HCX IRAPO L 25×/0.95 water-immersion objective, non-descanned detectors, and spectral detectors. GFP was excited with a Mai Tai DeepSee Ti:Sapphire laser (Newport/Spectra Physics, Santa Clara, CA, USA) at 900 nm. Scanning was performed with a resonant scanner (8000 Hz) with 16× line averaging. Images were taken in 12 bit for greater dynamic range. We took care to adjust the gain to maximize fluorescence without saturating pixels, which would lose data due to stack overflow. Absence of saturated pixels was verified with a LUT display. Sum projections were generated using MetaMorph 7.7, with the entire dataset multiplied by 0.65, empirically found to prevent stack overflow during sum-projection.

6.3 STATISTICS

Mean fluorescence was calculated for each neuron by MetaMorph. Average fluorescence for each fish and ordinary ANOVA comparisons were calculated by Prism version 7.0c for Mac, GraphPad Software, La

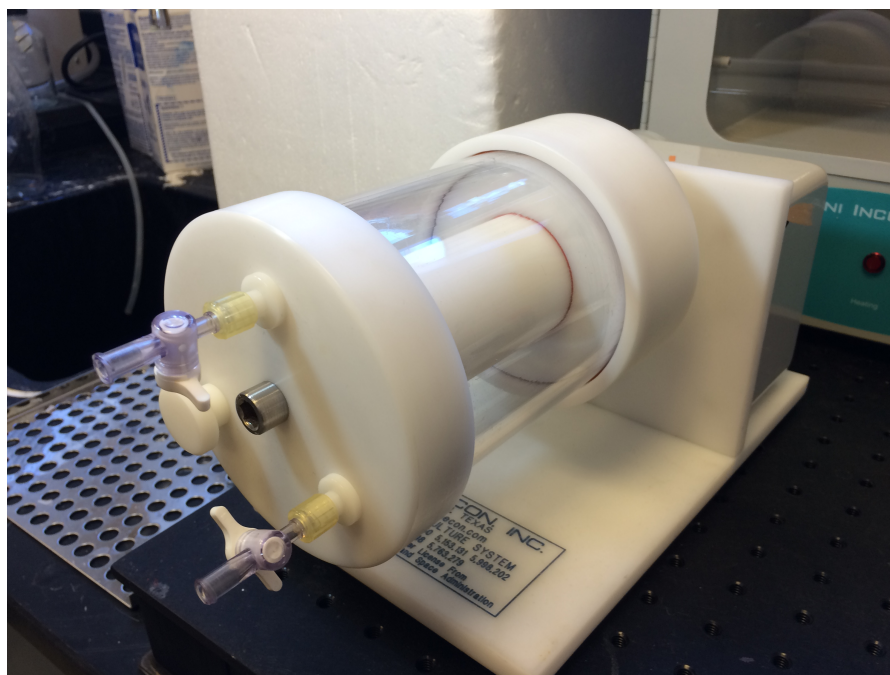


Figure 6.2: Photograph of RWV clinostat. Embryos are loaded into a clear Lexan cylinder filled with buffer and rotated around the teflon core. A variable motor keeps the eggs in circular orbit such that the gravity vector is constantly changing, resulting in time-averaged gravity compensation, a simulation of microgravity.

Jolla California USA, www.graphpad.com. Variation was calculated as mean squared error (MSE) to the best fit linear equation.

6.4 SIMULATED MICROGRAVITY

Zebrafish embryos were exposed to $5\mu g$ using a bioreactor designed by NASA (Synthecon, Houston, TX) as previously described [345]. Briefly, a clear Lexan cylinder 10-cm in diameter was filled with zebrafish eggs in 30% Danieau buffer. The cylinder was rotated around the x-axis so that the wall of water rotates around a Teflon core. A variable speed motor was adjusted to keep eggs in a circular orbit (15–20 RPM) which indicates a net force vector that constantly changes direction while maintaining the same magnitude, resulting in time-averaged mechanical deprivation [345]. Control and experimental conditions were both in a 28°C room with a 14:10 h light/dark cycle.

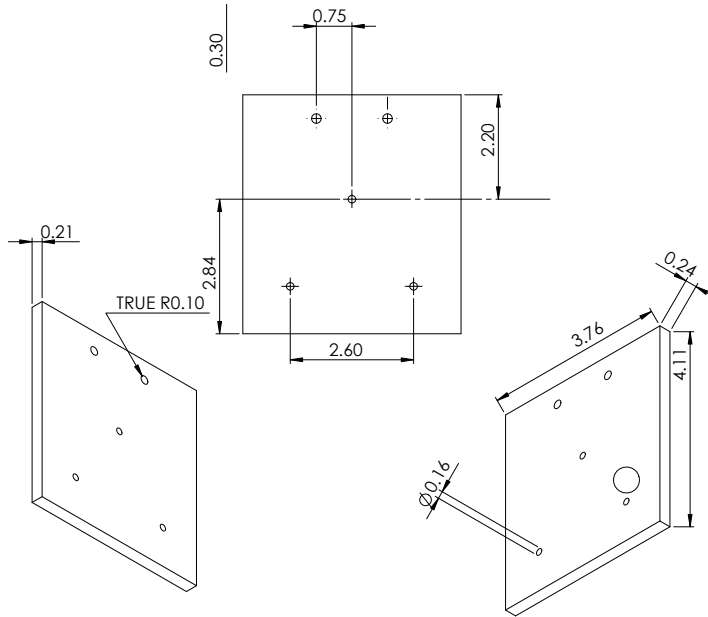


Figure 6.3: Schematic of a delrin adapter for mounting fan blades horizontally on a custom centrifuge (Fig. 6.5B). The adapter replaces the fan blades and contains screws to mount 15-mL falcon tubes. Numbers are inches.

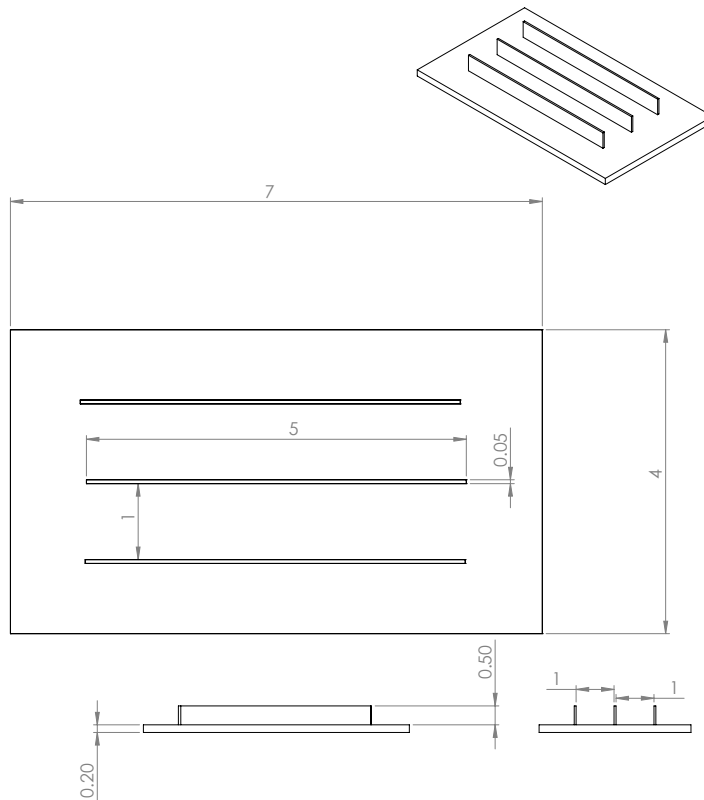


Figure 6.4: Schematic of a 3D-printed channel-forming stamp used in Fig. 6.8. Three parallel tracks are 500 μm wide, the width of zebrafish embryos. When agarose is allowed to gel around the channel, the resulting channels hold embryos dorsally. Numbers are cm.

RESULTS & DISCUSSION

6.5 CONSTRUCTION OF A CUSTOM CENTRIFUGE

To expose zebrafish embryos to hypergravity, we constructed a custom low-speed centrifuge. A ceiling fan was affixed upside-down to a plank of wood and coated with a waterproof polyurethane spray (Miniwax, Upper Saddle River, NJ). We created an adapter to hold the blades parallel to the ground (Fig. 6.5) using a TL-1 CNC toolroom lathe (HAAS, Warrendale, PA). On the blades, we mounted 15-mL round-bottom tubes (Thermo Fisher Scientific) perpendicular to the axis of rotation. Each embryo was directly against the wall of the tube, which applied a net force equally to each embryo. This allowed us to apply custom forces and avoids the accumulation of embryos pressing against each other at the bottom of the tube, which would occur in a conventional centrifuge. The number of embryos per tube was controlled to be less than 25; crowding precipitated morphological deformation. The speed of the centrifuge was adjusted by a variac (3PN1210B, Staco Energy) and verified with a laser tachometer (Omega). At 100 RPM, we applied 2g at a radius of 15.5 cm, and 3g at a radius of 25.3 cm.

Theoretical considerations

Unlike μg , hypergravity is not a simulation; acceleration is indistinguishable from gravity [158]. In our centrifuge, a rotating object experiences Earth's 1g and a perpendicular RCF. Both forces combine by vector addition to generate a net force:

$$F_{net} = \sqrt{(1g)^2 + (RCF)^2} \quad (6.1)$$

To apply a given net force, we choose an RCF such that

$$RCF = \sqrt{(F_{net})^2 - 1} \quad (6.2)$$

For example, to apply a net force of 3g, we want to apply an RCF of

$$RCF = \sqrt{(3g)^2 - (1g)^2} = \sqrt{8}g \quad (6.3)$$

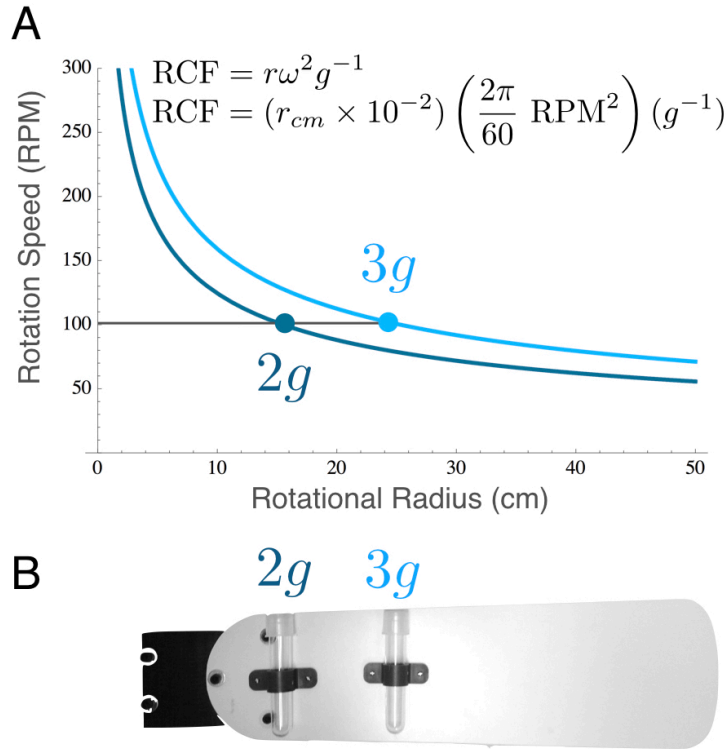


Figure 6.5: A custom centrifuge to expose embryos to hypergravity. To apply a net force of $2g$, we apply a RCF that combines with Earth's $1g$ such that $\sqrt{(RCF)^2 + (1g)^2} = 2g$. (A) To apply a given RCF , we choose a rotation speed and radius to satisfy this equation. To apply multiple conditions in parallel, we maintained the same RPM while varying the rotational radius, resulting in (B) two positions for holding embryos on the centrifuge. A delrin adapter, shown in black, holds the fan blade horizontally.

The RCF experienced by an object is a function of rotational radius r and angular velocity ω in radian per second, relative to Earth's gravitational acceleration g :

$$RCF = \frac{r\omega^2}{g} \quad (6.4)$$

This can be rewritten in terms of RPM and centimeters:

$$RCF = (r_{cm} \times 10^{-2}) \left(\frac{2\pi}{60} \text{RPM} \right)^2 (g^{-1}) \quad (6.5)$$

Which can also be combined along with Earth's g :

$$RCF = (1.118 \times 10^{-5})(r_{cm})(\text{RPM}^2) \quad (6.6)$$

Application of RCF

To apply a given RCF, we can choose a rotation radius and RPM that satisfies (6.2). The solutions for $F_{net} = 2g$ are in Fig. 6.5A. To increase hypergravity for $3g$, we could increase rotation speed. But a more convenient approach is to maintain the same RPM while varying rotational radius, resulting in Fig. 6.5B: two positions for holding embryos on the fan blade to apply $2g$ and $3g$ at the same time.

Generally, we can set (6.6) equal to (6.2) to say that we can apply a desired net force by choosing RPM such that

$$\text{RPM} = \sqrt{\frac{\sqrt{F_{net}}}{1.118 \times 10^{-5}(r_{cm})}} \quad (6.7)$$

6.6 DORSAL ALIGNMENT BY 3D-PRINTED STAMP

There are several benefits to rapid dorsal alignment of zebrafish embryos (Fig. 6.6). Rapid alignment allows for dozens of embryos to be prepared and imaged, and avoids having to search for embryos, or accidentally image the same one twice. Dorsal imaging preserves a consistent minimal distance between objective and RBN, which is significant because light attenuates in confocal scanning microscopy [346, 347]. RBN situate $25 \mu\text{m}$ under the dorsal surface, a value that is consistent within $5 \mu\text{m}$ (Fig. 6.6A, Fig. 6.7A). In contrast, lateral variance varies by $45 \mu\text{m}$ across the width of the embryo (Fig. 6.7B). Maintaining minimal distance preserves accuracy, while maintaining consistent distance preserves precision (Fig. 6.6B). Dorsal imaging also reduces overlap of neurons (Fig. 6.6C) allowing automated segmentation (Fig. 6.9).

Despite the advantages to dorsal imaging, conventional orientation methods are labor intensive, involving manually positioning embryos individually in random directions while agarose sets. So we created a 3D-printed stamp to form consistent $500 \mu\text{m}$ channels in agarose (Fig. 6.8). This allowed us to rapidly image and segment thousands of RBN.

Creating agarose channels: 2% SeaKem LE agarose in 30% Danieau was microwaved until liquid but not boiling. A small amount was poured into a petri dish such that the base was barely covered. This volume was further reduced by suctioning off liquid agarose with a pasteur pipette to leave behind a minimal continuous layer about 1 mm high. The 3D-printed mold was positioned on top (Fig. 6.8B), and the agarose was allowed to solidify for 5 minutes at room temperature. The mold was removed and the channels were flooded with buffer. Zebrafish embryos were added and pushed into the channels with a whisker eyelash

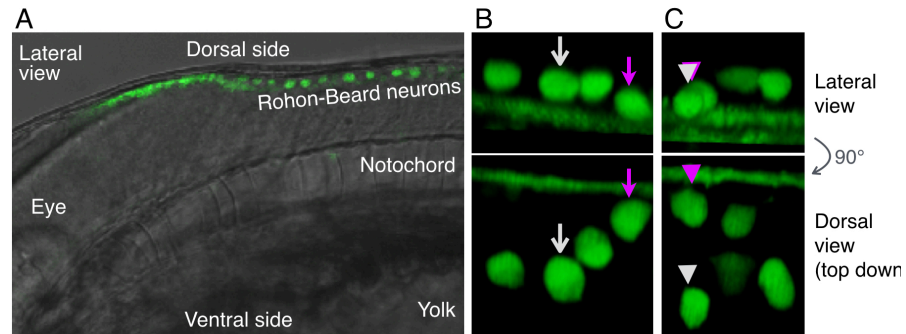


Figure 6.6: Fluorescent images of Rohon-Beard neuron with *neurogenin:GFP*. When quantifying Rohon-Beard fluorescence, two systematic biases in lateral imaging are addressed in dorsal imaging. (A) Lateral overview of a *ngn3.1:GFP* zebrafish embryo. *GFP* expresses selectively in Rohon-Beard neurons, just below the dorsal surface. (B) One lateral bias is the distance from the objective. Neurons distribute between longitudinal fasciculi. Like stars, more distant neurons (magenta arrows) appear dimmer when further away. Lateral imaging (top) conflates absolute magnitude and apparent magnitude; the magenta arrow appears coplanar with the white arrow, but is revealed to be further from the objective when imaged from the dorsal perspective (bottom). Imaging top-down preserves distance, isolating changes in absolute magnitude. (C) A second lateral bias is overlapping neurons, which are hard to differentiate laterally (top) but easily segmentable resolved when imaged dorsally (bottom).

(Fig. 6.8c). For long-term timelapse imaging, the buffer can be replaced with 0.6% agarose with Tricaine to seal the channels.

6.7 COMPUTATIONAL IMAGE ANALYSIS

High-throughput analysis requires not only the consistent orientation of zebrafish, but also a method of segmentation to extract morphological features (Fig. 6.9). Segmentation is the process of identifying and separating image regions that have different properties or are delineated by edges. In the biological context, segmentation consists of separating *RBN* from longitudinal fasciculi and background. This is somewhat imprecise; fluorescent sources often have unclear boundaries, both on the image and even physically. Segmentation is especially important when quantifying the gene transcription activity among cells; because zebrafish are transparent, transgenic reporter genes can show tissue-specific activity efficiently and rapidly [194, 348, 349]. Yet fluorescent reporter methods are limited by the lack of tools for automated segmentation. Manual segmentation by circling cells does not scale well to studies involving thousands of cell nuclei; the labor cost is high, and the output is slow.

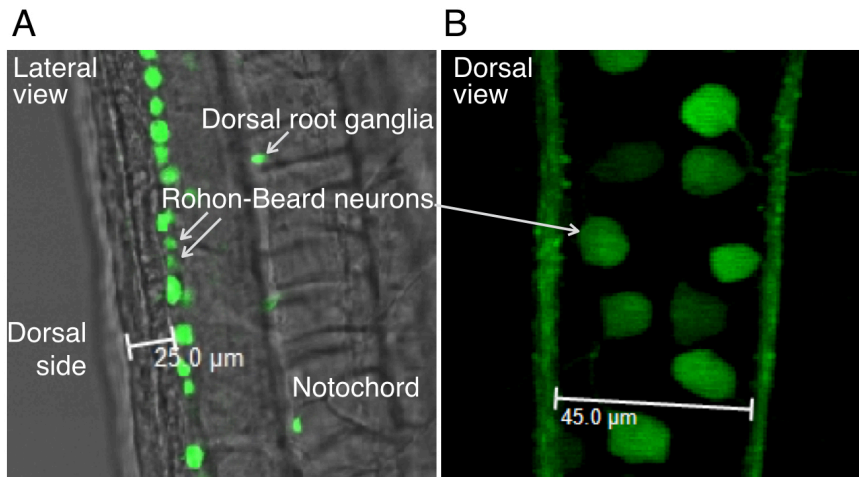


Figure 6.7: Anatomy of Rohon-Beard neurons (RBN). (A) Lateral view shows Rohon-Beard neurons are consistently below the dorsal surface. Therefore top-down imaging maintains a consistent and minimal distance between the objective and fluorescence source. (B) Dorsal view shows Rohon-Beard neurons distribute laterally between the longitudinal fasciculi, varying distance from the objective by as much as $45\ \mu\text{m}$; this implies lateral imaging could contribute to apparent variation in fluorescence.

Algorithmic segmentation is faster and more efficient once set up, but less accurate in specific situations such as determining objects in clusters [350]. There are several approaches to segmentation:

- **Thresholding techniques** assume adjacent pixels with values in a range belong to the same category [351]. However, thresholding is difficult in images that blur at object boundaries [352].
- **Boundary-based techniques** assume that pixels change rapidly at boundaries, however, they usually require post-processing to obtain a closed curve [353].
- **Region-based techniques** assume that adjacent pixels with similar values belong together, including split and merge [354, 355] and seed region growing [356], however, automated selection of seeds is still required. We also found that watershed segmentation alone miscounted the longitudinal fasciculi as neurons, and merged objects that touched.

Several fully automated pipelines exist that are more sophisticated, including warping experimental embryos onto a 2D reference shape [357], elastically deformable contours based on ellipsoidal centers [358], and supervised classification [359]. In practice, these techniques were optimized for the more typical lateral orientation, rather than dorsal views. Like many groups, we found it necessary to design custom algorithms and molds at the same time [357, 360] coupled with pre-processing

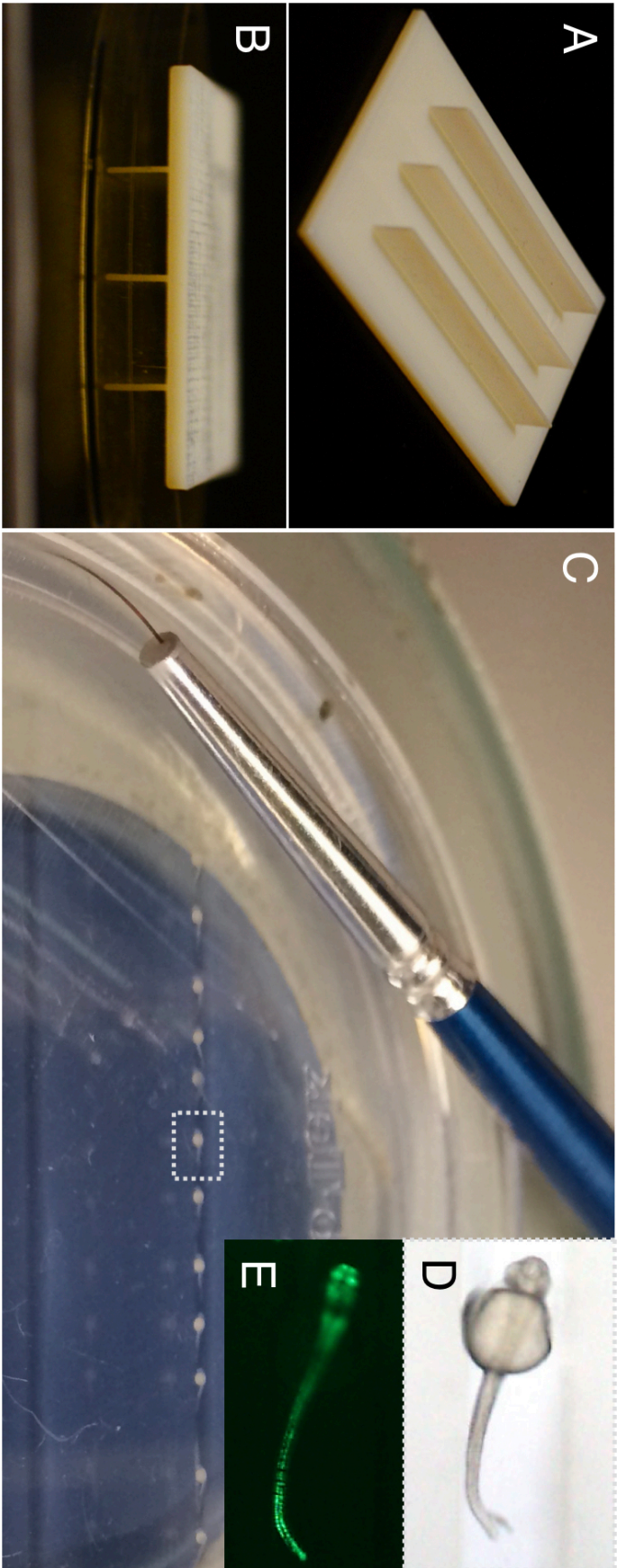


Figure 6.8: A 3D-printed stamp for rapid dorsal alignment of embryos. (A) 3D-printed stamp (B) is placed on top of a petri dish while agarose sets. (C) This approach creates reproducible 500 μm channels that spatially align embryos head to tail for rapid imaging. Embryos are placed into position by an eyelash brush (blue). (D) Image of embryo in dorsal orientation, which allows for segmentation of *RBN* (E) captured through fluorescent imaging of *ngn3.1:GFP*.

modifications [350, 357, 359]. Our procedure is a compromise that makes use of some human input:

Crop Z-stack to layers of interest, create a sum projection (Fig. 6.9.1), threshold the background and clip to 0, draw a line through the dorsal longitudinal fasciculi (Fig. 6.9.2). Metamorph does not support erasing, but a workaround is to generate boxes centered around a line and copy 0's into the boxes. With the fasciculi erased, the remaining objects can be morphometrically segmented by three parameters:

1. Circularity: RBN have a form factor of $\frac{4\pi a}{p^2} > 0.87$
2. Size: RBN are $12 \pm 3\mu\text{m}$ in diameter and:
3. Difference over background.

Using a for-loop, we generated 10 interpretations of segmentation by iterating through Metamorph's Integrated Morphometric Analysis parameters (Fig. 6.9.3) from which the user selects the best interpretation, which updates the morphometric parameters. We found these parameters to be region specific, and had to be optimized for each fish in the dataset. This process was conducted manually to provide added flexibility in processing this dataset; more automated methods are possible. Finally, the program generates a binary mask, which is multiplied by the original image, and finally segments the image (Fig. 6.9.4) and outputs mean intensity.

6.8 BIOLOGICAL RESULTS

Using these methods, we were able to collect data from 47 fish concurrently, measuring over 6,000 neurons (Fig. 6.10). This allowed us to analyze several phenomena that would otherwise be hard to observe. Compared to 1g controls, 0g fish show decreased *ngn3.1* fluorescence expression, and 2g and 3g fish showed increased *ngn3.1* expression by an ordinary one-way ANOVA with Dunnett's multiple comparisons test adjusted P value of $p < 0.0001$ for each condition, $n > 1,200$ neurons per condition (Fig. 6.10A). There was no significant difference between 2g and 3g. Gravity also affected stochastic distribution of neurons around their mean: 0g fish were more consistent, and hypergravity fish were less consistent compared to 1g controls (Fig. 6.10C). For additional statistical descriptions of the dataset, see Table 6.1.

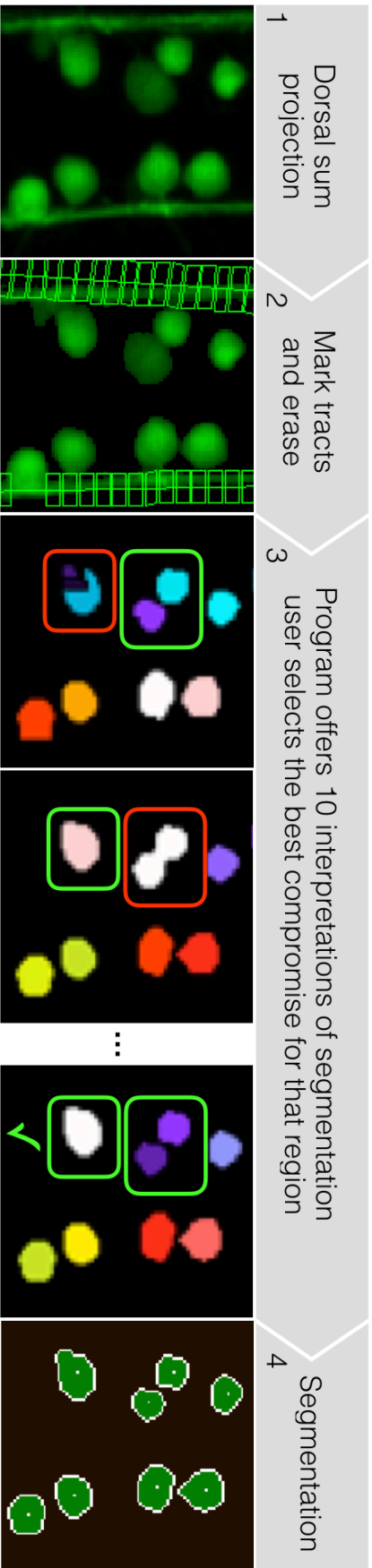


Figure 6.9: Pipeline of image processing for segmentation. To quantify $ngn3.1$ expression, *RBN* must be segmented into regions of interest. (1) Z-stack of dorsal images are sum-projected. Some variation in brightness can be seen by eye. (2) The user draws a line through the longitudinal fasciculi, and the program deletes around it. (3) Morphometric analysis excludes objects based on size, shape, and difference from background. A for-loop iterates through these parameters, generating multiple attempts at segmenting the same region. Note how the program initially over-splits one neuron (bottom red box). In the process of correctly segmenting that neuron (next panel, bottom green box) a new problem is generated: the top two neurons are merged. Although more sophisticated algorithms could solve this, we used human-computer collaboration to find a good compromise for that region (last panel). (4) Segmented images are used to measure fluorescence of regions of interest in the original image.

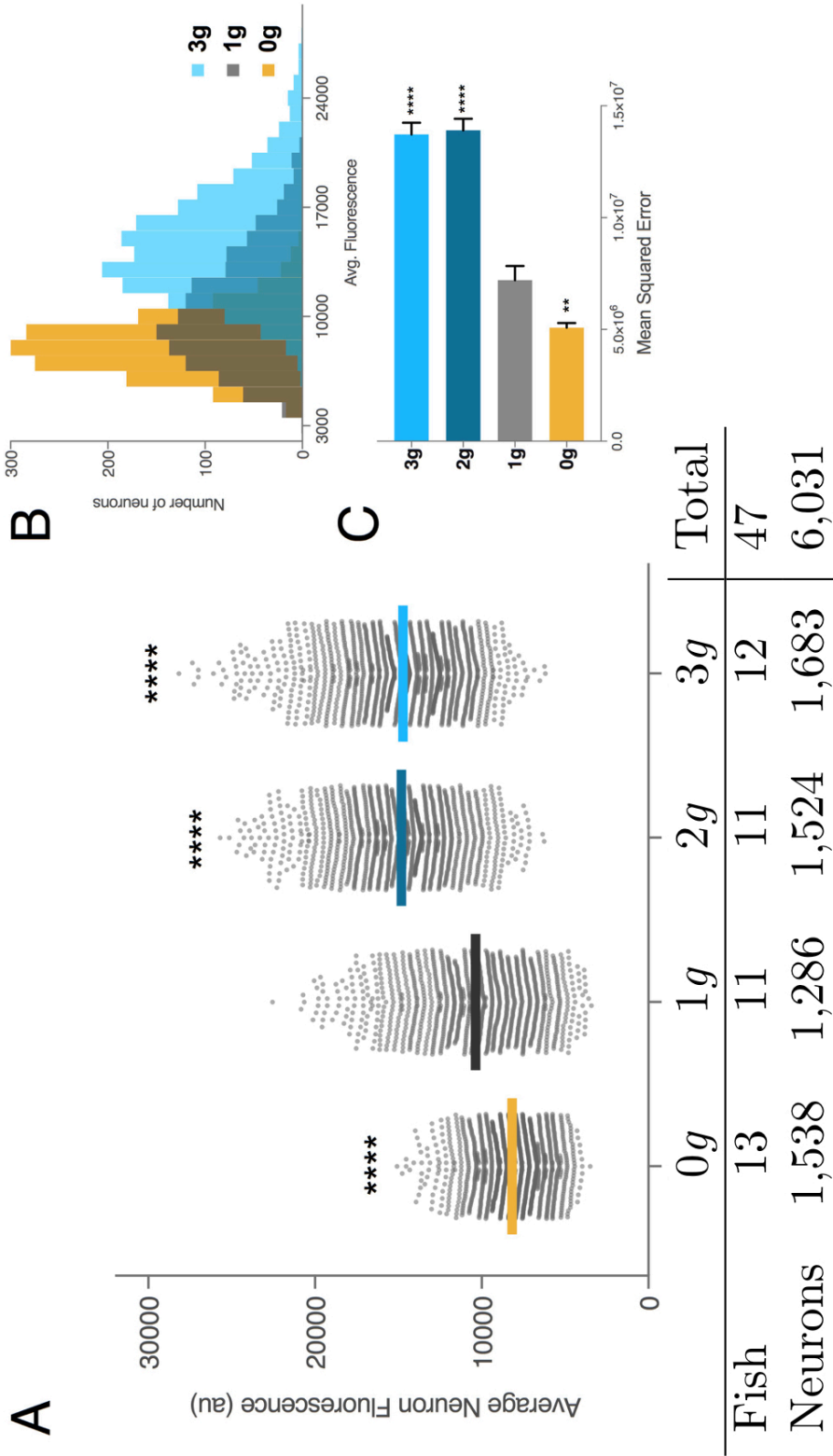


Figure 6.10: Gravity-induced changes in *ngn3.1* expression. (A) *ngn3.1:CFP* mean fluorescence decreased after exposure to *2g* and *3g* compared to *1g* controls (ANOVA $p < 0.0001$) and increased after exposure to hypergravity in both *2g* and *3g* (ANOVA $p < 0.0001$). These methods allow measurement from 47 fish and over 6,000 neurons; $n > 1,200$ neurons per condition. Gravity also affected stochastic distribution of individual cells around the collective mean in (A), and (C) as a histogram, and quantified by (B) *MSE*. (ANOVA $og\ p < 0.01$; $2g\ p < 0.0001$; $3g\ p < 0.0001$; 95% CI bars.)

	0g	1g	2g	3g
Fish	13	11	11	12
Neurons	1,538	1,286	1,524	1,683
Fluorescence Mean	8,194	10,380	14,840	14,740
Std. Deviation	1,933	3,516	3,348	3,491
Std. Error of Mean	49	99	86	85
Lower 95% CI of mean	8,097	10,186	14,670	14,572
Upper 95% CI of mean	8,291	10,573	15,009	14,907
Skewness	0.42	0.48	0.32	0.62
Kurtosis	0.19	-0.24	0.01	0.42
Mean Square Error ($\times 10^6$)	5.1	7.2	13.9	13.7

Table 6.1: Descriptive statistics of Rohon-Beard neurons

Descriptive statistics

CONCLUSIONS

Using a 3D-printed stamp to align zebrafish embryos is easy to implement at low cost. High-throughput dorsal imaging makes segmentation significantly more tractable, which enables measurement among thousands of individual Rohon-Beard cells, which enables the measurement of stochastic variation in an organ system.

The methods described here attempt to isolate variation in gene expression that is due to gravity by eliminating other sources of variation. Variation due to heterozygosity is reduced by generating embryos through pairwise crossing. Variation in apparent magnitude is reduced by imaging dorsally, which preserves a minimal and equal distance between the objective and each neuron (Fig. 6.6B). Dorsal imaging also resolves neurons that would overlap when imaged laterally (Fig. 6.6C). Variation due to off-target fluorescence is reduced by imaging with two-photon confocal microscopy: out-of-focus objects are rejected because excitation is restricted to a femtoliter focal volume; tissue is better penetrated because the excitation photons are near-IR, which reduces scattering and absorption by endogenous chromophores [361]; and scattered excitation photons are too dilute to cause appreciable fluorescence [362]. Taken together, these methods control for many of the most significant sources of gene expression variance, and allow future studies to detect changes in variation.

These methods also attempt to increase the tractable sample size of analysis without the burden of establishing full-scale automation. A

3D-printed channel-forming stamp rapidly orients many embryos dorsally, and a semi-supervised visual processing algorithm segments regions of interest in thousands of neurons. Taken together, these methods increase the statistical power of gene expression analysis by fluorescent reporters.

Part IV

MECHANOPROTEOMICS: COMPARATIVE PROTEOMIC ANALYSIS OF MECHANOTRANSDUCTION IN COMPRESSION, HYPERGRAVITY, AND SIMULATED MICROGRAVITY

Even small mechanical perturbations can have large effects on organismal health and disease. Here we consider three contexts of mechanical perturbation in *Drosophila* development: compression, hypergravity, and simulated microgravity (*sμg*). Each shows behavioral and transcriptomic responses, yet there is little agreement on mechanoresponsive pathways. One explanation is that mechanotransduction occurs primarily on the level of proteins and post-translational modification, which are more direct effectors of cell behavior, and not detectable by transcriptomic approaches. However, “mechanoproteomic” approaches have been limited by sample size – compression requires manual alignment of individual embryos. We developed a mesofluidic device to apply a precise uniaxial compressive strain to hundreds of embryos simultaneously. We also built a custom centrifuge to apply hypergravity, and use a NASA-designed clinostat to simulate microgravity. This enabled rapid mechanostimulation and recovery of hundreds of living embryos, which enabled a proteomic screen using difference gel electrophoresis (DIGE). The resulting protein differences show 14 reciprocal changes between *sμg* and hypergravity, and 7 overlapping proteins with compression, suggesting that mechanosensation in disparate contexts share a common proteomic link.

BACKGROUND

Mechanical forces profoundly impact living things. While much is known about mechanotransduction in specific sensory systems, little is known about generalized mechanosensation. A major barrier to understanding biomechanics is that the proteins involved in initially transducing general mechanical perturbation are not fully understood. A proteomic approach can help resolve conflicting theories of mechanotransduction. By understanding proteomic responses to mechanics, we can generate new approaches to understanding age-related disorders [139].

7.1 GRAVITY CAUSES DIVERSE BIOLOGICAL RESPONSES

in vivo responses to microgravity (μg) and simulated microgravity ($s\mu g$) have been observed in many model organisms, including *Drosophila* [75, 106, 121], zebrafish (*Danio rerio*) [37, 122], *E. coli* [123], yeast [124], rodents [79, 125–128], and others [74, 126, 129–132]. In vertebrate development, amphibians can ovulate, eggs develop, but fail to transition past tadpoles [133]. Rats and birds fail to develop motor skills for critical development [134].

In *Drosophila*, an integrative analysis of microarray data found subtle effects on the transcriptome in μg , with subtle opposite effects under hypergravity [187]. Specifically, μg and $s\mu g$ for 4 days had dramatic effects on gene expression in *Drosophila* larvae only when combined with the constraints of spaceflight [187]. In $s\mu g$ without environmental stressors, only five genes showed a > 2 -fold change; in $10g$, no genes cleared this threshold. Strikingly, the subthreshold pattern obtained in $s\mu g$ appears inverted in hypergravity [187]. This relationship was not present between $s\mu g$ and μg transcriptomes. This result suggests that the *Drosophila* transcriptome is finely tuned to changes in gravity.

A fundamental understanding of gravity's mechanism of transduction is still lacking. Despite responses to gravity across organisms and organ systems, the analysis of gravity-responsive genes has been inconclusive, with contradictory results, and limited commonality [189, 190]. While some proteomic work has been done in *Drosophila* adults [186], many effects were found to be from the magnetic levitation itself. Many genes show widespread sub-threshold changes [186–188]. It is also unclear how gravitational force is first transduced into a biological signal, or which proteins propagate that signal [34, 130, 198].

7.2 DEVELOPMENTAL MECHANICAL DEFORMATION

Developing embryos experience acute mechanical forces during gastrulation, the process by which a single-layered blastula folds into a multi-layered structure. In *Drosophila*, gastrulation begins with ventral furrow formation (VFF) when coordinated shape change induces a bending force to collapse the ventral furrow inwards, initiating mesoderm invagination [57]. The collective shape change during VFF is regulated by internal mechanical forces and the transcription factor Twist [57, 58]. Twist induces the expression of the secreted factor Fog [58], which activates the G-protein Concertina [59], leading to the reorganization of the actin cytoskeleton [59–61].

Surprisingly, both *twist* and VFF can also be regulated by the acute application of exogenous mechanical force [4, 66]. Although *twist* is normally expressed in ventral cells [63], acute mechanical deformation just before gastrulation leads to the expression of *twist* in all tissues, leading to a ventralized phenotype [65]. When *twist* expression is reduced by mutations in upstream genes or laser microsurgery, exogenous compression (indentation) with a blunt micro-needle recovers strong *twist* expression [3, 65, 67].

Although many mechanically responsive genes have been identified, the mechanisms behind transducing mechanical forces into biochemical signals have remained elusive [3, 10]. It remains unclear which molecules function as mechanosensors, whether they act independently, or to what extent their pathways integrate (76). A major limitation has been the manipulation of only one *Drosophila* embryo at a time, making proteomic techniques intractable. A mechanoproteomic approach can help resolve conflicting theories of mechanotransduction.

7.3 HIGH-THROUGHPUT PROTEOMIC APPROACHES

The literature on determining the biological effects of microgravity has a significant gap - it focuses on changes in transcription, without directly measuring changes in the proteins they encode [124, 190, 191]. Proteins are likely the initial sensors of gravity, which they then transduce to affect gene expression. Proteins mediate cell behavior more directly, and proteome abundance does not correlate with mRNA abundance [268]. A proteomic perspective will allow a more direct examination of how cells initially sense and respond to ubiquitous gravity deprivation.

A challenge in characterizing mechanical transduction pathways is that many organ systems are affected and interconnected. Using whole developing organisms *in vivo* has the advantage of capturing the complexity of a multicellular systems.

A challenge in characterizing mechanotransductive pathways *in vivo* is the manipulation of only one embryo at a time, making proteomic techniques intractable. We developed a novel mesofluidic device that can automatically align and immobilize hundreds of *Drosophila* embryos (Part ii). This device precisely compresses hundreds of embryos using pressure-actuated deformable sidewalls, allows for live imaging, and the retrieval of live embryos for post-analysis. The device itself does not affect survival or development, and does not induce anoxic arrest. Compressing embryos 7% for 4 hours or 22% for 10 minutes is sufficient to trigger the mechanical induction of *twist* (Chapter 5.5).

We have also developed and validated methods to apply *sμg* and hypergravity to meso-scale zebrafish embryos (Part iii Chapter 6.4). The principles behind *sμg* and hypergravity are discussed in 4.1 and 6.5. Here, we optimized these approaches for *Drosophila* embryos.

A powerful technique for discovering proteomic changes is DIGE. DIGE involves labeling proteins with pairs of differently colored fluorescent cyanine dyes that preserve protein charge, and have the same charge and mass. These properties allow two protein samples to be run together on the same gel under the same conditions, revealing differences in abundance, alternative splicing, and post-translational modification of all cellular proteins [290, 293].

In this context, DIGE provides several benefits over the more common liquid chromatography-mass spectrometry (LC-MS). Since proteins remain intact throughout the detection process, DIGE allows the detection of specific changes in the post-translational modification [290]. DIGE is more affordable [363, 364] allowing multiple biological and technical replicates to be run to a degree not possible with LC-MS. These properties create a unique opportunity for unbiased exploration of biological responses to mechanical forces at the proteomic level.

METHODS

7.4 ANIMALS

Oregon-R flies were a gift from Brooke McCartney, Carnegie Mellon University. Flies were kept at room temperature in plastic bottles filled with standard *Drosophila* breeding medium. For embryo collection, flies were transferred to 100 mL tri-corner beakers and capped with 60 mm Petri dishes (Fisher Scientific, Pittsburgh, USA) partially filled with a solution containing 1.5% agarose, 2.5% sucrose, 25% apple juice, and 0.15% p-hydroxybenzoic acid methyl ester (methyl paraben to inhibit mold growth) and allowed to gel. A dab of yeast paste (1:2 parts dry yeast to water) was added to each plate. Embryos were collected for three hours, dechorionated for 90 seconds in fresh 50% bleach, washed with distilled water, collected with a cell strainer (Bellco glass), and suspended in egg wash (0.7% NaCl and 0.4% Triton-X 100 in distilled water, 0.2 μ m-filtered, light-protected). Embryos were selected under stereoscope to collect those at early cellularization (Stage 5, 2-3 hours after laying) [309] so compression would occur before gastrulation.

7.5 APPLICATION OF MECHANICAL FORCE

Compression

Construction of a mesofluidic device has been described (Chapter 5). Stage 5 *Drosophila* embryos were sorted by stereoscope and loaded in batches of 130 into the mesofluidic device, which took approximately 10 minutes. Embryos were compressed by 22% for 10 minutes (5 PSI) and recovered, then lysed after 4 hours.

Simulated microgravity

Stage 5 *Drosophila* embryos were exposed to *smg* using a bioreactor (Synthecon, Houston, TX) as described (Chapter 6.4, Fig. 6.2). A 10-cm diameter cylinder was filled with *Drosophila* eggs in embryo egg wash solution. The cylinder was rotated around the x-axis so that the wall of water rotates around a Teflon core. A variable speed motor was adjusted to keep embryos in a circular orbit (15 RPM). After 4 hours, embryos were recovered and lysed.

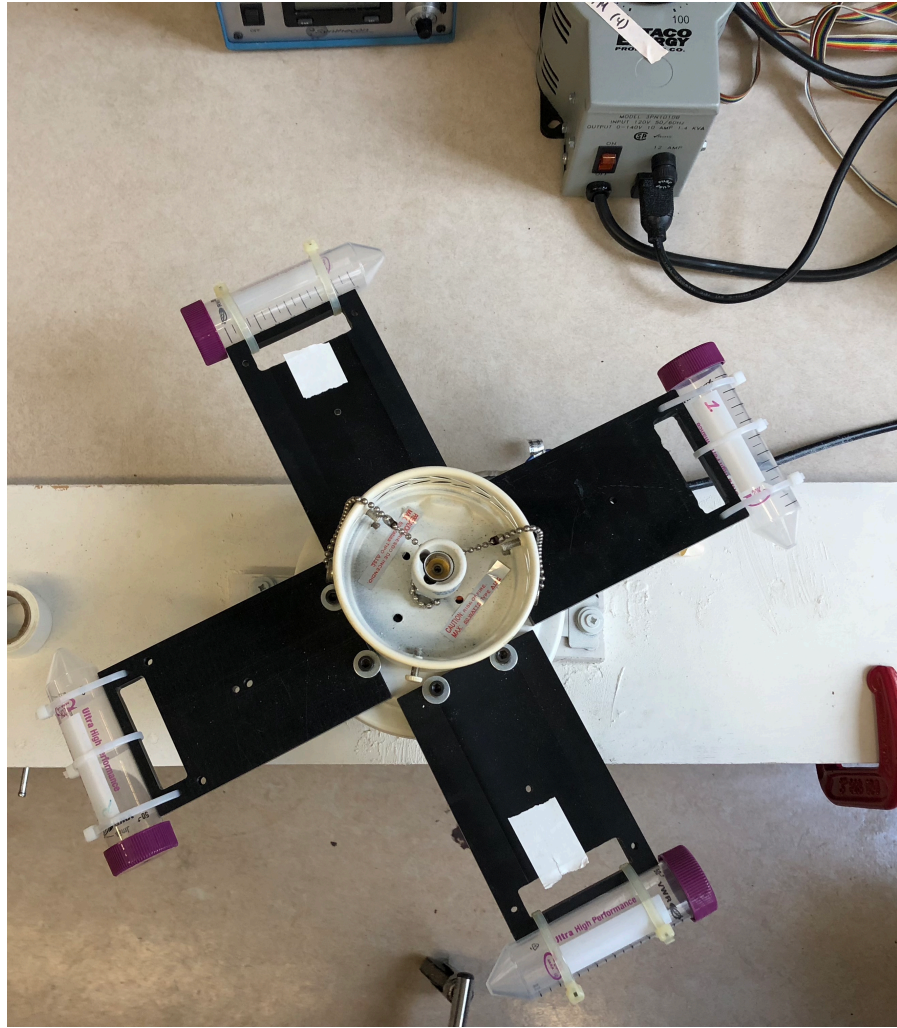


Figure 7.1: Custom centrifuge adapted to *Drosophila*. Fan blades were replaced by delrin adapters (Fig. 6.4). 50 mL centrifuge tubes accommodate embryos in 15 mL round-bottom tubes or adults in vials. A rheostat (upper right) controlled electrical power to customize the centrifuge speed.

Hypergravity

Stage 5 *Drosophila* embryos were placed in batches of 50 into 15-mL tubes filled with egg wash and sealed with parafilm. These were affixed to 50-mL centrifuge tubes zip-tied to the delrin fan blades described in Chapter 6.4. The fan was controlled by a rheostat, and speed was verified by tachometer, resulting in a net force of 3g for 4 hours. Control vials were placed horizontally near the centrifuge. After 4 hours, embryos were recovered and lysed.

Adult Drosophila

Drosophila were maintained as described in Chapter 5. Newly eclosed virgin adults were collected and sexed. 20 adults were placed in vials with molasses medium and loaded into 50-mL centrifuge tube portion of the custom centrifuge. The fan was spun for 9 days at 165 RPM resulting in a net force of 6g. The entire apparatus was placed in an empty dark room and undisturbed for 9 days. Control vials were positioned horizontally next to the centrifuge. After 9 days, flies were anaesthetized by CO₂ and decapitated by forceps. Heads and bodies were lysed separately.

7.6 LYSIS

Embryos were collected in a microfuge tube on ice. Egg wash was replaced three times with 0.01% DIGE wash buffer (diluted from 10x stock: 50 mg CHAPS, 250 μ L 1M Hepes 8.0 pH, DI water to 50 mL). This solution was replaced twice with lysis buffer (7 M urea, 2 M thiourea, 4% CHAPS, 10 mM DTT and 10 mM Na-Hepes pH 8.0). Tissue was homogenized with a fitted pestle and adjusted to 2 mg/mL protein concentration with lysis buffer as measured by Bradford assay.

7.7 DIGE

For an overview of 2D-difference gel electrophoresis (DIGE), see Fig. 4.2. Briefly, 100 μ g (micrograms) of protein were labeled with 2 μ L of either 1mM propyl-Cy3-NHS or 0.83 mM methyl-Cy5-NHS (CyDye DIGE Fluors; GE Healthcare) [292]. Reciprocal labeling was performed concurrently to control for dye-dependent changes and for technical replication. After 2DE [294], gels were fixed overnight in destain (40% methanol, 10% acetic acid). Fixed gels were imaged in a custom Structured Illumination Gel Imager [293].

The resulting image files were assigned a LUT of green (Cy3) or red (Cy5) and combined in Fiji (ImageJ) by converting to RGB color and adding. The resulting images were digitally morphed to a consensus image by overlaying them in Keynote (Apple Inc., Cupertino CA, USA), adjusting transparency, and aligning fiduciary markers (Fig. 7.7).

RESULTS & DISCUSSION

Groups of ≈ 300 *Drosophila* stage 5 embryos were subjected to 3g hypergravity, $s\mu g$, or 22% compression (5 PSI) in a mesofluidic device. Embryos were lysed, concentration measured by Bradford as described, diluted to 2 mg/mL, and analyzed by DIGE with reciprocal labeling.

The resulting proteomes showed subsets of 35 differences that repeated across technical and biological replicates. An overview of DIGE results are in Fig. 7.2. Spots were labeled with an arbitrary number following "A" for *above* the yolk – the large yellow streak at the center of gels – or "B" for *below* the yolk. Spot changes across all conditions are summarized in Table 7.1. Hypergravity showed 29 potential difference-proteins, $s\mu g$ showed 22. Compression gels resolved poorly, but with careful alignment, 12 potential differences were identified (Table 7.1). Two biological replicates for hypergravity and one for $s\mu g$ showed similar results. The process of identifying replicating spots has been described, with an example in Fig. 7.3.

7.8 MICROGRAVITY AND HYPERGRAVITY RECIPROCATE

Strikingly, 14 proteins showed reciprocal changes in simulated microgravity ($s\mu g$) and hypergravity. In $s\mu g$ compared to 1g controls, 9 enrichments and 5 depletions were also identified in hypergravity compared to 1g controls, where they showed the opposite response (Table 7.1).

The relationship between overlapping difference-proteins are visualized in Fig. 7.4. Differences in $s\mu g$ compared to 1g controls are represented by the X-axis, with depletion to the left and enrichment to the right. Differences in hypergravity compared to 1g controls are represented on the Y-axis, with no change on the X-intercept, enrichment above, and depletion below. For example, spots in quadrant IV (lower right) increased in $s\mu g$ and decreased in hypergravity.

Positions within a quadrant are arbitrary, except B6, A7, and B9, which showed a more extreme change, which was also reciprocated: the protein most highly enriched in hypergravity was also the protein most highly depleted in microgravity (Table 7.1). This result is preliminary and qualitative, and must be confirmed by photometric analysis. Nevertheless, the consistency across gels is intriguing, five of which can be seen in Fig. 7.2 along with a detail of the dotted box in Fig 7.3.

Notably, only one difference-protein increased slightly in both conditions compared to controls (A11), suggesting that these differences

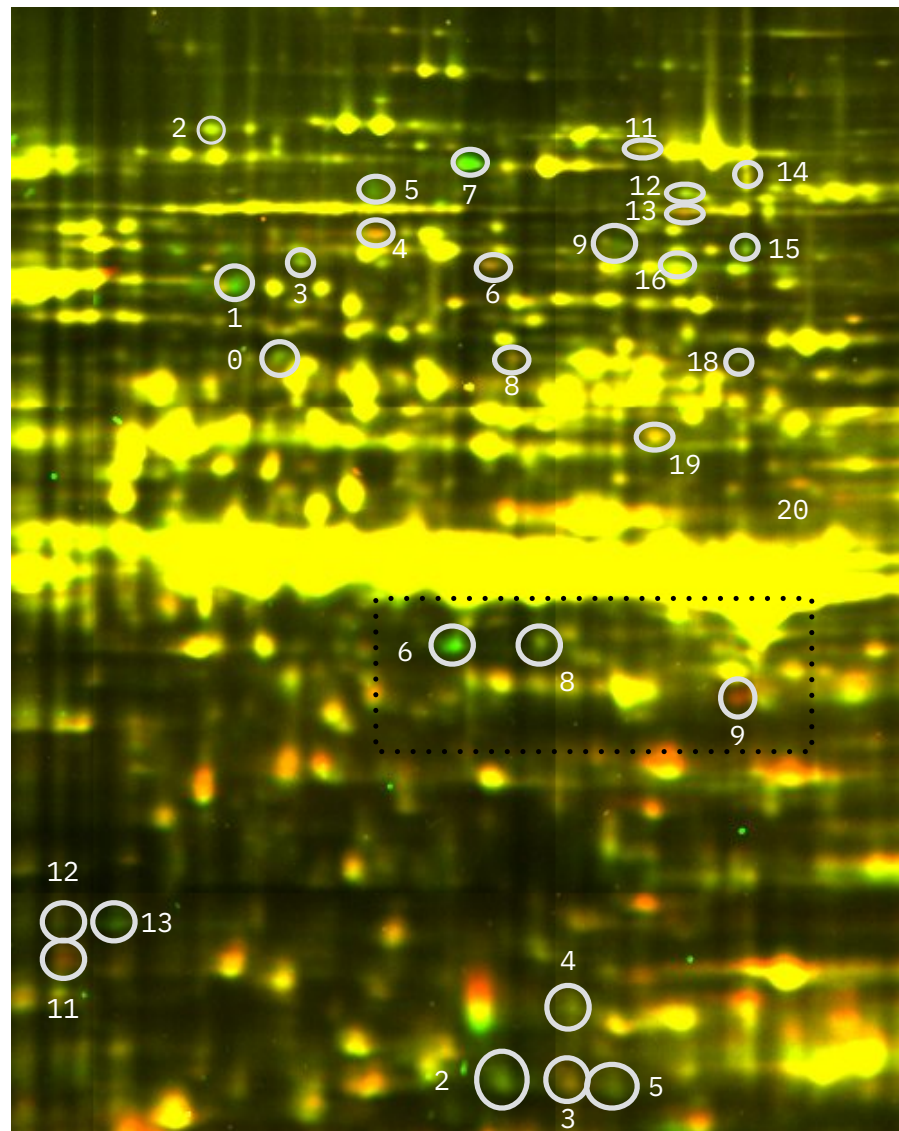


Figure 7.2: Representative DIGE comparing proteomes of ≈ 300 *Drosophila* embryos exposed to hypergravity (Cy5 red) or 1g control (Cy3 green). Two differentially labeled proteomes separate horizontally by IEF and vertically by SDS-PAGE. Proteins equally expressed appear yellow, proteins differentially expressed appear enriched in that color. Changes are confirmed by reciprocal labeling (dotted box detailed in Fig. 7.3) and summarized in Table 7.1. Uncircled differences were not sufficiently replicated and may be dye-dependent.

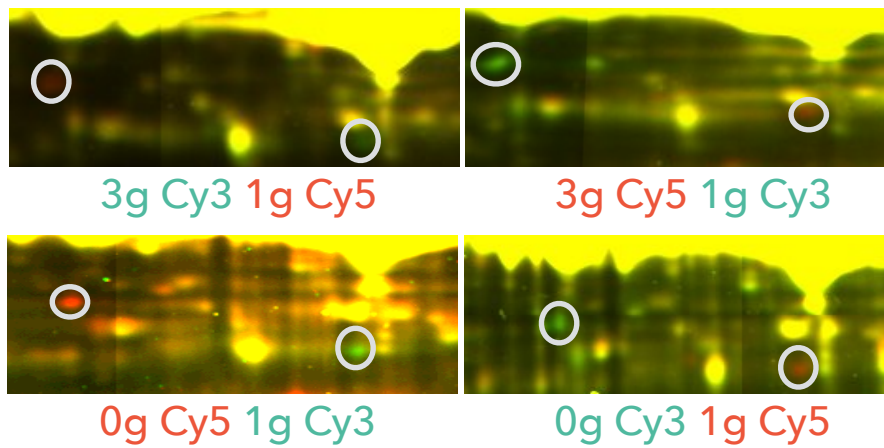


Figure 7.3: Reciprocal labeling confirms changes are not dye-dependent. Detail of dotted box in Fig. 7.2 from a biological replicate. Top row: proteins enriched $3g$ $Cy3$ appear reciprocally enriched in $3g$ $Cy5$. Bottom row: positioning and shape provides visual evidence that these same proteins differ in $s\mu g$ compared to $1g$ controls, which can be confirmed by LC-MS. Intriguingly, these proteins appear to change reciprocally between $3g$ and $s\mu g$.

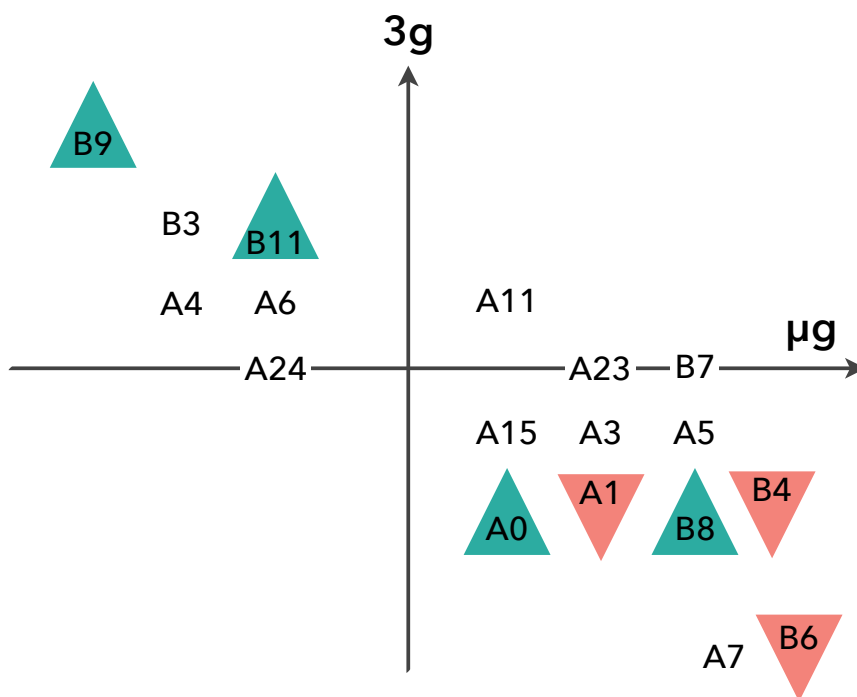


Figure 7.4: Visualization of relative protein changes across mechanical contexts. X-axis represents differences in $s\mu g$ compared to $1g$ controls, with depletion to the left and enrichment to the right of the Y-intercept. Y-axis represents differences in hypergravity compared to $1g$ controls. Protein differences also found in compression appear in up-green triangles (enriched) or down-red triangles (depleted). For example, spot names in quadrant IV (lower right) were enriched in $s\mu g$ and depleted in hypergravity, with $B6$ depleted after compression. Clustering in quadrants IV and II indicate reciprocal changes between $s\mu g$ and hypergravity (Table 7.1).

are not a generalized stress-response. Three differences appear unique to $s\mu g$ that were also identified in hypergravity, where they did not change compared to 1g controls. Ideally, all protein changes should be resolvable in both conditions, and may be informative. For example, two reciprocal differences in hypergravity – depleted A12 and enriched A13 – were not found in microgravity, but one enriched spot was found in its place, labeled A12.5. This potentially represents a PTM in hypergravity. Other potential PTM include A5/A4 and B11/B12, which could be confirmed by LC-MS.

If these shared differences across two disparate mechanical contexts are identified to be the same proteins by LC-MS, this presents proteomic evidence for a gravity-sensing pathway.

7.9 COMPRESSION FOLLOWS HYPERGRAVITY

Protein differences in compression are represented in Fig. 7.4 with an up-green triangle for enrichment or a down-red triangle for depletion. Twelve difference-proteins were identified after 10 minutes of 22% compression that were also found in $s\mu g$ or hypergravity (Fig. 7.5, Table 7.1). Of these, 83% (10/12) followed hypergravity: A1, B2, B4, B5, B6, B12, B13 decreased in both hypergravity and compression compared to controls; A19, B9, B11 increased in both hypergravity and compression compared to controls. Two compression differences opposed hypergravity and followed $s\mu g$: A0 and B8 were enriched in compression and $s\mu g$ but depleted in hypergravity. In contrast to reciprocation of changes between hypergravity and microgravity, protein differences in compression correlate with those in hypergravity (Fig. 7.5).

Notably, 7 proteins were found in all three conditions, with B6 and B9 showing the most extreme changes (Fig. 7.4). These present a target for future study to potentially link gravity-sensing pathways with compression-sensing pathways on the protein level.

7.10 PROTEOMIC COMPARISON IN ADULT *DROSOPHILA*

To test for hypergravity responses in adult *Drosophila*, 20 adult virgin males were spun in vials with food at 165 RPM (6g) for 9 days in darkness. Control vials were placed nearby, oriented horizontally to match the centrifuge, and match temperature, humidity, vibrational or magnetic effects. After 9 days, all flies showed 100% survival, and were decapitated. Separating heads eliminates confounding proteins that can be found due to eating. The bodies were lysed as described, and proteomes separated by DIGE as described. Representative gels are shown in Fig. 7.6. Six spots were consistently enriched in hypergravity com-



Figure 7.5: Shared protein differences in 3g and 22% compression. Visualization of results in Table 7.1. Alignment in quadrants I and III indicate strong correlation in difference proteins, suggesting that hypergravity and compression appear to share proteomic differences.

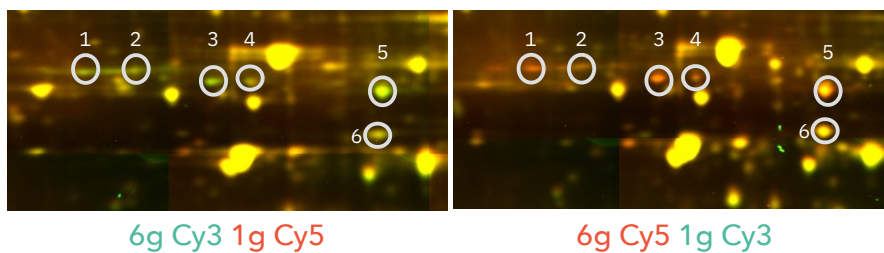


Figure 7.6: Representative pairs of reciprocally labeled DIGE from bodies of adult male *Drosophila* spun for 9 days at 6g compared to 1g controls. Spots identified by LC-MS in Table 7.2.

pared to 1g controls. These were cut from the gel and identified by LC-MS in Table 7.2.

Three of the six proteins identified match Hosamani 2016 [186], and three were novel, validating the approach of DIGE to find mechanoproteomic differences. No differences were found between sexes.

CONCLUSIONS

We report preliminary proteomic results from three modes of mechanical stimulation analyzed by DIGE for the first time.

In *Drosophila* stage-5 embryos, 35 differences were found, of which 14 showed reciprocal changes between *sμg* and 3g. Three proteins showed a more extreme enrichment/depletion, which was also reciprocated

in extremity in the opposite condition. Of these, 7 proteins were also found in compression. If confirmed by LC-MS, these may represent a shared proteomic link between disparate contexts of mechanotransduction. Proteins that are not shared may indicate unique responses to different modes of mechanostimulation.

In *Drosophila* adults, six proteins were enriched after exposure to 6g hypergravity for 9 days, and identified by LC-MS. The resulting proteins consistent with the literature on known changes in *Drosophila* under altered gravity.

This relatively small set of proteins contradicts the thousands of candidates seen by transcriptomic approaches, isobaric tagging LC-MS [186] and DIGE approaches in *Daphnia magna* [365]. With regards to DIGE in *Daphnia*, the resulting gels show almost no overlap between conditions, which is inconsistent with results the Minden lab has observed over decades in DIGE. Critically, no reciprocal control was reported, which validates that protein differences are due to conditions themselves and not dye-dependent.

However, this small set of changes is consistent, at least in order of magnitude, with the most carefully controlled studies in *Drosophila* [187]. By carefully controlling conditions, eliminating dye-dependent changes, working on the proteomic level, and using the sensitive power of DIGE, we can identify true changes in cell behavior due to altered gravity, and resolve some conflict from transcriptomic approaches.

The next critical hurdle for these difference-candidates is identification by LC-MS, especially for proteins that appear to be shared between conditions, to quantify changes in magnitude among gels, to resolve additional biological replicates of compression, and to validate these changes by RNAi knockdown to reverse the DIGE phenotype.

Just as DIGE aided comparison between varying 2DE gels, so too does DIGE itself require aids in comparison between variations in biological replicates (Fig. 7.7). Digitally morphing gels was extremely helpful in this regard, allowing rapid comparison between four gels at a time to identify differences in subtle proteomic shifts. It is my hope that this practice becomes standardized, and eventually automated. A similar principle has been demonstrated in zebrafish [357].

These results are incomplete, but the overlap between disparate modes of mechanostimulation is intriguing. A *Drosophila* – DIGE mechanoproteomic approach appears to be a powerful system to test the hypothesis that mechanosensation in disparate contexts shares a common proteomic link.

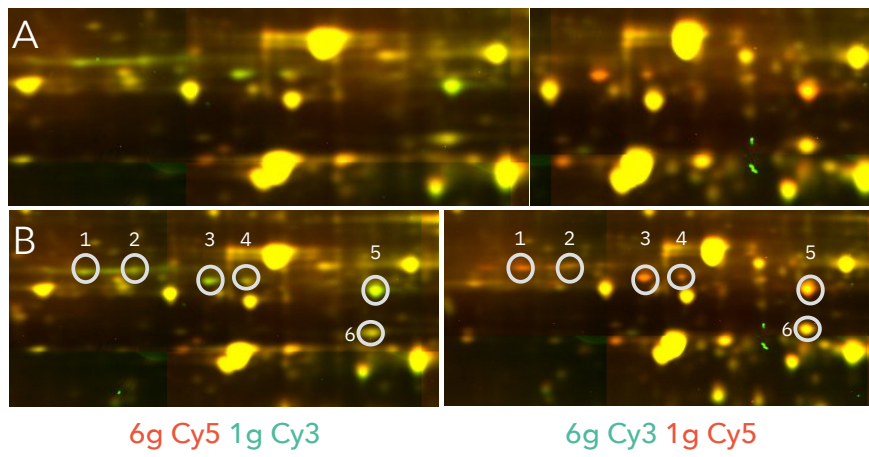


Figure 7.7: Example of digitally morphing *DIGE* gels to facilitate comparison. (A) Section of unmorphed gels from adult flies after 6g. (B) Morphing creates consistent alignment which facilitates identification of spots.

SPOT	38 Cy3	38 Cy5	sμg Cy3	sμg Cy5	22% Cy3
A0	↓	↓	↑	↑	↑
1	↓	↓		↑	↓
2	↓	↓			
3	↓	↓	↑	↑	
4	↑	↑	↓	↓	
5	↓	↓	↑	↑	
6	↑	↑	↓	↓	
7	↓↓	↓↓	↑↑	↑↑	
9	↓	↓			
11	↑	↑	↑	↑	
12	↓	↓			
12.5			↑	↑	
13	↑	↑			
14	↑	↑			
15	↓↓	↓	↑	↑	
16	↓	↓			
18	↓	↓			
19	↑	↑			↑
21			↓	↓	
22			↓	↓	
23	=	=	↓	↓	
24	=	=	↑	↑	
25			↑	↑	
26			↑	↑	
B2	↓	↓			↓
3	↑	↑	↓	↓	
4	↓	↓	↑	↑	↓
5	↓	↓			↓
6	↓↓	↓↓	↑	↑↑	↓
7	=	=	↑	↑	
8	↓	↓	↑	↑	↑
9	↑↑	↑↑	↓↓	↓↓	↑
11	↑	↑	↓		↑
12	↓	↓			↓
13	↓	↓			↓

Table 7.1: Summary of DIGE difference-proteins in Fig. 7.2 across three conditions. Each column is a technical replicate. Spots above midline are "A:" Above the yolk. Spots below: "B:" Below yolk. Color indicates spot color, arrow indicates change in abundance compared to control.

SPOT	PROTEIN	FUNCTION	NOVEL
1	Upheld	muscle related	*
2	NADH dehydrogenase	metabolic	*
3	Isocitrate dehydrogenase	metabolic	†
4	Serpine	immune activity	†
5	Actin	muscle related	†
6	Z-band protein	muscle related	*

Table 7.2: LC-MS identification of proteins enriched in adult *Drosophila* bodies after 9 days at 6g (Fig. 7.6). Proteins matching Hosamani 2016 [186] marked * novel proteins marked †.

Part V

CONCLUSIONS

THE HOW AND THE WHY

In her 2011 play *The How and the Why*, Sarah Treem writes that science consists of two essential questions. Although we spend most of our time answering *how* something happens, at some point we must step back to consider *why* it happens – of what benefit is this to an organism? That question certainly comes up in mechanotransduction: why do *Drosophila* have this alternative mechanical signaling pathway at all? Even more confounding is sensing gravity: why would an organism contain a response to something it never experienced over evolutionary history?

One answer in development is that mechanics are a form of long-range signaling. Developing tissue far away can synchronize and coordinate without waiting for chemical diffusion. This may be particularly useful in development when the signaling machinery is still developing. Another answer is that mechanics serve as a checkpoint: mechanical regulation of *Myo-II* ensures constriction is occurring before the embryo commits to mesoderm invagination.

Lately I've wondered if the entire distinction between biochemical and biomechanical signaling is a reductive model that holds us back. These categories seem increasingly permeable and tightly interwoven: cell apoptosis is well understood chemically, but also affects cell deformation and crowding. Substrate stiffness and buckling drive differentiation, which loops back to affect tension and stiffness. Perhaps the entire approach of explaining the cell through chemical signaling pathways is part of our intellectual heritage in Descartes – it's a form of mind-body dualism in which we desire to ignore, and thereby escape, the physical world.

As for sensing gravity, I've thought of this like a fish discovering water – it is only when we left Earth that we realized it mattered. Ten years ago I had some wild speculation on how gravitational signals could benefit an organism as a conserved circadian signal [8]; alas, some of those ideas are refuted by the results in Part [iii](#), and the rest I was unable to investigate.

I found the result of 14 reciprocal proteins in gravity truly surprising. One of my biggest regrets is not getting to that point sooner to pursue that question through protein identification. So much of this work has involved getting stuck, sometimes for months, and several times I've made the mistake of persisting in the same approach when I should have tried something different. I was troubleshooting imaging

for months until I realized I had contaminated the colony and lost the GFP line; I ran DIGE on 19-hour gravity exposures for almost a year before trying a 4-hour exposure at gastrulation, which immediately delivered results. These loops of persistence without results were demoralizing, instilled a habit of doubting every result, and made this process harder than it needed to be.

One of my best decisions was investing a little time in algorithmic thinking. Coding is unreasonably useful; I am constantly amazed at what I can do with almost zero knowledge.

This is a moment I've been looking forward to for about 20 years. It's easy for me to focus on what could have been better, what I wish I had done differently. At the same time, I am grateful for the unusual path this has taken, the persistence I've learned, and the study of interdisciplinary collaboration. I see this degree as the art of creating knowledge, which is both more messy and more sacred than I had imagined.

BIBLIOGRAPHY

- [1] C F Dewey, S R Bussolari, M A Gimbrone, and P F Davies. "The dynamic response of vascular endothelial cells to fluid shear stress." In: *Journal of biomechanical engineering* 103.3 (Aug. 1981), pp. 177–185.
- [2] F C Serluca, I A Drummond, and M C Fishman. "Endothelial signaling in kidney morphogenesis: A role for hemodynamic forces." In: *Current Biology* 12.6 (2002), pp. 492–497.
- [3] Eric Brouzés and Emmanuel Farge. "Interplay of mechanical deformation and patterned gene expression in developing embryos." In: *Current opinion in genetics & development* 14.4 (Aug. 2004), pp. 367–374.
- [4] María Elena Fernández-Sánchez, Thibaut Brunet, Jens-Christian Röper, and Emmanuel Farge. "Mechanotransduction's Impact on Animal Development, Evolution, and Tumorigenesis." In: *Annual Review of Cell and Developmental Biology* 31.1 (Nov. 2015), pp. 373–397.
- [5] P M Freeman, R N Natarajan, J H Kimura, and T P Andriacchi. "Chondrocyte Cells Respond Mechanically to Compressive Loads." In: *Journal of Orthopaedic Research* 12.3 (May 1994), pp. 311–320.
- [6] Elisabeth H Burger and Jenneke Klein-Nulend. "Mechanotransduction in bone—role of the lacuno-canalicular network." In: *The FASEB journal* 13 Suppl (1999), S101–12.
- [7] Adam J Engler, Shamik Sen, H Lee Sweeney, and Dennis E Discher. "Matrix Elasticity Directs Stem Cell Lineage Specification." In: *Cell* 126.4 (Aug. 2006), pp. 677–689.
- [8] Stephen J Moorman and Ardon Z Shorr. "The primary cilium as a gravitational force transducer and a regulator of transcriptional noise." In: 237.8 (Aug. 2008), pp. 1955–1959.
- [9] Donald E Ingber. "Cellular mechanotransduction: putting all the pieces together again." In: *The FASEB journal* 20.7 (May 2006), pp. 811–827.
- [10] Tatiana Merle and Emmanuel Farge. "ScienceDirect Trans-scale mechanotransductive cascade of biochemical and biomechanical patterning in embryonic development: the light side of the force." In: *Current opinion in cell biology* 55 (July 2018), pp. 111–118.

- [11] Thomas Lecuit and Pierre-François Lenne. "Cell surface mechanics and the control of cell shape, tissue patterns and morphogenesis." In: *Nature Reviews Molecular Cell Biology* 8.8 (Aug. 2007), pp. 633–644.
- [12] Huy Quang Le et al. "Mechanical regulation of transcription controls Polycomb-mediated gene silencing during lineage commitment." In: *Nature Cell Biology* 18.8 (July 2016), pp. 864–875.
- [13] B D Matthews. "Cellular adaptation to mechanical stress: role of integrins, Rho, cytoskeletal tension and mechanosensitive ion channels." In: *Journal of Cell Science* 119.3 (Feb. 2006), pp. 508–518.
- [14] J Matthew Barnes, Laralynne Przybyla, and Valerie M Weaver. "Tissue mechanics regulate brain development, homeostasis and disease." In: *Journal of Cell Science* 130.1 (Jan. 2017), pp. 71–82.
- [15] Diana E Jaalouk and Jan Lammerding. "Mechanotransduction gone awry." In: *Nature Reviews Molecular Cell Biology* 10.1 (Jan. 2009), pp. 63–73.
- [16] Florence Broders-Bondon, Thanh Huong Nguyen Ho-Boulidoires, María Elena Fernández-Sánchez, and Emmanuel Farge. "Mechanotransduction in tumor progression: The dark side of the force." In: *Journal of Cell Biology* 217.5 (May 2018), pp. 1571–1587.
- [17] Ahlke Heydemann and Elizabeth M McNally. "Consequences of Disrupting the Dystrophin-Sarcoglycan Complex in Cardiac and Skeletal Myopathy." In: *Trends in cardiovascular medicine* 17.2 (Feb. 2007), pp. 55–59.
- [18] A N Chang and J D Potter. "Sarcomeric protein mutations in dilated cardiomyopathy." In: *Heart Failure Reviews* 10.3 (Sept. 2005), pp. 225–235.
- [19] Jenneke Klein-Nulend, R G Bacabac, J P Veldhuijzen, and JJWA van Loon. "Microgravity and bone cell mechanosensitivity." In: *Advances in space research : the official journal of the Committee on Space Research (COSPAR)* 32.8 (2003), pp. 1551–1559.
- [20] M A Gimbrone, J N Topper, T Nagel, K R Anderson, and G Garcia-Cardena. "Endothelial dysfunction, hemodynamic forces, and atherogenesis." In: *Atherosclerosis v: the Fifth Saratoga Conference* 902 (2000), pp. 230–240.
- [21] Surya M Nauli et al. "Polycystins 1 and 2 mediate mechanosensation in the primary cilium of kidney cells." In: *Nature Genetics* 33.2 (Feb. 2003), pp. 129–137.
- [22] Derek A Affonce and Kenneth R Lutchen. "New perspectives on the mechanical basis for airway hyperreactivity and airway hypersensitivity in asthma." In: *Journal of Applied Physiology* 101.6 (Dec. 2006), pp. 1710–1719.

- [23] Parth Patwari and Richard T Lee. "Mechanical Control of Tissue Morphogenesis." In: *Circulation Research* 103.3 (Aug. 2008), pp. 234–243.
- [24] S Nonaka et al. "Randomization of left-right asymmetry due to loss of nodal cilia generating leftward flow of extraembryonic fluid in mice lacking KIF3B motor protein." In: *Cell* 95.6 (Dec. 1998), pp. 829–837.
- [25] S Huang and D E Ingber. "The structural and mechanical complexity of cell-growth control." In: *Nature Cell Biology* 1.5 (Sept. 1999), E131–E138.
- [26] Subra Suresh. "Biomechanics and biophysics of cancer cells." In: *Acta biomaterialia* 3.4 (July 2007), pp. 413–438.
- [27] Sui Huang and Donald E Ingber. "Cell tension, matrix mechanics, and cancer development." In: *Cancer cell* 8.3 (Sept. 2005), pp. 175–176.
- [28] Matthew J Paszek et al. "Tensional homeostasis and the malignant phenotype." In: *Cancer cell* 8.3 (Sept. 2005), pp. 241–254.
- [29] Martin Chalfie. "Neurosensory mechanotransduction." In: *Nature Reviews Molecular Cell Biology* 10.1 (Jan. 2009), pp. 44–52.
- [30] Jeffrey R Holt and David P Corey. "Two Mechanisms for Transducer Adaptation in Vertebrate Hair Cells." In: *Proceedings of the National Academy of Sciences of the United States of America* 97.22 (Oct. 2000), pp. 11730–11735.
- [31] Melissa A Vollrath, Kelvin Y Kwan, and David P Corey. "The Micromachinery of Mechanotransduction in Hair Cells." In: *Annual Review of Neuroscience* 30.1 (July 2007), pp. 339–365.
- [32] Popi Syntichaki and Nektarios Tavernarakis. "Genetic Models of Mechanotransduction: The Nematode *Caenorhabditis elegans*." In: *Physiological reviews* 84.4 (Oct. 2004), pp. 1097–1153.
- [33] D F Eberl, R W Hardy, and M J Kernan. "Genetically similar transduction mechanisms for touch and hearing in *Drosophila*." In: *Journal of Neuroscience* 20.16 (2000), pp. 5981–5988.
- [34] A Wayne Orr, Brian P Helmke, Brett R Blackman, and Martin A Schwartz. "Mechanisms of Mechanotransduction." In: *Developmental Cell* 10.1 (Jan. 2006), pp. 11–20.
- [35] Viola Vogel and Michael Sheetz. "Local force and geometry sensing regulate cell functions." In: *Nature Reviews Molecular Cell Biology* 7.4 (Feb. 2006), pp. 265–275.
- [36] H R Wirtz and L G Dobbs. "The effects of mechanical forces on lung functions." In: *Respiration physiology* 119.1 (Jan. 2000), pp. 1–17.

- [37] Stephen J Moorman, Naoko Shimada, Gbalabo Sokunbi, and Cynthia Pfirrmann. "Simulated-microgravity induced changes in gene expression in zebrafish embryos suggest that the primary cilium is involved in gravity transduction." In: *Gravitational and Space Biology* 20.2 (2007).
- [38] Donald Ingber. "Mechanobiology and diseases of mechanotransduction." In: *Annals of Medicine* 35.8 (July 2009), pp. 564–577.
- [39] Thomas Iskratsch, Haguy Wolfenson, and Michael P Sheetz. "Appreciating force and shape — the rise of mechanotransduction in cell biology." In: *Nature Publishing Group* 15.12 (Oct. 2014), pp. 825–833.
- [40] B Martinac and C D Cox. "Mechanosensory Transduction: Focus on Ion Channels." In: *Reference Module in Life Sciences*. Elsevier, 2017, pp. 1–48.
- [41] Michele A Wozniak and Christopher S Chen. "Mechanotransduction in development: a growing role for contractility." In: *Nature Reviews Molecular Cell Biology* 10.1 (Jan. 2009), pp. 34–43.
- [42] Dennis E Discher, Paul Janmey, and Yu-li Wang. "Tissue Cells Feel and Respond to the Stiffness of Their Substrate." In: *Science* 310.5751 (Nov. 2005), pp. 1139–1143.
- [43] Tyler J Kirby and Jan Lammerding. "Emerging views of the nucleus as a cellular mechanosensor." In: *Nature Cell Biology* (Mar. 2018), pp. 1–9.
- [44] Sangkyun Cho, Jerome Irianto, and Dennis E Discher. "Mechanosensing by the nucleus: From pathways to scaling relationships." In: *The Journal of cell biology* 105.2 (Jan. 2017), jcb.201610042–11.
- [45] Gregory R Fedorchak, Ashley Kaminski, and Jan Lammerding. "Cellular mechanosensing: Getting to the nucleus of it all." In: *Progress in biophysics and molecular biology* 115.2-3 (Aug. 2014), pp. 76–92.
- [46] Yekaterina A Miroshnikova, Michele M Nava, and Sara A Wickström. "Emerging roles of mechanical forces in chromatin regulation." In: *Journal of Cell Science* 130.14 (July 2017), pp. 2243–2250.
- [47] Arash Tajik et al. "Transcription upregulation via force-induced direct stretching of chromatin." In: *Nature Materials* 15.12 (Aug. 2016), pp. 1287–1296.
- [48] Ning Wang, Jessica D Tytell, and Donald E Ingber. "Mechanotransduction at a distance: mechanically coupling the extracellular matrix with the nucleus." In: *Nature Reviews Molecular Cell Biology* 10.1 (Jan. 2009), pp. 75–82.

- [49] Mir H Ali and Paul T Schumacker. "Endothelial responses to mechanical stress: where is the mechanosensor?" In: *Critical care medicine* 30.5 Suppl (May 2002), S198–206.
- [50] Nitzan Resnick et al. "Fluid shear stress and the vascular endothelium: for better and for worse." In: *Progress in biophysics and molecular biology* 81.3 (Apr. 2003), pp. 177–199.
- [51] Donald E Ingber. "Tensegrity II. How structural networks influence cellular information processing networks." In: *Journal of Cell Science* 116.Pt 8 (Apr. 2003), pp. 1397–1408.
- [52] Nicolas Di-Poï et al. "Changes in Hox genes' structure and function during the evolution of the squamate body plan." In: *Nature* 464.7285 (Mar. 2010), pp. 99–103.
- [53] D St Johnston and C Nüsslein-Volhard. "The origin of pattern and polarity in the Drosophila embryo." In: *Cell* 68.2 (Jan. 1992), pp. 201–219.
- [54] Victoria E Foe. "Mitotic Domains Reveal Early Commitment of Cells in Drosophila Embryos." In: *Development* 107.1 (Sept. 1989), pp. 1–22.
- [55] Zvi Kam, Jonathan S Minden, David A Agard, John W Sedat, and Maria Leptin. "Drosophila gastrulation: analysis of cell shape changes in living embryos by three-dimensional fluorescence microscopy." In: *dev.biologists.org* ().
- [56] D Sweeton, S Parks, M Costa, and E Wieschaus. "Gastrulation in Drosophila: the formation of the ventral furrow and posterior midgut invaginations." In: *Development* 112.3 (July 1991), pp. 775–789.
- [57] Y T Ip and T Gridley. "Cell movements during gastrulation: Snail dependent and independent pathways." In: *Current opinion in genetics & development* 12.4 (Aug. 2002), pp. 423–429.
- [58] M Costa, E T Wilson, and E Wieschaus. "A Putative Cell Signal Encoded by the Folded Gastrulation Gene Coordinates Cell-Shape Changes During Drosophila Gastrulation." In: *Cell* 76.6 (1994), pp. 1075–1089.
- [59] S Parks and E Wieschaus. "The Drosophila gastrulation gene *concertina* encodes a G α -like protein." In: *Cell* 64.2 (1991), pp. 447–458.
- [60] K Barrett, Maria Leptin, and J Settleman. "The Rho GTPase and a putative RhoGEF mediate a signaling pathway for the cell shape changes in Drosophila gastrulation." In: *Cell* 91.7 (Dec. 1997), pp. 905–915.

- [61] U Häcker and N Perrimon. "DRhoGEF2 encodes a member of the Dbl family of oncogenes and controls cell shape changes during gastrulation in *Drosophila*." In: *Genes & Development* 12.2 (Jan. 1998), pp. 274–284.
- [62] B Thisse, C Stoetzel, C Gorostiza-Thisse, and F Perrin-Schmitt. "Sequence of the twist gene and nuclear localization of its protein in endomesodermal cells of early *Drosophila* embryos." In: *The EMBO Journal* 7.7 (July 1988), pp. 2175–2183.
- [63] J L Boulay, C Dennefeld, and A Alberga. "The *Drosophila* developmental gene snail encodes a protein with nucleic acid binding fingers." In: *Nature* 330.6146 (Dec. 1987), pp. 395–398.
- [64] Lei Gong et al. "*Drosophila* ventral furrow morphogenesis: a proteomic analysis." In: *Development* 131.3 (Feb. 2004), pp. 643–656.
- [65] Emmanuel Farge. "Mechanical Induction of Twist in the *Drosophila* Foregut/Stomodeal Primordium." In: *Current Biology* 13.16 (Aug. 2003), pp. 1365–1377.
- [66] Alyssa J Manning and Stephen L Rogers. "The Fog signaling pathway: Insights into signaling in morphogenesis." In: *Developmental Biology* 394.1 (Oct. 2014), pp. 6–14.
- [67] Philippe-Alexandre Pouille, Padra Ahmadi, Anne-Christine Brunet, and Emmanuel Farge. "Mechanical signals trigger Myosin II redistribution and mesoderm invagination in *Drosophila* embryos." In: *Science Signaling* 2.66 (Apr. 2009), ra16.
- [68] Alyssa J Manning, Kimberly A Peters, Mark Peifer, and Stephen L Rogers. "Regulation of epithelial morphogenesis by the G protein-coupled receptor mist and its ligand fog." In: *Science Signaling* 6.301 (Nov. 2013), ra98–ra98.
- [69] R E Dawes-Hoang et al. "folded gastrulation, cell shape change and the control of myosin localization." In: *Development* 134.24 (Dec. 2007), pp. 4507–4507.
- [70] Adam C Martin, Matthias Kaschube, and Eric F Wieschaus. "Pulsed contractions of an actin-myosin network drive apical constriction." In: *Nature* 457.7228 (Jan. 2009), pp. 495–501.
- [71] M Janmaleki, M Pachenari, S M Seyedpour, R Shahghadami, and A Sanati-Nezhad. "Impact of Simulated Microgravity on Cytoskeleton and Viscoelastic Properties of Endothelial Cell." In: *Scientific Reports* (Aug. 2016), pp. 1–11.
- [72] F A Cucinotta et al. "Space radiation and cataracts in astronauts." In: *Radiation Research* 156.5 (Nov. 2001), pp. 460–466.

- [73] Erica K Low et al. "Microgravity Impairs DNA Damage Repair in Human Hematopoietic Stem/Progenitor Cells and Inhibits Their Differentiation into Dendritic Cells." In: *Stem Cells and Development* (July 2018), scd.2018.0052–31.
- [74] Cécile Huin-Schohn et al. "Gravity changes during animal development affect IgM heavy-chain transcription and probably lymphopoiesis." In: *The FASEB journal* 27.1 (Jan. 2013), pp. 333–341.
- [75] Katherine Taylor et al. "Toll mediated infection response is altered by gravity and spaceflight in *Drosophila*." In: *PLoS ONE* 9.1 (2014), e86485.
- [76] C Drummer, R Gerzer, F Baisch, and M Heer. "Body fluid regulation in microgravity differs from that on Earth: an overview." In: *Pflügers Archiv* (2000).
- [77] R M Bagdigian, D L Carter, and J Bedard. "Status of the regenerative ECLSS water recovery system." In: *International Conference On Environmental Systems* 1 (2007).
- [78] T F Lang. "What do we know about fracture risk in long-duration spaceflight?" In: *J Musculoskelet Neuronal Interact* 6.4 (Oct. 2006), pp. 319–321.
- [79] R T Turner. "Invited review: what do we know about the effects of spaceflight on bone?" In: *Journal of applied physiology (Bethesda, Md. : 1985)* 89.2 (Aug. 2000), pp. 840–847.
- [80] Daniel D Bikle, Takeshi Sakata, and Bernard P Halloran. "The impact of skeletal unloading on bone formation." In: *Gravitational and space biology bulletin : publication of the American Society for Gravitational and Space Biology* 16.2 (June 2003), pp. 45–54.
- [81] Millie Hughes-Fulford, Raymond Tjandrawinata, Jamie Fitzgerald, Kim Gasuad, and Vicki Gilbertson. "Effects of Microgravity on Osteoblast Growth." In: *Gravitational and Space Biology* 11.2 (May 2007).
- [82] Yasir Arfat et al. "Physiological Effects of Microgravity on Bone Cells." In: *Calcified Tissue International* 94.6 (Apr. 2014), pp. 569–579.
- [83] Scott M Smith et al. "Men and women in space: bone loss and kidney stone risk after long-duration spaceflight." In: *Journal of Bone and Mineral Research* 29.7 (July 2014), pp. 1639–1645.
- [84] H Vandenburg, J Chromiak, J Shansky, M Del Tatto, and J Lemaire. "Space travel directly induces skeletal muscle atrophy." In: *The FASEB journal* 13.9 (June 1999), pp. 1031–1038.
- [85] A I Grigoriev. "Summing-up cosmonaut participation in long-term space flights." In: *Advances in Space Research* 12.1 (1992), pp. 323–328.

- [86] Scott M Smith et al. "Benefits for bone from resistance exercise and nutrition in long-duration spaceflight: Evidence from biochemistry and densitometry." In: *Journal of Bone and Mineral Research* 27.9 (Aug. 2012), pp. 1896–1906.
- [87] P A Whitson, R A Pietrzyk, and CYC Pak. "Renal stone risk assessment during space shuttle flights." In: *Journal of Urology* 158.6 (Dec. 1997), pp. 2305–2310.
- [88] P A Whitson, R A Pietrzyk, Morukov, BV, and C F Sams. "The risk of renal stone formation during and after long duration space flight." In: *Nephron* 89.3 (Nov. 2001), pp. 264–270.
- [89] Nicholas Rt Drinnan and Alexandra Begougne De Juniac. "The effects of microgravity on the urological system: a review." In: *Journal of Clinical Urology* 6.6 (Nov. 2013), pp. 391–394.
- [90] Michael S Leapman et al. "Up and Away: Five Decades of Urologic Investigation in Microgravity." In: *Urology* 106 (Aug. 2017), pp. 18–25.
- [91] André E Aubert, Frank Beckers, and Bart Verheyden. "Cardiovascular function and basics of physiology in microgravity." In: *Acta cardiologica* 60.2 (Apr. 2005), pp. 129–151.
- [92] Joan Vernikos and Victor S Schneider. "Space, gravity and the physiology of aging: parallel or convergent disciplines? A mini-review." In: *Gerontology* 56.2 (2010), pp. 157–166.
- [93] DC Holley, C W DeRoshia, M M Moran, and C E Wade. "Chronic centrifugation (hypergravity) disrupts the circadian system of the rat." In: *Journal of applied physiology (Bethesda, Md. : 1985)* 95.3 (Sept. 2003), pp. 1266–1278.
- [94] Danilo Ranieri, Alessandra Cucina, Mariano Bizzarri, Maurizio Alimandi, and Maria Rosaria Torrisi. "Microgravity influences circadian clock oscillation in human keratinocytes." In: *FEBS OPEN BIO* 5.C (2015), pp. 717–723.
- [95] DC Holley, C W DeRoshia, M M Moran, and C E Wade. "Chronic centrifugation (hypergravity) disrupts the circadian system of the rat." In: *Journal of Applied Physiology* 95.3 (Sept. 2003), pp. 1266–1278.
- [96] G C Sieck. "Highlighted topics series: cellular responses to mechanical stress." In: *Journal of Applied Physiology* 89.4 (Oct. 2000), pp. 1253–1254.
- [97] M V Narici and M D de Boer. "Disuse of the musculo-skeletal system in space and on earth." In: *European Journal of Applied Physiology* 111.3 (July 2010), pp. 403–420.
- [98] Gerald Sonnenfeld, Janet S Butel, and William T Shearer. "Effects of the space flight environment on the immune system." In: *Reviews on environmental health* 18.1 (Jan. 2003), pp. 1–17.

- [99] J M Davidson, A M Aquino, S C Woodward, and W W Wilfinger. "Sustained microgravity reduces intrinsic wound healing and growth factor responses in the rat." In: *The FASEB journal* 13.2 (Feb. 1999), pp. 325–329.
- [100] D J Anderson, M F Reschke, J E Homick, and S A Werness. "Dynamic posture analysis of Spacelab-1 crew members." In: *Experimental Brain Research* 64.2 (1986), pp. 380–391.
- [101] Viktor S Kokhan, Marina I Matveeva, Azat Mukhametov, and Andrey S Shtemberg. "Risk of defeats in the central nervous system during deep space missions." In: *Neuroscience and Biobehavioral Reviews* 71 (Oct. 2016), pp. 1–53.
- [102] R Marco et al. "Microgravity effects on *Drosophila melanogaster* development and aging: comparative analysis of the results of the Fly experiment in the Biokosmos 9 biosatellite flight." In: *Advances in space research : the official journal of the Committee on Space Research (COSPAR)* 12.1 (1992), pp. 157–166.
- [103] E de Juan et al. "The "ageing" experiment in the spanish soyuz mission to the international space station." In: *Microgravity Science and Technology* 19.5-6 (2007), pp. 170–174.
- [104] R Herranz, D A Laván, C E Dijkstra, and O J Larkin. "Drosophila Behaviour & Gene expression in altered gravity conditions: Comparison between Space and ground facilities." In: (2008).
- [105] R Marco, I Vernos, J González, and M Calleja. "Embryogenesis and aging of *Drosophila melanogaster* flown in the space shuttle. Preliminary analysis of experiment fly 15E." In: *Die Naturwissenschaften* 73.7 (July 1986), pp. 431–432.
- [106] A Benguria et al. "Microgravity effects on *Drosophila melanogaster* behavior and aging. Implications of the IML-2 experiment." In: *Journal of Biotechnology* 47.2-3 (1996), pp. 191–201.
- [107] Camillo Di Giulio. "Do we age faster in absence of gravity?" In: *Frontiers in Physiology* 4 (June 2013), pp. 1–2.
- [108] Susan E Celniker and Gerald M Rubin. "The *Drosophila melanogaster* genome." In: *Annual Review of Genomics and Human Genetics* 4 (2003), pp. 89–117.
- [109] A Bernards and I K Hariharan. "Of flies and men—studying human disease in *Drosophila*." In: *Current opinion in genetics & development* 11.3 (June 2001), pp. 274–278.
- [110] Udai Bhan Pandey and Charles D Nichols. "Human disease models in *Drosophila melanogaster* and the role of the fly in therapeutic drug discovery." In: *Pharmacological reviews* 63.2 (June 2011), pp. 411–436.

- [111] Ethan Bier. "Drosophila, the golden bug, emerges as a tool for human genetics." In: *Nature Reviews Genetics* 6.1 (Jan. 2005), pp. 9–23.
- [112] L T Reiter, L Potocki, S Chien, M Gribskov, and E Bier. "A systematic analysis of human disease-associated gene sequences in *Drosophila melanogaster*." In: *Genome research* 11.6 (June 2001), pp. 1114–1125.
- [113] Sergey Doronkin and Lawrence T Reiter. "Drosophila Orthologues to Human Disease Genes: An Update on Progress." In: Elsevier, 2008, pp. 1–32.
- [114] Matthew J Wolf et al. "Drosophila as a model for the identification of genes causing adult human heart disease." In: *Proceedings of the National Academy of Sciences of the United States of America* 103.5 (Jan. 2006), pp. 1394–1399.
- [115] Ethan Bier and Rolf Bodmer. "Drosophila, an emerging model for cardiac disease." In: *Gene* 342.1 (Nov. 2004), pp. 1–11.
- [116] Alyce Finelli, Anju Kelkar, Ho-Juhn Song, Haidi Yang, and Mary Konsolaki. "A model for studying Alzheimer's A β 42-induced toxicity in *Drosophila melanogaster*." In: *Molecular and Cellular Neuroscience* 26.3 (July 2004), pp. 365–375.
- [117] Angela Fortner McKoy, Jermont Chen, Trudi Schupbach, and Michael H Hecht. "A novel inhibitor of amyloid β (A β) peptide aggregation: from high throughput screening to efficacy in an animal model of Alzheimer disease." In: *Journal of Biological Chemistry* 287.46 (Nov. 2012), pp. 38992–39000.
- [118] Damian C Crowther, Richard Page, Dhianjali Chandraratna, and David A Lomas. "A *Drosophila* Model of Alzheimer's Disease." In: *Amyloid, Prions, and Other Protein Aggregates, Part B*. Elsevier, 2006, pp. 234–255.
- [119] I Greeve. "Age-Dependent Neurodegeneration and Alzheimer-Amyloid Plaque Formation in Transgenic *Drosophila*." In: *Journal of Neuroscience* 24.16 (Apr. 2004), pp. 3899–3906.
- [120] C W Wittmann et al. "Tauopathy in *Drosophila*: neurodegeneration without neurofibrillary tangles." In: *Science* 293.5530 (July 2001), pp. 711–714.
- [121] Oana Marcu et al. "Innate Immune Responses of *Drosophila melanogaster* Are Altered by Spaceflight." In: *PLoS ONE* 6.1 (Jan. 2011), e15361.
- [122] Naoko Shimada and Stephen J Moorman. "Changes in gravitational force cause changes in gene expression in the lens of developing zebrafish." In: 235.10 (Oct. 2006), pp. 2686–2694.

- [123] Luis Zea et al. "A Molecular Genetic Basis Explaining Altered Bacterial Behavior in Space." In: *PLoS ONE* 11.11 (Nov. 2016), e0164359–23.
- [124] Kathy B Sheehan, Kate McInnerney, Boloroo Purevdorj-Gage, Sara D Altenburg, and Linda E Hyman. "Yeast genomic expression patterns in response to low-shear modeled microgravity." In: 8.1 (2007), p. 3.
- [125] D B Thomason et al. "Altered actin and myosin expression in muscle during exposure to microgravity." In: *Journal of applied physiology (Bethesda, Md. : 1985)* 73.2 Suppl (Aug. 1992), 90S–93S.
- [126] Emily Morey-Holton, E.L. Hill, and Kenneth A. Souza. "Animals and spaceflight: From survival to understanding." In: *J Musculoskelet Neuronal Interact* 7 (Mar. 2007), pp. 17–25.
- [127] N Gueguinou et al. "Could spaceflight-associated immune system weakening preclude the expansion of human presence beyond Earth's orbit?" In: *Journal of Leukocyte Biology* 86.5 (Oct. 2009), pp. 1027–1038.
- [128] Janet Tou, April Ronca, Richard Grindeland, and Charles Wade. "Models to study gravitational biology of Mammalian reproduction." In: *Biology of Reproduction* 67.6 (Dec. 2002), pp. 1681–1687.
- [129] R Bellairs. "Experiments on embryos in space: an overview." In: *Advances in space research : the official journal of the Committee on Space Research (COSPAR)* 14.8 (1994), pp. 179–187.
- [130] Mariano Bizzarri, Monica Monici, and Jack J W A van Loon. "How Microgravity Affects the Biology of Living Systems." In: *BioMed Research International* 2015.9 (2015), pp. 1–4.
- [131] Susan J Crawford-Young. "Effects of microgravity on cell cytoskeleton and embryogenesis." In: *The International journal of developmental biology* 50.2-3 (2006), pp. 183–191.
- [132] H Rahmann, K Slenzka, R Hilbig Research in Space, and 1994. "Influence of hyper-and hypo-gravity on the early ontogenetic development of cichlid fish. Behavioural and ultrastructural investigations: first Spacelab D2 ..." In: *adsabs.harvard.edu* ().
- [133] Kenneth A. Souza, Steven D Black, and Richard J Wassersug. "Amphibian Development in the Virtual Absence of Gravity." In: *Proceedings of the National Academy of Sciences of the United States of America* 92.6 (1995), pp. 1975–1978.
- [134] K Walton. "Postnatal development under conditions of simulated weightlessness and space flight." In: *Brain Research Reviews* 28.1-2 (Nov. 1998), pp. 25–34.

- [135] Marina Feric and Clifford P Brangwynne. "A nuclear F-actin scaffold stabilizes ribonucleoprotein droplets against gravity in large cells." In: *Nature Cell Biology* 15.10 (Oct. 2013), pp. 1253–1259.
- [136] Augusto Cogoli. "The effect of hypogravity and hypergravity on cells of the immune system." In: *Journal of Leukocyte Biology* 54.3 (Sept. 1993), pp. 259–268.
- [137] Philip J Rijken et al. "Altered Gravity Conditions Affect Early EGF-Induced Signal Transduction in Human Epidermal A431 Cells." In: *Gravitational and Space Biology* 5.2 (Nov. 2007).
- [138] M Ingram et al. "Three-dimensional growth patterns of various human tumor cell lines in simulated microgravity of a NASA bioreactor." In: *In Vitro Cellular & Developmental Biology-Animal* 33.6 (June 1997), pp. 459–466.
- [139] Jeanne L Becker and Glauco R Souza. "Using space-based investigations to inform cancer research on Earth." In: (Apr. 2013), pp. 1–14.
- [140] S Dinarelli et al. "Erythrocyte's aging in microgravity highlights how environmental stimuli shape metabolism and morphology." In: *Scientific Reports* (Mar. 2018), pp. 1–12.
- [141] J W Wilson et al. "Space flight alters bacterial gene expression and virulence and reveals a role for global regulator Hfq." In: *Proceedings of the National Academy of Sciences of the United States of America* 104.41 (Oct. 2007), pp. 16299–16304.
- [142] Aurélie Crabbé et al. "Transcriptional and Proteomic Responses of *Pseudomonas aeruginosa* PAO1 to Spaceflight Conditions Involve Hfq Regulation and Reveal a Role for Oxygen." In: *Applied and Environmental Microbiology* 77.4 (Feb. 2011), pp. 1221–1230.
- [143] A J Ricco, M Parra, M Piccini, D Ly Tech Dig Solid-State, and 2010. "PharmaSat: drug dose dependence results from an autonomous microsystem-based small satellite in low Earth orbit." In: *researchgate.net* ().
- [144] R Tixador et al. "Preliminary results of Cytos 2 experiment." In: *Acta Astronautica* 12.2 (Feb. 1985), pp. 131–134.
- [145] O Ciferri, O Tiboni, G Di Pasquale, A M Orlandoni, and M L Marchesi. "Effects of microgravity on genetic recombination in *Escherichia coli*." In: *Die Naturwissenschaften* 73.7 (July 1986), pp. 418–421.
- [146] Gerda Horneck, David M Klaus, and Rocco L Mancinelli. "Space microbiology." In: *Microbiology and molecular biology reviews : MMBR* 74.1 (Mar. 2010), pp. 121–156.

- [147] David M. Klaus, S Simske, P Todd, and L Stodieck. "Investigation of space flight effects on *Escherichia coli* and a proposed model of underlying physical mechanisms." In: *Microbiology (Reading, England)* 143 (Pt 2) (Feb. 1997), pp. 449–455.
- [148] Neva Çiftçioğlu, Ruwaida S Haddad, D C Golden, Dennis R Morrison, and David S McKay. "A potential cause for kidney stone formation during space flights: enhanced growth of nanobacteria in microgravity." In: *Kidney international* 67.2 (Feb. 2005), pp. 483–491.
- [149] R J McLean, J M Cassanto, M B Barnes, and J H Koo. "Bacterial biofilm formation under microgravity conditions." In: *FEMS microbiology letters* 195.2 (Feb. 2001), pp. 115–119.
- [150] Wooseong Kim et al. "Spaceflight Promotes Biofilm Formation by *Pseudomonas aeruginosa*." In: *PLoS ONE* 8.4 (Apr. 2013), e62437–8.
- [151] Robert B Brown, David M. Klaus, and P Todd. "Effects of space flight, clinorotation, and centrifugation on the substrate utilization efficiency of *E. coli*." In: *Microgravity Science and Technology* 13.4 (2002), pp. 24–29.
- [152] David M. Klaus. "Microgravity and its implications for fermentation biotechnology." In: *Trends in Biotechnology* 16.9 (Sept. 1998), pp. 369–373.
- [153] Michael R Benoit and David M Klaus. "Microgravity, bacteria, and the influence of motility." In: *Advances in Space Research* 39.7 (Jan. 2007), pp. 1225–1232.
- [154] Kesheng Dai et al. "Effects of microgravity and hypergravity on platelet functions." In: *Thrombosis and Haemostasis* (Mar. 2009), pp. 1–9.
- [155] Suping Li et al. "Mechanism of platelet functional changes and effects of anti-platelet agents on in vivo hemostasis under different gravity conditions." In: *Journal of applied physiology (Bethesda, Md. : 1985)* 108.5 (May 2010), pp. 1241–1249.
- [156] Tae Young Jang, Ah-Yeoun Jung, Soonjo Kwon, and Young Hyo Kim. "Hypergravity enhances the therapeutic effect of dexamethasone in allergic asthma and rhinitis animal model." In: *PLoS ONE* 13.5 (May 2018), e0197594–15.
- [157] Jeonghyun Kim, Kevin Montagne, Hidetoshi Nemoto, Takashi Ushida, and Katsuko S Furukawa. "Hypergravity down-regulates c-fos gene expression via ROCK/Rho-GTP and the PI3K signaling pathway in murine ATDC5 chondroprogenitor cells." In: *PLoS ONE* 12.9 (Sept. 2017), e0185394–11.

- [158] Albert Einstein. "Über das Relativitätsprinzip und die aus demselben gezogenen Folgerungen." In: *Jahrbuch der Radioaktivität und Elektronik* 4 (1908), pp. 411–462.
- [159] G C Pitts, L S Bull, and J Oyama. "Regulation of Body Mass in Rats Exposed to Chronic Acceleration." In: *American Journal of Physiology* 228.3 (1975), pp. 714–717.
- [160] B C Daligcon and J Oyama. "Increased Uptake and Utilization of Glucose by Diaphragms of Rats Exposed to Chronic Centrifugation." In: *American Journal of Physiology* 228.3 (1975), pp. 742–746.
- [161] A C Economos et al. "Effects of simulated increased gravity on the rate of aging of rats: implications for the rate of living theory of aging." In: *Archives of Gerontology and Geriatrics* 1.4 (Dec. 1982), pp. 349–363.
- [162] F A Lints, P Bullens, and E LeBourg. "Hypergravity and Aging in *Drosophila-Melanogaster* .7. New Longevity Data." In: *Experimental Gerontology* 28.6 (1993), pp. 611–615.
- [163] E LeBourg, F A Lints, N Fresquet, and P Bullens. "Hypergravity, Aging and Longevity in *Drosophila-Melanogaster*." In: *Comparative Biochemistry and Physiology a-Physiology* 105.3 (July 1993), pp. 389–396.
- [164] E LeBourg and F A Lints. "Hypergravity and Aging in *Drosophila-Melanogaster* .2. Longevity." In: *Gerontology* 35.5-6 (1989), pp. 244–252.
- [165] E LeBourg and F A Lints. "Hypergravity and Aging in *Drosophila-Melanogaster* .4. Climbing Activity." In: *Gerontology* 38.1-2 (1992), pp. 59–64.
- [166] E LeBourg and F A Lints. "Hypergravity and Aging in *Drosophila-Melanogaster* .5. Patterns of Movement." In: *Gerontology* 38.1-2 (1992), pp. 65–70.
- [167] E Le Bourg Gerontology. "Hypergravity and aging in *Drosophila melanogaster*: 8. Proboscis-extension-response threshold to sucrose." In: *search.proquest.com* ().
- [168] Nadege Minois and E LeBourg. "Hypergravity and aging in *Drosophila melanogaster* .9. Conditioned suppression and habituation of the proboscis extension response." In: *Aging-Clinical and Experimental Research* 9.4 (Aug. 1997), pp. 281–291.
- [169] Robert A Krebs and Volker Loeschke. "Effects of Exposure to Short-Term Heat-Stress on Fitness Components in *Drosophila-Melanogaster*." In: *Journal of Evolutionary Biology* 7.1 (Jan. 1994), pp. 39–49.

- [170] Eric Le Bourg and Nadege Minois. "Increased longevity and resistance to heat shock in *Drosophila melanogaster* flies exposed to hypergravity." In: *Comptes Rendus de l'Académie des Sciences - Series III - Sciences de la Vie* 320.3 (Mar. 1997), pp. 215–221.
- [171] E Le Bourg and Nadege Minois. "A mild stress, hypergravity exposure, postpones behavioral aging in *Drosophila melanogaster*." In: *Experimental Gerontology* 34.2 (Apr. 1999), pp. 157–172.
- [172] Nadege Minois and E Le Bourg. "Resistance to stress as a function of age in *Drosophila melanogaster* living in hypergravity." In: *Mechanisms of Ageing and Development* 109.1 (1999), pp. 53–64.
- [173] Irina V Ogneva, Stepan N Belyakin, and Svetlana V Sarantseva. "The Development Of *Drosophila Melanogaster* under Different Duration Space Flight and Subsequent Adaptation to Earth Gravity." In: *PLoS ONE* 11.11 (Nov. 2016), e0166885–20.
- [174] Nadege Minois. "Longevity and aging: beneficial, effects of exposure to mild stress." In: *Biogerontology* 1.1 (2000), pp. 15–29.
- [175] Suresh IS Rattan. "Hormetic modulation of aging and longevity by mild heat stress." In: *Dose-Response* 3.4 (May 2006), pp. 533–546.
- [176] Marion J Lamb. "The Effects of Radiation on the Longevity of Female *Drosophila-Subobscura*." In: *Journal of Insect Physiology* 10.3 (1964), pp. 487–497.
- [177] Nadege Minois and S Vaynberg. "Fecundity and life span in transgenic *Drosophila melanogaster* overexpressing hsp70." In: *Biogerontology* 3.5 (2002), pp. 301–306.
- [178] E Le Bourg, Nadege Minois, P Bullens, and P Baret. "A mild stress due to hypergravity exposure at young age increases longevity in *Drosophila melanogaster* males." In: *Biogerontology* 1.2 (2000), pp. 145–155.
- [179] Nadege Minois. "The Hormetic Effects of Hypergravity on Longevity and Aging." In: *Dose-Response* 4.2 (Apr. 2006), dose-response.0–10.
- [180] LiuDeng. "Effects of Simulated Microgravity on Vascular Development in Zebrafish." In: (Jan. 2018), pp. 1–16.
- [181] Torsten N Wiesel and David H Hubel. "Single-cell responses in striate cortex of kittens deprived of vision in one eye." In: *Journal of neurophysiology* 26 (Nov. 1963), pp. 1003–1017.
- [182] David H Hubel and Torsten N Wiesel. "Receptive fields and functional architecture in two nonstriate visual areas (18 and 19) of the cat." In: *Journal of neurophysiology* 28 (Mar. 1965), pp. 229–289.

- [183] D J Simons and P W Land. "Early experience of tactile stimulation influences organization of somatic sensory cortex." In: *Nature* 326.6114 (Apr. 1987), pp. 694–697.
- [184] Stephen J Moorman, N Shimada Gravitational, Gbalabo Sokunbi, and Cynthia Pfirrmann. "Simulated-microgravity induced changes in gene expression in zebrafish embryos suggest that the primary cilium is involved in gravity transduction." In: *gravitation-alandspacebiology.org* ().
- [185] Stefan Hammerschmidt, Hartmut Kuhn, Christian Gessner, Hans-Jurgen Seyfarth, and Hubert Wirtz. "Stretch-induced alveolar type II cell apoptosis: role of endogenous bradykinin and PI₃K-Akt signaling." In: *American journal of respiratory cell and molecular biology* 37.6 (Dec. 2007), pp. 699–705.
- [186] Ravikumar Hosamani, Ryan Leib, Shilpa R Bhardwaj, Christopher M Adams, and Sharmila Bhattacharya. "Elucidating the "Gravome": Quantitative Proteomic Profiling of the Response to Chronic Hypergravity in *Drosophila*." In: *Journal of Proteome Research* 15.12 (Dec. 2016), pp. 4165–4175.
- [187] Raul Herranz et al. "Spaceflight-related suboptimal conditions can accentuate the altered gravity response of *Drosophila* transcriptome." In: *Molecular ecology* 19.19 (Oct. 2010), pp. 4255–4264.
- [188] Raul Herranz et al. "Microgravity simulation by diamagnetic levitation: effects of a strong gradient magnetic field on the transcriptional profile of *Drosophila melanogaster*." In: 13.1 (2012).
- [189] Jade Q Clement and Hiroki Yokota. "Genomics in Space Life Sciences." In: *Genomics, Proteomics & Bioinformatics* 6.1 (Jan. 2008), pp. 1–3.
- [190] J Q Clement. "Gene Expression Microarrays in Microgravity Research: Toward the Identification of Major Space Genes." In: *Innovations in Biotechnology* (2012).
- [191] T G Hammond et al. "Mechanical culture conditions effect gene expression: gravity-induced changes on the space shuttle." In: *Physiological genomics* 3.3 (2000), pp. 163–173.
- [192] James W Wilson et al. "Microarray analysis identifies *Salmonella* genes belonging to the low-shear modeled microgravity regulon." In: *Proceedings of the National Academy of Sciences of the United States of America* 99.21 (Oct. 2002), pp. 13807–13812.
- [193] Shannon Hateley, Ravikumar Hosamani, Shilpa R Bhardwaj, Lior Pachter, and Sharmila Bhattacharya. "Transcriptomic response of *Drosophila melanogaster* pupae developed in hypergravity." In: *Genomics* 108.3-4 (Oct. 2016), pp. 158–167.

- [194] Naoko Shimada, Gbolabo Sokunbi, and Stephen J Moorman. "Changes in gravitational force affect gene expression in developing organ systems at different developmental times." In: *BMC developmental biology* 5 (May 2005), p. 10.
- [195] Timothy Hammond and Patricia Allen. "The Bonn Criteria: Minimal Experimental Parameter Reporting for Clinostat and Random Positioning Machine Experiments with Cells and Tissues." In: *Microgravity Science and Technology* 23.2 (July 2010), pp. 271–275.
- [196] Raul Herranz et al. "Ground-Based Facilities for Simulation of Microgravity: Organism-Specific Recommendations for Their Use, and Recommended Terminology." In: *Astrobiology* 13.1 (Jan. 2013), pp. 1–17.
- [197] Allan H Brown, A O Dahl, and D K Chapman. "Limitation on the use of the horizontal clinostat as a gravity compensator." In: *Plant Physiology* 58.2 (Aug. 1976), pp. 127–130.
- [198] Daniela Grimm et al. "The impact of microgravity-based proteomics research." In: *Expert Review of Proteomics* 11.4 (Aug. 2014), pp. 465–476.
- [199] Bingxin Xu et al. "Simulated microgravity affects ciprofloxacin susceptibility and expression of *acrAB-tolC* genes in *E. coli* ATCC25922." In: *International journal of clinical and experimental pathology* 8.7 (2015), pp. 7945–7952.
- [200] John O Kessler. "The internal dynamics of slowly rotating biological systems." In: *Gravitational and Space Biology* 5.2 (2007).
- [201] D M Klaus. "Clinostats and bioreactors." In: *Gravitational and space biology bulletin : publication of the American Society for Gravitational and Space Biology* 14.2 (June 2001), pp. 55–64.
- [202] G Albrecht-Buehler. "The simulation of microgravity conditions on the ground." In: *Gravitational and Space Biology* 5.2 (Oct. 1992), pp. 3–10.
- [203] Wolfgang Briegleb. "Some qualitative and quantitative aspects of the fast rotating clinostat as a research tool." In: (Aug. 1992), pp. 1–8.
- [204] S Brungs, J Hauslage, and R Hilbig. "Effects of simulated weightlessness on fish otolith growth: clinostat versus rotating-wall vessel." In: *Advances in Space ...* (2011).
- [205] T G Hammond and J M Hammond. "Optimized suspension culture: the rotating-wall vessel." In: *American Journal of Physiology-Renal Physiology* 281.1 (July 2001), F12–F25.

- [206] Mahmut N Cinbiz, R Seda Tıǧlı, Işıl Gerçek Beşkardeş, Memişe Gümüşderelioǧlu, and Üner Çolak. "Computational fluid dynamics modeling of momentum transport in rotating wall perfused bioreactor for cartilage tissue engineering." In: *Journal of Biotechnology* 150.3 (Nov. 2010), pp. 389–395.
- [207] Simon L Wuest, Stéphane Richard, Sascha Kopp, Daniela Grimm, and Marcel Egli. "Simulated microgravity: critical review on the use of random positioning machines for mammalian cell culture." In: *BioMed Research International* 2015 (2015), p. 971474.
- [208] Marianne Cogoli. "The fast rotating clinostat: a history of its use in gravitational biology and a comparison of ground-based and flight experiment results." In: (Aug. 2000), pp. 1–9.
- [209] Erwin Berthier, Edmond W K Young, and David Beebe. "Engineers are from PDMS-land, Biologists are from Polystyrenia." In: *Lab on a Chip* 12.7 (Apr. 2012), pp. 1224–1237.
- [210] Manuel Théry et al. "Anisotropy of cell adhesive microenvironment governs cell internal organization and orientation of polarity." In: *Proceedings of the National Academy of Sciences of the United States of America* 103.52 (Dec. 2006), pp. 19771–19776.
- [211] Kyung Eun Sung et al. "Transition to invasion in breast cancer: a microfluidic in vitro model enables examination of spatial and temporal effects." In: *Integr. Biol.* 3.4 (2011), pp. 439–450.
- [212] R G Harrison. "On the stereotropism of embryonic cells." In: *Science* 34.1 (1911), pp. 279–281.
- [213] Olivia Harvey. "Culturing Life: How Cells Became Technologies." In: *Annals of Science* 66.4 (Oct. 2009), pp. 585–588.
- [214] G D Aumiller, E A Chandross, W J Tomlinson, and H P Weber. "Submicrometer resolution replication of relief patterns for integrated optics." In: *Journal of Applied Physics* 45.10 (Oct. 1974), pp. 4557–4562.
- [215] A Manz, N Graber, and H M Widmer. "Miniaturized Total Chemical-Analysis Systems - a Novel Concept for Chemical Sensing." In: *Sensors and Actuators B: Chemical* 1.1-6 (Jan. 1990), pp. 244–248.
- [216] I Papautsky, J Brazzle, T Ameel, and Frazier, AB. "Laminar fluid behavior in microchannels using micropolar fluid theory." In: *Sensors and Actuators A: Physical* 73.1-2 (1999), pp. 101–108.
- [217] D Jed Harrison, Andreas Manz, Zhonghui Fan, Hans Luedi, and H Michael Widmer. "Capillary electrophoresis and sample injection systems integrated on a planar glass chip." In: *Analytical Chemistry* 64.17 (May 2002), pp. 1926–1932.
- [218] Paul C H Li and D Jed Harrison. "Transport, Manipulation, and Reaction of Biological Cells On-Chip Using Electrokinetic Effects." In: *Analytical Chemistry* 69.8 (Apr. 1997), pp. 1564–1568.

- [219] David C Duffy, J Cooper McDonald, Olivier J A Schueller, and George M Whitesides. "Rapid Prototyping of Microfluidic Systems in Poly(dimethylsiloxane)." In: *Analytical Chemistry* 70.23 (Dec. 1998), pp. 4974–4984.
- [220] Takeshi Saito et al. "Oxygen consumption of cell suspension in a poly(dimethylsiloxane) (PDMS) microchannel estimated by scanning electrochemical microscopy." In: *The Analyst* 131.9 (2006), pp. 1006–6.
- [221] Kwanghun Chung et al. "A microfluidic array for large-scale ordering and orientation of embryos." In: *Nature Methods* 8.2 (Dec. 2010), pp. 171–176.
- [222] John L Tan et al. "Cells Lying on a Bed of Microneedles: An Approach to Isolate Mechanical Force." In: *Proceedings of the National Academy of Sciences of the United States of America* 100.4 (Feb. 2003), pp. 1484–1489.
- [223] Christopher Moraes, Jan-Hung Chen, Yu Sun, and Craig A Simmons. "Microfabricated arrays for high-throughput screening of cellular response to cyclic substrate deformation." In: *Lab on a Chip* 10.2 (2010), pp. 227–234.
- [224] Michael Murrell, Roger Kamm, and Paul Matsudaira. "Substrate Viscosity Enhances Correlation in Epithelial Sheet Movement." In: *Biophysj* 101.2 (July 2011), pp. 297–306.
- [225] Jennifer S Gewandter, Rhonda J Staversky, and Michael A O'Reilly. "Hyperoxia augments ER-stress-induced cell death independent of BiP loss." In: *Free Radical Biology and Medicine* 47.12 (Dec. 2009), pp. 1742–1752.
- [226] Yun Seok Heo et al. "Characterization and Resolution of Evaporation-Mediated Osmolality Shifts That Constrain Microfluidic Cell Culture in Poly(dimethylsiloxane) Devices." In: *Analytical Chemistry* 79.3 (Feb. 2007), pp. 1126–1134.
- [227] Erwin Berthier, Jay Warrick, Hongmeiy Yu, and David J Beebe. "Managing evaporation for more robust microscale assays : Part 1. Volume loss in high throughput assays." In: *Lab on a Chip* 8.6 (2008), pp. 852–21.
- [228] Michael W Toepke and David J Beebe. "PDMS absorption of small molecules and consequences in microfluidic applications." In: *Lab on a Chip* 6.12 (2006), pp. 1484–3.
- [229] Keil J Regehr et al. "Biological implications of polydimethylsiloxane-based microfluidic cell culture." In: *Lab on a Chip* 9.15 (2009), pp. 2132–8.

- [230] Xiaojing Su, Ashleigh B Theberge, Craig T January, and David J Beebe. "Effect of Microculture on Cell Metabolism and Biochemistry: Do Cells Get Stressed in Microchannels?" In: *Analytical Chemistry* 85.3 (Jan. 2013), pp. 1562–1570.
- [231] Hirotaka Sasaki, Hiroaki Onoe, Toshihisa Osaki, Ryuji Kawano, and Shoji Takeuchi. "Parylene-coating in PDMS microfluidic channels prevents the absorption of fluorescent dyes." In: *Sensors and Actuators B: Chemical* 150.1 (Sept. 2010), pp. 478–482.
- [232] Kangning Ren, Yihua Zhao, Jing Su, Declan Ryan, and Hongkai Wu. "Convenient Method for Modifying Poly(dimethylsiloxane) To Be Airtight and Resistive against Absorption of Small Molecules." In: *Analytical Chemistry* 82.14 (July 2010), pp. 5965–5971.
- [233] Jessamine Ng Lee, Cheolmin Park, and George M Whitesides. "Solvent Compatibility of Poly(dimethylsiloxane)-Based Microfluidic Devices." In: *Analytical Chemistry* 75.23 (Dec. 2003), pp. 6544–6554.
- [234] C C Chen et al. "Design and operation of a microfluidic sorter for *Drosophila* embryos." In: *Sensors and Actuators B: Chemical* 102.1 (Sept. 2004), pp. 59–66.
- [235] Thomas J Levario, Mei Zhan, Bomyi Lim, Stanislav Y Shvartsman, and Hang Lu. "Microfluidic trap array for massively parallel imaging of *Drosophila* embryos." In: *Nature Protocols* 8.4 (Mar. 2013), pp. 721–736.
- [236] Ralph W Bernstein et al. "Characterization of fluidic microassembly for immobilization and positioning of *Drosophila* embryos in 2-D arrays." In: *Sensors and Actuators A: Physical* 114.2-3 (Sept. 2004), pp. 191–196.
- [237] Xiaojing Zhang et al. "Microoptical characterization and modeling of positioning forces on *drosophila* embryos self-assembled in two-dimensional arrays." In: *Journal of Microelectromechanical Systems* 14.5 (Sept. 2005), pp. 1187–1197.
- [238] Xiquan Cui et al. "Lensless high-resolution on-chip optofluidic microscopes for *Caenorhabditis elegans* and cell imaging." In: *Proceedings of the National Academy of Sciences* 105.31 (Aug. 2008), pp. 10670–10675.
- [239] Gabriel T Dagani et al. "Microfluidic self-assembly of live *Drosophila* embryos for versatile high-throughput analysis of embryonic morphogenesis." In: *Biomedical Microdevices* 9.5 (Oct. 2007), pp. 681–694.
- [240] Marc Gershow et al. "Controlling airborne cues to study small animal navigation." In: *Nature Methods* 9.3 (Jan. 2012), pp. 290–296.

- [241] Tomoko Ohyama et al. "High-Throughput Analysis of Stimulus-Evoked Behaviors in *Drosophila* Larva Reveals Multiple Modality-Specific Escape Strategies." In: *PLoS ONE* 8.8 (Aug. 2013), e71706–21.
- [242] Reza Ghaemi, Pouya Rezai, Balaji G Iyengar, and Ponnambalam Ravi Selvaganapathy. "Microfluidic devices for imaging neurological response of *Drosophila melanogaster* larva to auditory stimulus." In: *Lab on a Chip* 15 (Jan. 2015), pp. 1116–1122.
- [243] Wei Zhang, Zhiqiang Yan, Lily Yeh Jan, and Yuh Nung Jan. "Sound response mediated by the TRP channels NOMPC, NANCHUNG, and INACTIVE in chordotonal organs of *Drosophila* larvae." In: *Proceedings of the National Academy of Sciences of the United States of America* 110.33 (2013), pp. 13612–13617.
- [244] S R Lockery et al. "Artificial Dirt: Microfluidic Substrates for Nematode Neurobiology and Behavior." In: *Journal of neurophysiology* 99.6 (June 2008), pp. 3136–3143.
- [245] Sungsu Park et al. "Enhanced *Caenorhabditis elegans* Locomotion in a Structured Microfluidic Environment." In: *PLoS ONE* 3.6 (June 2008), e2550–5.
- [246] Stefan Zappe, Matthew Fish, Matthew P Scott, and Olav Solgaard. "Automated MEMS-based *Drosophila* embryo injection system for high-throughput RNAi screens." In: *Lab on a Chip* 6.8 (2006), pp. 1012–8.
- [247] Daniel Delubac et al. "Microfluidic system with integrated microinjector for automated *Drosophila* embryo injection." In: *Lab on a Chip* 12.22 (2012), pp. 4911–9.
- [248] Venkataragavalu Sivagnanam and Martin A M Gijs. "Exploring Living Multicellular Organisms, Organs, and Tissues Using Microfluidic Systems." In: *Chemical Reviews* 113.5 (Mar. 2013), pp. 3214–3247.
- [249] Felix Kurth, Klaus Eyer, Alfredo Franco-Obregón, and Petra S Dittrich. "A new mechanobiological era: microfluidic pathways to apply and sense forces at the cellular level." In: *Current Opinion in Chemical Biology* 16.3-4 (Aug. 2012), pp. 400–408.
- [250] Jean R Fakhoury, John C Sisson, and Xiaojing Zhang. "Microsystems for controlled genetic perturbation of live *Drosophila* embryos: RNA interference, development robustness and drug screening." In: *Microfluidics and Nanofluidics* 6.3 (Feb. 2009), pp. 299–313.
- [251] Daniel T Chiu et al. "Small but Perfectly Formed? Successes, Challenges, and Opportunities for Microfluidics in the Chemical and Biological Sciences." In: *CHEMPR* 2.2 (Feb. 2017), pp. 201–223.

- [252] Cody E Narciso, Nicholas M Contento, Thomas J Storey, David J Hoelzle, and Jeremiah J Zartman. "Release of Applied Mechanical Loading Stimulates Intercellular Calcium Waves in *Drosophila* Wing Discs." In: *Biophysical Journal* 113.2 (July 2017), pp. 491–501.
- [253] Matthew M Crane, Kwanghun Chung, Jeffrey Stirman, and Hang Lu. "Microfluidics-enabled phenotyping, imaging, and screening of multicellular organisms." In: *Lab on a Chip* 10.12 (2010), pp. 1509–9.
- [254] Karine Guevorkian, Marie-Josée Colbert, Mélanie Durth, Sylvie Dufour, and Françoise Brochard-Wyart. "Aspiration of biological viscoelastic drops." In: *Physical Review Letters* 104.21 (May 2010), p. 218101.
- [255] Benjamen A Filas, Gang Xu, and Larry A Taber. "Probing regional mechanical properties of embryonic tissue using microindentation and optical coherence tomography." In: *Methods in molecular biology (Clifton, N.J.)* 1189. Chapter 1 (2015), pp. 3–16.
- [256] Abbas Mgharbel, H el ene Delano e Ayari, and Jean Paul Rieu. "Measuring accurately liquid and tissue surface tension with a compression plate tensiometer." In: *HFSP Journal* 3.3 (Sept. 2010), pp. 213–221.
- [257] F S Collins, M S Guyer, and A Charkravarti. "Variations on a theme: cataloging human DNA sequence variation." In: *Science* 278.5343 (Nov. 1997), pp. 1580–1581.
- [258] J D Watson. "The human genome project: past, present, and future." In: *Science* 248.4951 (Apr. 1990), pp. 44–49.
- [259] F S Collins and V A McKusick. "Implications of the Human Genome Project for medical science." In: *JAMA : the journal of the American Medical Association* 285.5 (Feb. 2001), pp. 540–544.
- [260] M P Sawicki, G Samara, M Hurwitz, and E Passaro. "Human Genome Project." In: *American journal of surgery* 165.2 (Feb. 1993), pp. 258–264.
- [261] J C Venter et al. "The sequence of the human genome." In: *Science* 291.5507 (Feb. 2001), pp. 1304–1351.
- [262] Rebecca A Burrell, Nicholas McGranahan, Jiri Bartek, and Charles Swanton. "The causes and consequences of genetic heterogeneity in cancer evolution." In: *Nature* 501.7467 (Sept. 2013), pp. 338–345.
- [263] Jon McClellan and Mary-Claire King. "Genetic Heterogeneity in Human Disease." In: *Cell* 141.2 (Apr. 2010), pp. 210–217.
- [264] Eric H Davidson. "Emerging properties of animal gene regulatory networks." In: *Nature* 468.7326 (Dec. 2010), pp. 911–920.

- [265] Tatjana Sauka-Spengler and Marianne Bronner-Fraser. "A gene regulatory network orchestrates neural crest formation." In: *Nature Reviews Molecular Cell Biology* 9.7 (June 2008), pp. 557–568.
- [266] Manel Esteller. "Non-coding RNAs in human disease." In: *Nature Publishing Group* 12.12 (Dec. 2011), pp. 861–874.
- [267] Sarah Geisler and Jeff Collier. "RNA in unexpected places: long non-coding RNA functions in diverse cellular contexts." In: *Nature Reviews Molecular Cell Biology* 14.11 (Oct. 2013), pp. 699–712.
- [268] Jon M Laurent et al. "Protein abundances are more conserved than mRNA abundances across diverse taxa." In: *PROTEOMICS* 10.23 (Nov. 2010), pp. 4209–4212.
- [269] S P Gygi, Y Rochon, B R Franza, and R Aebersold. "Correlation between protein and mRNA abundance in yeast." In: *Molecular and cellular biology* 19.3 (Mar. 1999), pp. 1720–1730.
- [270] Samreen Riaz et al. "Proteomic Identification of Human Urinary Biomarkers in Diabetes Mellitus Type 2." In: *Diabetes Technology & Therapeutics* 12.12 (Dec. 2010), pp. 979–988.
- [271] Urban A Kiernan, Dobrin Nedelkov, and Randall W Nelson. "Multiplexed mass spectrometric immunoassay in biomarker research: a novel approach to the determination of a myocardial infarct." In: *Journal of Proteome Research* 5.11 (Nov. 2006), pp. 2928–2934.
- [272] Qing-Yu He et al. "Serum biomarkers of hepatitis B virus infected liver inflammation: A proteomic study." In: *PROTEOMICS* 3.5 (May 2003), pp. 666–674.
- [273] Karin D van Dijk et al. "Diagnostic cerebrospinal fluid biomarkers for Parkinson's disease: A pathogenetically based approach." In: *Neurobiology of Disease* 39.3 (Sept. 2010), pp. 229–241.
- [274] Kaj Blennow. "Biomarkers in Alzheimer's disease drug development." In: *Nature Publishing Group* 16.11 (Sept. 2010), pp. 1218–1222.
- [275] Timo Gemoll, Uwe Johannes Roblick, Gert Auer, Hans Jörnvall, and Jens Karsten Habermann. "SELDI-TOF serum proteomics and colorectal cancer: A current overview." In: *Archives of Physiology and Biochemistry* 116.4-5 (Sept. 2010), pp. 188–196.
- [276] Poh-Kuan Chong et al. "Upregulation of plasma C9 protein in gastric cancer patients." In: *PROTEOMICS* 10.18 (July 2010), pp. 3210–3221.
- [277] Sho Minami et al. "Proteomic study of sera from patients with bladder cancer: usefulness of S100A8 and S100A9 proteins." In: *Cancer genomics & proteomics* 7.4 (July 2010), pp. 181–189.

- [278] Jennifer C Byrne et al. "2D-DIGE as a Strategy To Identify Serum Markers for the Progression of Prostate Cancer." In: *Journal of Proteome Research* 8.2 (Feb. 2009), pp. 942–957.
- [279] Richard Frank and Richard Hargreaves. "Clinical biomarkers in drug discovery and development." In: *Nature Reviews Drug Discovery* 2.7 (July 2003), pp. 566–580.
- [280] Sarah C Sim and Magnus Ingelman-Sundberg. "Pharmacogenomic biomarkers: new tools in current and future drug therapy." In: *Trends in Pharmacological Sciences* 32.2 (Feb. 2011), pp. 72–81.
- [281] Mariana P Torrente, Willard M Freeman, and Kent E Vrana. "Protein biomarkers of alcohol abuse." In: *Expert Review of Proteomics* 9.4 (Jan. 2014), pp. 425–436.
- [282] Charalampos Pierrakos and Jean-Louis Vincent. "Sepsis biomarkers: a review." In: *Critical Care* 14.1 (2010), R15–18.
- [283] Vinitha Ganesan, Dana P Ascherman, and Jonathan S Minden. "Immunoproteomics technologies in the discovery of autoantigens in autoimmune diseases." In: *Biomolecular Concepts* 7.2 (Apr. 2016), pp. 1–11.
- [284] Patrick H O'Farrell. "High resolution two-dimensional electrophoresis of proteins." In: *Journal of Biological Chemistry* 250.10 (May 1975), pp. 4007–4021.
- [285] George A Scheele. "Two-dimensional gel analysis of soluble proteins. Characterization of guinea pig exocrine pancreatic proteins." In: *Journal of Biological Chemistry* 250.14 (July 1975), pp. 5375–5385.
- [286] J Klose. "Protein mapping by combined isoelectric focusing and electrophoresis of mouse tissues." In: *Springer* (Aug. 1975).
- [287] Angelika Görg, Wilhelm Postel, and Siegfried Günther. "The Current State of Two-Dimensional Electrophoresis with Immobilized Ph Gradients." In: *Electrophoresis* 9.9 (Sept. 1988), pp. 531–546.
- [288] Mark J Miller, Arthur D Olson, and Snorri S Thorgeirsson. "Computer-Analysis of Two-Dimensional Gels - Automatic Matching." In: *Electrophoresis* 5.5 (1984), pp. 297–303.
- [289] Andrew W Dowsey et al. "Image analysis tools and emerging algorithms for expression proteomics." In: *PROTEOMICS* 10.23 (Nov. 2010), pp. 4226–4257.
- [290] M Unlü, M E Morgan, and Jonathan S Minden. "Difference gel electrophoresis: a single gel method for detecting changes in protein extracts." In: *Electrophoresis* 18.11 (Oct. 1997), pp. 2071–2077.

- [291] Jonathan S Minden, Susan R Dowd, Helmut E Meyer, and Kai Stühler. "Difference gel electrophoresis." In: *Electrophoresis* 30 Suppl 1 (June 2009), S156–61.
- [292] Jonathan S Minden. "Two-Dimensional Difference Gel Electrophoresis (2D DIGE)." In: *Laboratory Methods in Cell Biology*. Elsevier, 2012, pp. 111–141.
- [293] Phu T Van, Victor Bass, Dan Shiwerski, Frederick Lanni, and Jonathan Minden. "High dynamic range proteome imaging with the structured illumination gel imager." In: *Electrophoresis* 35.18 (Aug. 2014), pp. 2642–2655.
- [294] Phu T Van et al. "In-gel equilibration for improved protein retention in 2DE-based proteomic workflows." In: *Electrophoresis* 35.20 (Aug. 2014), pp. 3012–3017.
- [295] Surya Viswanathan, Mustafa Unlü, and Jonathan S Minden. "Two-dimensional difference gel electrophoresis." In: *Nature Protocols* 1.3 (Oct. 2006), pp. 1351–1358.
- [296] Vinitha Ganesan et al. "Immuno-proteomics: Development of a novel reagent for separating antibodies from their target proteins." In: *Biochimica et Biophysica Acta (BBA) - Proteins and Proteomics* 1854.6 (June 2015), pp. 592–600.
- [297] Vinitha Ganesan. "Immunological Enrichment of Low-Abundance Proteins for Comparative Proteomics." PhD thesis. Aug. 2017.
- [298] M H Hamdan and P G Righetti. *Proteomics today: protein assessment and biomarkers using mass spectrometry, 2D electrophoresis, and microarray technology*. 2005.
- [299] Mamta Puri, Anupam Goyal, Nina Senutovich, Susan R Dowd, and Jonathan S Minden. "Building proteomic pathways using *Drosophila* ventral furrow formation as a model." In: *Molecular bioSystems* 4.11 (Nov. 2008), pp. 1126–1135.
- [300] Malachi A Blundon et al. "Proteomic analysis reveals APC-dependent post-translational modifications and identifies a novel regulator of β -catenin." In: *Development* 143.14 (July 2016), pp. 2629–2640.
- [301] M A Blundon. "Using Gel Based Proteomics to Study Signaling, Physiology, and Behavior in *Drosophila Melanogaster*." PhD thesis. 2017.
- [302] Eric Brouzés, Willy Supatto, and Emmanuel Farge. "Is mechano-sensitive expression of twist involved in mesoderm formation?" In: *Biology of the Cell* 96.7 (Sept. 2004), pp. 471–477.
- [303] Willy Supatto et al. "In vivo modulation of morphogenetic movements in *Drosophila* embryos with femtosecond laser pulses." In: *Proceedings of the National Academy of Sciences of the United States of America* 102.4 (Jan. 2005), pp. 1047–1052.

- [304] Nicolas Desprat, Willy Supatto, Philippe-Alexandre Pouille, Emmanuel Beaurepaire, and Emmanuel Farge. "Tissue deformation modulates twist expression to determine anterior midgut differentiation in *Drosophila* embryos." In: *Developmental Cell* 15.3 (Sept. 2008), pp. 470–477.
- [305] Albert Folch. *Introduction to bioMEMS*. 2016.
- [306] Y N Xia and G M Whitesides. "Soft lithography." In: *Annual Review of Materials Science* 28.1 (1998), pp. 153–184.
- [307] Hun Lee et al. "A new fabrication process for uniform SU-8 thick photoresist structures by simultaneously removing edge bead and air bubbles." In: *Journal of Micromechanics and Microengineering* 21.12 (Nov. 2011), p. 125006.
- [308] Dong Qin, Younan Xia, and George M Whitesides. "Soft lithography for micro- and nanoscale patterning." In: *Nature Protocols* 5.3 (Feb. 2010), pp. 491–502.
- [309] J A Campos-Ortega and V Hartenstein. *The embryonic development of *Drosophila melanogaster**. 2013.
- [310] Robyn H Pritchard, Pascal Lava, Dimitri Debruyne, and Eugene M Terentjev. "Precise determination of the Poisson ratio in soft materials with 2D digital image correlation." In: *Soft Matter* 9.26 (2013), pp. 6037–6045.
- [311] Johannes Schindelin et al. "Fiji: an open-source platform for biological-image analysis." In: *Nature Methods* 9.7 (July 2012), pp. 676–682.
- [312] J.A.M. Carrer, W. J. Mansur, R. F. Scuciato, and S A Fleischfresser. "Analysis of Euler-Bernoulli and Timoshenko beams by the boundary element method." In: *researchgate.net* (May 2014).
- [313] G R Cowper. "The Shear Coefficient in Timoshenko's Beam Theory." In: *Journal of Applied Mechanics* 33.2 (June 1966), pp. 335–340.
- [314] Warren C Young and Richard G Budynas. *Roark's Formulas for Stress and Strain*. 7th ed. New York: McGraw-Hill, Sept. 2006.
- [315] Francis I. Baratta. "When Is a Beam a Plate?" In: *Journal of the American Ceramic Society* 64.5 (1981), pp. C86–C86.
- [316] R D Cook and Warren C Young. *Advanced mechanics of materials*. Vol. 2. Upper Saddle River, NJ: Prentice Hall, May 1999.
- [317] Y J Chuang, F G Tseng, and W K Lin. "Reduction of diffraction effect of UV exposure on SU-8 negative thick photoresist by air gap elimination." In: *Microsystem Technologies* 8.4-5 (Aug. 2002), pp. 308–313.

- [318] Zhong G Ling, Kun Lian, and Linke Jian. "Improved patterning quality of SU-8 microstructures by optimizing the exposure parameters." In: *Microolithography 2000*. Ed. by Francis M Houlihan. SPIE, June 2000, pp. 1019–10.
- [319] H Lorenz, M Despont, P Vettiger, and P Renaud. "Fabrication of photoplastic high-aspect ratio microparts and micromolds using SU-8 UV resist." In: *Microsystem Technologies* 4.3 (May 1998), pp. 143–146.
- [320] Che-Hsin Lin, Gwo-Bin Lee, Bao-Wen Chang, and Guan-Liang Chang. "A new fabrication process for ultra-thick microfluidic microstructures utilizing SU-8 photoresist." In: *Journal of Micromechanics and Microengineering* 12.5 (June 2002), pp. 590–597.
- [321] I D Johnston, D K McCluskey, C K L Tan, and M C Tracey. "Mechanical characterization of bulk Sylgard 184 for microfluidics and microengineering." In: *Journal of Micromechanics and Microengineering* 24.3 (Feb. 2014), p. 035017.
- [322] Zhixin Wang, Alex A Volinsky, and Nathan D Gallant. "Crosslinking effect on polydimethylsiloxane elastic modulus measured by custom-built compression instrument." In: *Journal of Applied Polymer Science* 131.22 (June 2014), n/a–n/a.
- [323] Miao Liu, Jianren Sun, Ying Sun, Christopher Bock, and Quanfang Chen. "Thickness-dependent mechanical properties of polydimethylsiloxane membranes." In: *Journal of Micromechanics and Microengineering* 19.3 (Feb. 2009), p. 035028.
- [324] V Placet and P Delobelle. "Mechanical properties of bulk polydimethylsiloxane for microfluidics over a large range of frequencies and aging times." In: *Journal of Micromechanics and Microengineering* 25.3 (Feb. 2015), p. 035009.
- [325] Yantao Shen, Ning Xi, and Rui Zhang. "In-situ mechanical property evaluation of different stage *Drosophila* embryos with a minimally invasive microforce sensing tool." In: *ieeexplore.ieee.org* (), pp. 31–36.
- [326] Victoria E Foe and Bruce M Alberts. "Reversible Chromosome Condensation Induced in *Drosophila* Embryos by Anoxia - Visualization of Interphase Nuclear-Organization." In: *Journal of Cell Biology* 100.5 (1985), pp. 1623–1636.
- [327] C Coralli, M Cemazar, C Kanthou, G M Tozer, and G U Dachs. "Limitations of the reporter green fluorescent protein under simulated tumor conditions." In: *Cancer Research* 61.12 (2001), pp. 4784–4790.
- [328] Muh-Hwa Yang and Kou-Juey Wu. "TWIST activation by hypoxia inducible factor-1 (HIF-1): Implications in metastasis and development." In: *Cell Cycle* 7.14 (Oct. 2014), pp. 2090–2096.

- [329] Muh-Hwa Yang et al. "Direct regulation of TWIST by HIF-1 α promotes metastasis." In: *Nature Cell Biology* 10.3 (Feb. 2008), pp. 295–305.
- [330] Raul Herranz et al. "The behavioural-driven response of the *Drosophila* imago transcriptome to different types of modified gravity." In: *Genomics Discovery* 1.1 (2013), pp. 1–7.
- [331] April E Ronca, Joshua S Alwood, Ruth K Globus, and Kenneth A Souza. "Mammalian Reproduction and Development on the International Space Station (ISS): Proceedings of the Rodent Mark III Habitat Workshop." In: *Gravitational and Space Research* 1.1 (2013), e32243.
- [332] Peter J Thul et al. "A subcellular map of the human proteome." In: *Science* 356.6340 (May 2017), eaal3321–14.
- [333] Albert Goldbeter. "Computational approaches to cellular rhythms." In: *Nature* 420.6912 (2002), pp. 238–245.
- [334] José M G Vilar, Hao Yuan Kueh, Naama Barkai, and Stanislas Leibler. "Mechanisms of Noise-Resistance in Genetic Oscillators." In: *Proceedings of the National Academy of Sciences of the United States of America* 99.9 (Apr. 2002), pp. 5988–5992.
- [335] Juliane Zantke et al. "Circadian and Circalunar Clock Interactions in a Marine Annelid." In: *CellReports* (Sept. 2013), pp. 1–15.
- [336] J A Williams et al. "Programmed Cell Death in Zebrafish Rohon Beard Neurons Is Influenced by TrkC₁/NT-3 Signaling." In: *Developmental Biology* 226.2 (Oct. 2000), pp. 220–230.
- [337] J Y Kuwada, R R Bernhardt, and N Nguyen. "Development of spinal neurons and tracts in the zebrafish embryo." In: *The Journal of comparative neurology* 302.3 (Dec. 1990), pp. 617–628.
- [338] Erica F Andersen, Namrata S Asuri, and Mary C Halloran. "In vivo imaging of cell behaviors and F-actin reveals LIM-HD transcription factor regulation of peripheral versus central sensory axon development." In: *Neural development* 6.1 (May 2011), p. 27.
- [339] Patrick Blader, Charles Plessy, and Uwe Strähle. "Multiple regulatory elements with spatially and temporally distinct activities control neurogenin1 expression in primary neurons of the zebrafish embryo." In: *Mechanisms of development* 120.2 (Feb. 2003), pp. 211–218.
- [340] Benjamin B Kaufmann and Alexander van Oudenaarden. "Stochastic gene expression: from single molecules to the proteome." In: *Current opinion in genetics & development* 17.2 (2007), pp. 107–112.

- [341] C H Kim et al. "Overexpression of neurogenin induces ectopic expression of HuC in zebrafish." In: *Neuroscience letters* 239.2-3 (Dec. 1997), pp. 113–116.
- [342] Monte Westerfield. *The Zebrafish Book*. 5th ed. A Guide for the Laboratory Use of Zebrafish (*Danio rerio*), 5th Edition. University of Oregon Press, Eugene, Jan. 2007.
- [343] Christian Lawrence. "The husbandry of zebrafish (*Danio rerio*): A review." In: *Aquaculture* 269.1-4 (Sept. 2007), pp. 1–20.
- [344] Arndt F Siekmann, Clive Standley, Kevin E Fogarty, Scot A Wolfe, and Nathan D Lawson. "Chemokine signaling guides regional patterning of the first embryonic artery." In: *Genes & Development* 23.19 (Oct. 2009), pp. 2272–2277.
- [345] Stephen J Moorman. "Stimulus Dependence of the Development of the Zebrafish (*Danio rerio*) Vestibular System." In: (Jan. 1999), pp. 1–12.
- [346] A Liljeborg, M Czader, and A Porwit. "A method to compensate for light attenuation with depth in three-dimensional DNA image cytometry using a confocal scanning laser microscope." In: *Journal of microscopy* 177.Pt 2 (Feb. 1995), pp. 108–114.
- [347] F Margadant, T Leemann, and P Niederer. "A precise light attenuation correction for confocal scanning microscopy with $O(n(4/3))$ computing time and $O(n)$ memory requirements for n voxels." In: *Journal of microscopy* 182 (May 1996), pp. 121–132.
- [348] Monte Westerfield, Jeremy Wegner, Beatrice G Jegalian, Eddy M DeRobertis, and Andreas W Püschel. "Specific Activation of Mammalian Hox Promoters in Mosaic Transgenic Zebrafish." In: *Genes & Development* 6.4 (Apr. 1992), pp. 591–598.
- [349] F Muller et al. "Intronic enhancers control expression of zebrafish sonic hedgehog in floor plate and notochord." In: *Development* 126.10 (May 1999), pp. 2103–2116.
- [350] Gang Lin et al. "A hybrid 3D watershed algorithm incorporating gradient cues and object models for automatic segmentation of nuclei in confocal image stacks." In: *Cytometry* 56A.1 (Oct. 2003), pp. 23–36.
- [351] N R Pal and S K Pal. "A review on image segmentation techniques." In: *Pattern Recognition* (Feb. 1993), pp. 1–18.
- [352] Jianping Fan, D K Y Yau, A K Elmagarmid, and W G Aref. "Automatic image segmentation by integrating color-edge extraction and seeded region growing." In: *IEEE Transactions on Image Processing* 10.10 (2001), pp. 1454–1466.
- [353] P L Palmer, H Dabis, and J Kittler. "A Performance Measure for Boundary Detection Algorithms." In: *Computer Vision and Image Understanding* 63.3 (May 1996), pp. 476–494.

- [354] C A Glasbey. "An Analysis of Histogram-Based Thresholding Algorithms." In: *Cvgip-Graphical Models and Image Processing* 55.6 (Nov. 1993), pp. 532–537.
- [355] S A Hojjatoleslami and J Kittler. "Region growing: a new approach." In: *IEEE transactions on image processing : a publication of the IEEE Signal Processing Society* 7.7 (1998), pp. 1079–1084.
- [356] Rolf Adams and Leanne Bischof. "Seeded Region Growing." In: *IEEE Transactions on Pattern Analysis and Machine Intelligence* (June 1994), pp. 1–7.
- [357] Jochen Gehrig et al. "Automated high-throughput mapping of promoter-enhancer interactions in zebrafish embryos." In: 6.12 (Nov. 2009), pp. 911–916.
- [358] A Kelemen, H W Reist, G Gerig, and G Szekely. "Automatic segmentation of cell nuclei from confocal laser scanning microscopy images." In: (Dec. 2016), pp. 1–13.
- [359] Andreas Vogt et al. "Automated image-based phenotypic analysis in zebrafish embryos." In: *Developmental dynamics* 238.3 (Mar. 2009), pp. 656–663.
- [360] Ravindra Peravali et al. "Automated feature detection and imaging for high-resolution screening of zebrafish embryos." In: *BioTechniques* 50.5 (May 2011), pp. 319–324.
- [361] Martin Oheim, Emmanuel Beaurepaire, Emmanuelle Chaigneau, Jerome Mertz, and Serge Charpak. "Two-photon microscopy in brain tissue: parameters influencing the imaging depth." In: *Journal of neuroscience methods* 111.1 (Oct. 2001), pp. 29–37.
- [362] Karel Svoboda and Ryohei Yasuda. "Principles of Two-Photon Excitation Microscopy and Its Applications to Neuroscience." In: *Neuron* 50.6 (June 2006), pp. 823–839.
- [363] H Koehn and M K Oehler. "Proteins' promise–progress and challenges in ovarian cancer proteomics." In: *Menopause international* 13.4 (Dec. 2007), pp. 148–153.
- [364] F Dautel, S Kalkhof, S Trump, and I Lehmann. "Large-scale 2-D DIGE studies-guidelines to overcome pitfalls and challenges along the experimental procedure." In: *Journal of Integrated ...* (2010).
- [365] Benjamin Trotter et al. "The influence of simulated microgravity on the proteome of *Daphnia magna*." In: *Nature Publishing Group* (Sept. 2015), pp. 1–10.

*Our knowledge is so weak that no philosopher
will ever be able to completely explore the nature of even a fly...*

— Thomas Aquinas, *In Symbolum Apostolorum*

ACKNOWLEDGMENTS

I'm lucky to have a lot of people to thank.

Thanks to my advisors, Phil LeDuc and Jon Minden. It took me a long time to appreciate how much you work behind the scenes to clear the path for your students. I've learned I can either take your advice now, or come back in two months to say you were right. Thank you for taking me into your lab. You've been incredibly kind and generous, and your dedication to mentorship is a gift.

Thanks to my committee: Dr. Fred Lanni for getting into the details, your profound interest in the world, and one of my favorite classes of all time. You have been a phenomenal resource for my learning. Thanks to Dr. Rebecca Taylor for making research look fun. Thanks to Dr. Woolford for reminding me that science is creative, and modeling what it means to be trustworthy, loyal, helpful, friendly, courteous, kind, obedient, cheerful, thrifty, brave, clean, and reverent.

Thanks to the LeDuc lab (Fig. ??) and alumni not pictured: Doctors Kristin Warren, Melis Hazar, Cheemeng Tan, Mary Beth Wilson. Thanks especially to Dr. Lina Gonzalez and Dr. Kyle Justus, who helped with early modeling of hypergravity. Dr. Mark Whiting, working with you is always a pleasure, and I hope we have a long road of collaboration ahead.

Thanks to the Minden lab for being my academic home and teaching me the value of a scientific community. Thanks to Dr. Emily Furbee, Dr. Malachi Blundon, and Dr. Vanitha Ganesan, for teaching me everything I know about flies and DIGE. Thanks especially to Amber Lucas for keeping me sane, and never parading on somebody's rain. Dan Crosby, you were a phenomenal rotato. Thanks to the wonderful platoon members I've had the privilege to work with: Rachel Willen, Tiffany Lau, and Ian Griswold.

Thanks to Dr. Brooke McCartney who made all of this fly work possible. Thanks to the Strähle Lab in KIT and Dr. Mary Halloran at University of Wisconsin for the zebrafish line, and to the Roman lab. Thanks to Alexandra Elbakyan, without whom I would not have been able to read half the papers I did for this project. Thanks to Dr. Jarvik and Dr. Ettensohn for your mentorship, Haibing for microscopy training,

and Rachel Koh for discussions on analytical models of wall deflection. Thanks to Dr. Suzie Laurich-McIntyre for making *Public Communication for Researchers* possible.

Thanks to Dr. Jesse Dunietz and Adona Iosif for teaching me how to talk about my work and why it matters.

I'm grateful to Dr. Liz Ransey, who mentored me through feeling like an outsider, and Emily Simon, who brightens any day. Thanks to Dr. Jeremy Siegman, Shae, Anya, Sophie, and Shira for being a part of my life. Thanks to Dr. Sylke Hoehnel for reminding me to make more pictures.

Thank you to my Pittsburgh community – you are the reason I want to stay. Thanks to Dr. Avigail Orren for teaching me *sitzfleisch*, Dr. Samantha Finkelstein for being pure magic, and phenomenal study buddies Emily, Claire, Lili, Judah, and Lev. Thanks to Emily Payne for asking the hard questions like, "is that a good thing?" Thanks to Ren and Diana for their skill in observation, and for help with cancer research.

Thanks to Pearlann Porter and John Lambert for creating the *Invisible Jazz Labs*, for your collaboration, discussion, and inspiration. Thanks to Troy Patrick, Sarah Friedlander, Roberta Guido, Lauren Gerlowski, John Lambert, Jenni Walkup, and PJ Roduta for making a movie with me about proteins.

Thanks to Dr. Stephen Moorman who started this project of sensing gravity, and for teaching me that data are data. Thanks to Vicky DiBona for teaching me everything I know about zebrafish. Thanks to Dr. Storch, Dr. Sherrell, Dr. Langer, and Dr. Hecht for introducing me to the lab. Thank you Dr. Judy Swan for teaching me scientific writing; learning from you is a blessing. Thanks to Dr. Weber, my first mentor and inspiration in science.

Thanks to my parents for fostering curiosity even when it was disassembled on the living room floor, and for what ended up being the most useful concept in lab work, *עבודה במקביל*. Thanks for pushing me to explain everything I learned, and for never releasing the footage where I "explain" that the people on Mars are 1,000 years old.

Thanks to Arielle for keeping me humble. Who knows how much worse I'd be without you.

Thanks to Moriah Ella Mason for your incredible support. Thanks for introducing me to dance, staying up late to talk about science, making up songs about spin coating, and being the best part of a hard day. I love learning with you, and I'm grateful to have you in my life.

Lastly, I want to acknowledge the animals whose lives I've sacrificed in the pursuit of knowledge.

COLOPHON

This thesis was typeset in *Palatino* by Hermann Zapf, based on the 16th century Italian calligrapher Giambattista Palatino. Layout was developed in *A Classic Thesis Style*, by André Miede and Ivo Pletikosić for L^AT_EX based on Robert Bringhurst's "*The Elements of Typographic Style*."